

A Study of Atmospheric Reactions of
Neutral Sodium Species and Other Metals
of Meteoric Origin

J.A. Silver
C.E. Kolb

Aerodyne Research, Inc.
45 Manning Road
Billerica, MA 01821

Date of Report
10 February 1986

Final Report
10 November 1982 - 9 February 1986

APPROVED FOR PUBLIC RELEASE; DISTRIBUTION UNLIMITED

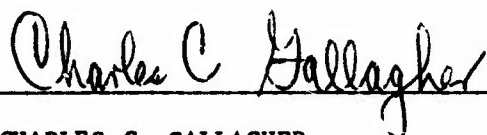
AIR FORCE GEOPHYSICS LABORATORY
AIR FORCE SYSTEMS COMMAND
UNITED STATES AIR FORCE
HANSCOM AIR FORCE BASE, MASSACHUSETTS 01731

DTIC
ELECTE
APR 15 1986
S D
B


AD-A166 561

DTIC FILE COPY

This technical report has been reviewed and is approved for publication.

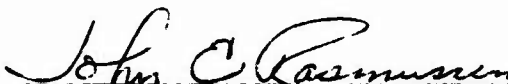


CHARLES C. GALLAGHER
Contract Manager



JOHN E. RASMUSSEN, Chief
Ionospheric Interactions Branch

FOR THE COMMANDER



JOHN E. RASMUSSEN, Acting Director
Ionospheric Physics Division

This report has been reviewed by the ESD Public Affairs Office (PA) and is releasable to the National Technical Information Service (NTIS).

Qualified requestors may obtain additional copies from the Defense Technical Information Center. All others should apply to the National Technical Information Service.

If your address has changed, or if you wish to be removed from the mailing list, or if the addressee is no longer employed by your organization, please notify AFGL/DAA, Hanscom AFB, MA 01731. This will assist us in maintaining a current mailing list.

REPORT DOCUMENTATION PAGE

1a. REPORT SECURITY CLASSIFICATION Unclassified			1b. RESTRICTIVE MARKINGS		
2a. SECURITY CLASSIFICATION AUTHORITY			3. DISTRIBUTION/AVAILABILITY OF REPORT Approved for public release; distribution unlimited		
2b. DECLASSIFICATION/DOWNGRADING SCHEDULE					
4. PERFORMING ORGANIZATION REPORT NUMBER(S) ARI-RR-508			5. MONITORING ORGANIZATION REPORT NUMBER(S) AFGL-TR-86-0010		
6a. NAME OF PERFORMING ORGANIZATION Aerodyne Research, Inc.		6b. OFFICE SYMBOL (If applicable)	7a. NAME OF MONITORING ORGANIZATION Air Force Geophysics Laboratory		
6c. ADDRESS (City, State, and ZIP Code) 45 Manning Road Billerica, MA 01821			7b. ADDRESS (City, State, and ZIP Code) Hanscom AFB Massachusetts 01731		
8a. NAME OF FUNDING/SPONSORING ORGANIZATION		8b. OFFICE SYMBOL (If applicable)	9. PROCUREMENT INSTRUMENT IDENTIFICATION NUMBER F19628-83-C-0010		
8c. ADDRESS (City, State, and ZIP Code)			10. SOURCE OF FUNDING NUMBERS		
			PROGRAM ELEMENT NO. 61102F	PROJECT NO 2310	TASK NO G3
					WORK UNIT ACCESSION NO. AY
11. TITLE (Include Security Classification) A STUDY OF ATMOSPHERIC REACTIONS OF NEUTRAL SODIUM SPECIES AND OTHER METALS OF METEORIC ORIGIN					
12. PERSONAL AUTHOR(S) J.A. Silver and C.E. Kolb					
13a. TYPE OF REPORT FINAL		13b. TIME COVERED FROM 11/10/82 TO 2/9/86		14. DATE OF REPORT (Year, Month, Day) 1986 February 10	
				15. PAGE COUNT 114	
16. SUPPLEMENTARY NOTATION					
17. COSATI CODES			18. SUBJECT TERMS (Continue on reverse if necessary and identify by block number)		
FIELD	GROUP	SUB-GROUP			
			Meteor Metal Reactions, Atmospheric Sodium		
19. ABSTRACT (Continue on reverse if necessary and identify by block number) The reactions of metallic species introduced into the atmosphere by meteor ablation may play a significant role in the chemistry of the lower thermosphere and upper stratosphere. The work described in this report summarizes a series of experimental rate constant measurements for reactions pertinent to these atmospheric regions. Prior to this work, virtually no direct kinetic parameters had been measured for the reactions of alkalis, and in particular sodium, which are believed to occur between 30 and 100 km in altitude. Model predictions of excited sodium emissions, expected concentration levels of the various alkali species, and the potential impact of alkali chemistry on the ozone balance all depended on theoretical estimates of reaction rate constants and product branching ratios. Using a high temperature fast flow reactor and a variety of atomic and molecular species source and detection techniques, we have measured rate constants for over a dozen reactions.					
20. DISTRIBUTION/AVAILABILITY OF ABSTRACT <input type="checkbox"/> UNCLASSIFIED/UNLIMITED <input type="checkbox"/> SAME AS RPT. <input type="checkbox"/> DTIC USERS			21. ABSTRACT SECURITY CLASSIFICATION UNCLASSIFIED		
22a. NAME OF RESPONSIBLE INDIVIDUAL Charles Gallagher			22b. TELEPHONE (Include Area Code)		22c. OFFICE SYMBOL AFGL/LID

19. ABSTRACT (Continued)

The results of these measurements lead to the following conclusions:

- a) Below 85 km, the prime reaction for removal of atomic sodium is the termolecular reaction with O_2 to form NaO_2 , not the reaction with ozone as had been previously believed.
- b) The major alkali species which leaves the mesosphere is most likely NaO_2 or $NaOH$, but not NaO .
- c) In the upper stratosphere, it is possible that alkali reactions have a significant effect on the concentration of ozone. The reactions of NaO , $NaOH$, and NaO_2 with HCl are all very rapid, leading to the formation of $NaCl$, which subsequently photodissociates. The rates of these processes are such that sodium can act as a catalytic agent in the release of free chlorine, which then attacks ozone.
- d) More detailed in situ atmospheric measurements of both atomic and molecular forms of sodium and other meteor metals should be performed.
- e) Investigation of heterogeneous loss processes for gaseous meteor metals are recommended.

Accession For	
NTIS GRA&I	<input checked="" type="checkbox"/>
DTIC TAB	<input type="checkbox"/>
Unannounced	<input type="checkbox"/>
Justification	
By	
Distribution/	
Availability Codes	
Dist	Avail and/or Special
A1	



DTIC
ELECTE
APR 15 1986
S B D

TABLE OF CONTENTS

<u>Section</u>		<u>Page</u>
	EXECUTIVE SUMMARY	iv
1	OBJECTIVE	1-1
	1.1 Introduction	1-1
	1.2 References	1-7
2	SECTION 2 - Temperature Dependent Termolecular Reaction Rate Constants for Potassium and Sodium Superoxide Formation	2-1
3	SECTION 3 - Determination of the Absolute Rate Constant for the Room Temperature Reactions of Atomic Sodium With Ozone and Nitrous Oxide	3-1
4	SECTION 4 - Gas-Phase Reaction Rate of Sodium Hydroxide With Hydrochloric Acid	4-1
5	SECTION 5 - Gas-Phase Reaction of Sodium Superoxide With Hydrochloric Acid	5-1
6	SECTION 6 - Absolute Photodissociation Cross Sections of Gas-Phase Sodium Chloride at Room Temperature	6-1
7	RATE CONSTANT FOR THE REACTION OF NaOH with CO ₂ 7.1 Introduction 7.2 Formation of Gas Phase Sodium Hydroxide 7.3 Detection of NaOH 7.4 Results 7.5 References	7-1 7-1 7-2 7-3 7-5 7-7
8	DISCUSSION AND SUMMARY OF RESULTS 8.1 References	8-1 8-4
9	PAPERS AND PUBLICATIONS 9.1 Publications 9.2 Presentations	9-1 9-1 9-1

EXECUTIVE SUMMARY

The reactions of metallic species introduced into the atmosphere by meteor ablation may play a significant role in the chemistry of the lower thermosphere and upper stratosphere. The work described in this report summarizes a series of experimental rate constant measurements for reactions pertinent to these atmospheric regions.

Prior to this work, virtually no direct kinetic parameters had been measured for the reactions of alkalis, and in particular sodium, which are believed to occur between 30 and 100 km in altitude. Model predictions of excited sodium emissions, expected concentration levels of the various alkali species, and the potential impact of alkali chemistry on the ozone balance all depended on theoretical estimates of reaction rate constants and product branching ratios.

Using a high temperature fast flow reactor and a variety of atomic and molecular species source and detection techniques, we have measured rate constants for over a dozen reactions. The results of these measurements lead to the following conclusions:

- a) Below 85 km, the prime reaction for removal of atomic sodium is the termolecular reaction with O_2 to form NaO_2 , not the reaction with ozone as had been previously believed.
- b) The major alkali species which leaves the mesosphere is most likely NaO_2 or $NaOH$, but not NaO .
- c) In the upper stratosphere, it is possible that alkali reactions have a significant effect on the concentration of ozone. The reactions of NaO , $NaOH$, and NaO_2 with HCl are all very rapid, leading to the formation of $NaCl$, which subsequently photodissociates. The rates of these processes are such that sodium can act as a catalytic agent in the release of free chlorine, which then attacks ozone.
- d) More detailed in situ atmospheric measurements of both atomic and molecular forms of sodium and other meteor metals should be performed.
- e) Investigation of heterogeneous loss processes for gaseous meteor metals are recommended.

1. OBJECTIVE

1.1 Introduction

Metallic elements volatilized during meteor entry into the Earth's upper atmosphere play a significant role in the structure of the D and E regions of the ionosphere,¹⁻² and, at least in the case of sodium, the visible day and nightglow emissions from the mesosphere and lower thermosphere.³⁻⁵ Recently, it was suggested that sodium and other meteor metals may be important in stratospheric chemistry by affecting ozone reduction by the catalytic chlorine cycle.⁶⁻⁸

The influx of meteor metals into the upper atmosphere has been estimated⁹ to be 3.5×10^6 kg yr⁻¹, with a sodium abundance of 2% leading to a calculated sodium flux of 1.2×10^4 atoms cm⁻² s⁻¹. Other estimates of sodium flux run as high as 2×10^4 cm⁻² s⁻¹.¹⁰ The flux of other metallic species such as Mg, Ca, Al, Si and Fe will be as much as 10 times higher and speculative concerns about their influence on upper atmospheric homogeneous and heterogeneous chemistry have been published.^{1-2, 7-8, 10}

Unfortunately, all attempts to model the role of volatilized meteor metals (particularly sodium) in the mesosphere and stratosphere^{3-4, 7, 9-15} have suffered from an almost total lack of measured rate constants. All such models start with the oxidation of sodium or other metallic species in reaction with atmospheric O, O₂, or O₃. Through 1982, the only measured chemical rate constants available for any meteor metal oxidation reactions were the three body recombination reactions of alkali atoms (Na, K) with O₂.¹⁶⁻¹⁸



Flame studies by Hynes et al¹⁹ and direct measurements at 724 and 844 K by Husain and Plane¹⁸ showed that this reaction rate is 1000 times faster than previously believed.¹⁶⁻¹⁷ Recent direct flow tube measurements²⁰ in our laboratory have extended these results from 700 K down to 300 K, and show that the reaction rates vary inversely with temperature, and confirm the larger values for the rate constants.

As an indication of the effect that the availability of chemical rate data has on aeronomic modeling studies, consider the theoretical calculation of several important sodium oxidation reaction rate constants:



and



performed at Aerodyne Research, Inc.²¹ The adoption of realistic values for just these three rate constants has led to a major revision in the understanding of the structure of the mesospheric sodium layer,²² the magnitude of the sodium D line nightglow,^{5,21} and the understanding of long-lived luminous meteor trails.^{8,21}

From the recent modeling work^{7-8,10,13,21-22} and comparison of these models with atmospheric measurements,^{12,14-15} neutral sodium is believed to be transformed via a series of chemical reactions involving NaO, NaO₂, and NaOH. A survey of the relevant literature^{6-8,10,13} provides a fairly complete list of possible neutral sodium reactions of importance. These are listed in Table 1, in four groups, which to some extent, reflect the sequence of events from the introduction of neutral sodium at 110 km altitude to its disappearance near 70 km. Also listed are reaction enthalpies, with associated uncertainties.

Table 1 - Atmospheric Reactions of Neutral Sodium Species

I. Sodium Atom Reactions		$-\Delta H^\circ_r (\text{kJ mol}^{-1})$
$\text{Na} + \text{O}_2 \xrightarrow{\text{M}} \text{NaO}_2$		163 \pm 21
$\text{Na} + \text{O}_3 \rightarrow \text{NaO} + \text{O}_2$		167 \pm 42
$\text{Na} + \text{HO}_2 \rightarrow \text{NaOH} + \text{O}$		77 \pm 15
$\text{NaH} + \text{O}_2$		4 \pm 21
$\text{NaO} + \text{OH}$		
$\text{Na} + \text{O} \xrightarrow{\text{M}} \text{NaO}$		273 \pm 42
II. Sodium Oxide Reactions		
$\text{NaO} + \text{O}_3 \rightarrow \text{NaO}_2 + \text{O}_2$		282 \pm 47
$\text{NaO} + \text{O}_3 \rightarrow \text{Na} + 2\text{O}_2$		119 \pm 42
$\text{NaO} + \text{H}_2\text{O} \rightarrow \text{NaOH} + \text{OH}$		1 \pm 44
$\text{NaO} + \text{H}_2 \rightarrow \text{NaOH} + \text{H}$		64 \pm 44
$\text{NaO} + \text{CH}_4 \rightarrow \text{NaOH} + \text{CH}_3$		61 \pm 44
$\text{NaO} + \text{HCl} \rightarrow \text{NaCl} + \text{OH}$		134 \pm 42
$\text{NaO} + \text{O} \rightarrow \text{Na} + \text{O}_2$		225 \pm 42
$\text{NaO} + \text{HO}_2 \rightarrow \text{NaOH} + \text{O}_2$		303 \pm 44
$\text{NaO} + \text{H} \rightarrow \text{Na} + \text{OH}$		155 \pm 42
$\text{NaO} + \text{ClO} \rightarrow \text{NaOCl} + \text{O}$		
$\text{NaO}_2 + \text{HCl} \rightarrow \text{NaCl} + \text{HO}_2$		13 \pm 23
$\text{NaO}_2 + \text{Cl} \rightarrow \text{NaCl} + \text{O}_2$		247 \pm 21
$\text{NaO}_2 + \text{ClO} \rightarrow \text{NaCl} + \text{O}_3$		84 \pm 21
$\text{NaO}_2 + \text{H}_2 \rightarrow \text{NaOH} + \text{OH}$		103 \pm 24
$\text{NaO}_2 + \text{H}_2 \rightarrow \text{NaO} + \text{H}_2\text{O}$		103 \pm 47
$\text{NaO}_2 + \text{O} \rightarrow \text{NaO} + \text{O}_2$		110 \pm 47
$\text{NaO}_2 + \text{OH} \rightarrow \text{NaOH} + \text{O}_2$		181 \pm 24
$\text{NaO}_2 + \text{H} \rightarrow \text{NaOH} + \text{O}$		111 \pm 24
$\text{NaO}_2 + \text{H} \rightarrow \text{Na} + \text{HO}_2$		34 \pm 23
III. Sodium Hydroxide Reactions		
$\text{NaOH} + \text{HCl} \rightarrow \text{NaCl} + \text{H}_2\text{O}$		133 \pm 13
$\text{NaOH} + \text{Cl} \rightarrow \text{NaCl} + \text{OH}$		67 \pm 13
$\text{NaOH} + \text{ClO} \rightarrow \text{NaCl} + \text{HO}_2$		63 \pm 15
$\text{NaOH} + \text{H} \rightarrow \text{Na} + \text{H}_2\text{O}$		154 \pm 13
$\text{NaOH} + \text{CO}_2 \xrightarrow{\text{M}} \text{NaHCO}_3$		
$\text{NaOH} + \text{HNO}_3 \rightarrow \text{NaNO}_3 + \text{H}_2\text{O}$		
$\text{NaHCO}_3 + \text{HCl} \rightarrow \text{NaCl} + \text{Products}$		
IV. Photolysis Reactions		
$\text{NaOH} + h\nu \rightarrow \text{Na} + \text{OH}$		
$\text{NaO} + h\nu \rightarrow \text{Na} + \text{O}$		
$\text{NaO}_2 + h\nu \rightarrow \text{Na} + \text{O}_2$		
$\text{NaCl} + h\nu \rightarrow \text{Na} + \text{Cl}$		

The main removal mechanisms of sodium are by reaction with O_2 or O_3 , the latter reaction used by Chapman²³ to describe the Na nightglow. The recent rate measurements of reaction (1) however, lead us to believe that below 80 km most of the Na is converted to NaO_2 .

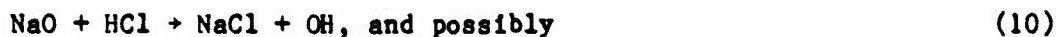
The fate of NaO_2 , however, is uncertain. Recent measurements by Figger et al²⁴ and flame studies by Hynes et al¹⁹ imply that the Na- O_2 bond strength is much weaker than previously believed, with a value of ca. 163 kJ mol⁻¹. As a result, NaO_2 will react exothermically with atomic oxygen to produce NaO. Sodium oxide can react either with ozone to reform NaO_2 or Na, or react with water to produce NaOH.



Unfortunately, none of these rates had been measured, leading the various modelers to speculate on the importance of each.^{10,12-15} As shown by Sze et al,¹³ the predominant alkali species below 70 km may be NaO, NaO_2 , and/or NaOH, depending on ones choice for k_5 , k_6 , and k_7 .

In a recent paper by Murad et al,⁸ it was proposed that the reactions of metal hydroxides and superoxides with chlorine compounds between 40 and 70 km may have an impact on the depletion of stratospheric ozone. In the case of sodium, the exothermic bimolecular reactions





might be expected to proceed rapidly and act as a sink for Cl, given that NaCl can readily polymerize and condense via heterogeneous nucleation.⁸ Analogous reactions also can occur with Cl and ClO. The inclusion of sodium bicarbonate (in reaction 11) comes about due to the possible occurrence of the reaction



Murad et al calculated that if the reaction rate of these sodium species with HCl were $\sim 10^{-11} \text{ cm}^3 \text{ molecule}^{-1} \text{ s}^{-1}$, they might be comparable to the major Cl regeneration mechanism,



While previously published studies have viewed NaCl as a potential sink for stratospheric chlorine,⁷⁻⁸ more recent analyses by F.S. Rowland²⁵ indicate that photolysis of NaCl may in fact release free Cl. Given the potentially large J values (atmospheric photolysis rate) for this process,²⁵⁻²⁶ reactions (8)-(11) could effectively supplement, rather than remove, reaction (13) as a release mechanism for Cl from the inactive HCl stratospheric reservoir and thereby determine the extent to which ozone might be depleted by chlorine compounds in the stratosphere. However, to fully understand the role of alkali species in the stratosphere one must also consider the effects of NaO₂ and NaOH photodissociation on those processes,^{13,27} as well as homonuclear and heteronuclear sinks for meteoric metal species.

The objective of this program was to provide direct experimental measurements of key rate constants. Obtaining accurate reaction rates for the sodium atmospheric system will enable more accurate modeling of the sodium

emission and density profiles. Once this is completed, these results can be extended toward the larger goal of understanding the chemistry of the more abundant meteor metals.

Over the three years of work on this program, we have measured rate constants for over a dozen alkali reactions and believe that these results will lead to a much improved understanding of the role of meteor metals in atmospheric chemical processes. The remainder of this report details and summarizes our findings. Section 2 is a reprint of our studies of the termolecular recombination of sodium and potassium with molecular oxygen. Section 3 is a preprint of a paper detailing the reaction of Na with O_3 and N_2O , and NaO with O_3 . A reprint discussing our measurements of the reaction of NaO and NaOH with HCl comprises Section 4 and a preprint of the analogous reaction of NaO_2 with HCl forms Section 5. Section 6 is a preprint of a paper describing our measurements of the absolute photodissociation cross sections for NaCl. Section 7 describes our work on the measurement of the rate constant for the reaction of $NaOH + CO_2 + M$. A summary of the results obtained from this program is contained in Section 8 and a listing of papers and presentations made during the course of this contract is given in Section 9.

1.2 References

1. Murad, E., J. Geophys. Res. 83, 5525 (1978).
2. Brown, T.L., Chem. Rev. 73, 645 (1973).
3. Blamont, J.E. and Donahue, T.M., J. Geophys. Res. 69, 4093 (1964).
4. Hunten, D.M., Space Sci. Rev. 6, 493 (1967).
5. a) Kirchhoff, V.W.J.H., Clemesha, B.R., and Simonich, D.M., J. Geophys. Res. 84, 1323 (1979);
b) Bates, D.R. and Ojha, P.C., Nature 286, 790 (1980).
6. Ferguson, E.E., Geophys. Res. Lett. 5, 1035 (1978).
7. Murad, E. and Swider, W., Geophys. Res. Lett. 6, 929 (1979).
8. Murad, E., Swider, W., and Benson, S.W., Nature 289, 273 (1981).
9. Richter, E.S. and Sechrist, C.F., Jr., J. Atmos. and Terres. Phys. 41, 579 (1979), Geophys. Res. Lett. 6, 183 (1979).
10. Liu, S.C. and Reid, G.C., Geophys. Res. Lett. 6, 283 (1979).
11. a) Baggaley, W.J., Nature 257, 567 (1975);
b) Baggaley, W.J., Nature 267, 376 (1977);
c) Hapgood, M.A., Nature 286, 582 (1980).
12. Kirchhoff, V.W.J.H., Clemesha, B.R., and Simonich, D.M., J. Geophys. Res. 86, 6892 (1981).
13. Sze, N.D., Ko, M.K.W., Swider, W., and Murad, E., Geophys. Res. Lett. 9, 1187 (1982).
14. Kirchhoff, V.W.J.H., Geophys. Res. Lett. 10, 721 (1983).
15. Thomas, L., Isherwood, M.C., and Bowman, M.R., J. Atm. Terrestrial Phys. 45, 587 (1983).
16. Carabetta, R. and Kaskan, W.E., J. Phys. Chem. 72, 2483 (1968).
17. McEwen, M.J. and Phillips, L.F., Trans. Faraday Soc. 62, 717 (1966).
18. Husain, D. and Plane, J.M.C., J. Chem. Soc. Far. Trans. 2, 78, 163 (1982).

19. Hynes, A.J., Steinberg, M., and Schofield, K., J. Chem. Phys. 80, 2585 (1984).
20. Silver, J.A., Stanton, A.C., Zahmiser, M.S., and Kolb, C.E., 20th Symposium (International) on Combustion, 605 (1984).
21. Kolb, C.E. and Elgin, J.B., Nature 263, 488 (1976).
22. Simonich, D.M., Clemesha, B.R., and Kirchoff, V.W.J.H., J. Geophys. Res. 84, 1543 (1979).
23. Chapman, S., Astrophys. J. 90, 309 (1939).
24. Figger, H., Schrepp, W. and Zhu, Xu-hui, J. Chem. Phys. 79, 1 (1983).
25. Rowland, F.S. and Rogers, P.J., Proc. Natl. Acad. Sci. USA 79 (1982).
26. Davidovits, P. and Brodhead, D.C., J. Chem. Phys. 46, 2968 (1967).
27. Rowland, F.S. and Makide, Y., Geophys. Res. Lett. 9, 473 (1982).

SECTION 2

TEMPERATURE DEPENDENT TERMOLICULAR REACTION RATE CONSTANTS FOR POTASSIUM AND SODIUM SUPEROXIDE FORMATION

TEMPERATURE DEPENDENT TERMOLLECULAR REACTION RATE CONSTANTS FOR POTASSIUM AND SODIUM SUPEROXIDE FORMATION

J. A. SILVER, M. S. ZAHNISER, A. C. STANTON, AND C. E. KOLB

Center for Chemical and Environmental Physics
Aerodyne Research, Inc.
45 Manning Road
Billerica, MA 01821

Rate constants for the recombination reactions of alkali atoms with molecular oxygen, $K + O_2 + M \rightarrow KO_2 + M$ and $Na + O_2 + M \rightarrow NaO_2 + M$, have been measured as a function of temperature from 300 to 700 K using a fast flow reactor. Laser induced fluorescence is used to monitor the disappearance of Na or K as a function of O_2 and M. The reactions are studied in their low pressure third order limit from 1 to 8 torr total pressure with N_2 , He, and Ar as third bodies. The rate constants are found to have the expected negative temperature dependence. The values for k ($Na + O_2 + M$) are $(1.9 \pm 0.4) \times 10^{-30} (T/300)^{-1.1 \pm 0.5}$ with $M = N_2$, $(1.4 \pm 0.3) \times 10^{-30} (T/300)^{-0.9 \pm 0.5}$ with $M = He$, and $(1.2 \pm 0.3) \times 10^{-30}$ at $T = 324$ K with $M = Ar$, all in units of $cm^6 \text{ molecules}^{-2} \text{ s}^{-1}$. The values for the corresponding reactions with potassium are larger than those for sodium with k ($K + O_2 + M$) = $(5.4 \pm 0.2) \times 10^{-30} (T/300)^{-0.9 \pm 0.20}$ with $M = N_2$, $(2.0 \pm 0.5) \times 10^{-30} (T/300)^{-0.9 \pm 0.5}$ with $M = He$, and $(3.5 \pm 1.0) \times 10^{-30}$ at $T = 300$ K with $M = Ar$. The results are compared with other recent measurements from flame and flash photolysis studies and with theoretical expectations based on an energy transfer RRKM mechanism for the NaO_2^* activated complex.

Introduction

The chemistry of alkali metals in flames commands our attention for both scholarly and practical reasons. From a scientific standpoint reactions of alkali atoms, with their single valence electron, form a natural test bed to extend our theoretical understanding honed on reactions of atomic hydrogen. Furthermore, the low ionization potentials of alkali atoms open the possibility of electron transfer reaction mechanisms and allow determination of the role of ionic potential surfaces in reaction dynamics. Finally, incredibly sensitive methods of detecting alkali atoms, including hot wire surface ionization, laser induced resonance fluorescence, and laser induced resonance ionization now allow the design of elegant experimental studies for environments ranging from molecular beams to high pressure flames.

From a practical standpoint, gas phase alkali chemistry has long been recognized to be important in flame suppression,¹⁻⁵ and is also involved in the conversion of alkali-containing minerals in coal to alkali sulfates.⁶⁻⁸ These sulfates are a major cause of fouling and corrosion of boiler-tube surfaces, heat exchangers, and turbine blades. Alkali atoms introduced into the atmosphere by meteor ablation also play a role in mesospheric chemistry,⁹⁻¹² and it has

been suggested¹³⁻¹⁴ that alkali molecules may affect stratospheric ozone reduction through the catalytic chlorine cycle.

However, for all the intrinsic theoretical and experimental interest in alkali reactions, our understanding of the gas phase oxidation chemistry of alkali atoms has only recently progressed, first back to, and then beyond the level gained in the 1930's in pioneering sodium diffusion flame studies by Halber and Sachse¹⁵ and Bawn and Evans.¹⁶ While these low pressure studies of the reaction of Na with O_2 showed it proceeded with a termolecular rate constant in excess of $10^{-30} \text{ cm}^6 \text{ s}^{-1}$, subsequent work (primarily in the mid 1960's) using flame photometric methods by Kaskan¹⁷⁻¹⁹ and McEwan and Phillips¹⁹⁻²⁰ indicated much lower MO_2 formation rates ($M = Na, K$)¹⁷⁻¹⁹ as well as relatively high dissociation energies for the $M-O_2$ bond ($M = Na, Li$).¹⁹⁻²⁰

Analyses of thermochemical cycles by Herm and Herschbach²¹ and Alexander²² clearly indicated that the strengths of $M-O_2$ bonds deduced from flame photometric data by McEwan and Phillips were greatly overestimated. This was recently confirmed by Figger and co-workers who analyzed observations of chemiluminescence between crossed molecular beams of alkali dimers and molecular oxygen to yield alkali superoxide bond energies.²³

Reinterpretation of the earlier flame experiments²⁴ as well as newly performed flame studies²⁵ are also consistent with lower alkali superoxide bond energies.

The low sodium and potassium termolecular reaction rates deduced from the flame photometry studies¹⁷⁻¹⁹ are also incorrect. Recently published flash photolysis studies over limited temperature ranges for Li (393 and 463 K),²⁶ Cs (321 K),²⁷ Na (724 and 844 K),²⁸ and K (753 and 853 K),²⁹ as well as flame photometry studies for Na,²⁵ all clearly show fast termolecular rates for alkali superoxide formation.

In this paper we report termolecular rate constants for superoxide formation from sodium and potassium over a much wider temperature range than previously available, yielding the first clear, direct measurement of the temperature dependence of these processes. Third body dependencies are illustrated by separate measurements for N₂, He and Ar. These measurements were made in a high temperature, fast flow reactor³⁰ utilizing laser induced resonance fluorescence detection of atomic alkali species. A discussion of these results in terms of their importance in testing termolecular association reaction theory is also presented.

Experimental

The high temperature fast flow reactor used in these experiments has been described in detail previously³⁰ and is shown in Fig. 1 in the configuration used in this study. Briefly, a 7.26 cm diameter, 120 cm long alumina tube is heated with Kanthal resistance heaters. The helium, argon or nitrogen carrier gas enters the flow tube through two mullite multichannel arrays which both preheat and laminarize the flow upstream of the reaction zone. A sufficient distance (20 cm) is allowed downstream of these arrays for the carrier gas to develop a parabolic flow profile before reaching the reaction

zone. Carrier gas flow rates are measured with calibrated rotameters. Total pressures are measured with a capacitance manometer at the downstream end of the reaction zone. Gas temperatures are obtained with a chromel-alumel thermocouple which is movable throughout the reaction zone. The lowest reaction temperatures are slightly above room temperature due to the heating of the carrier gas as it passes over the resistively heated alkali oven. The maximum axial temperature gradient due to this effect over the region in which decay measurements are taken is 10 to 20 degrees depending on flow velocity, pressure, and identity of carrier gas. The temperature at the mid point of the reaction zone as measured by the movable thermocouple is used in the data analysis. Axial profiles are more uniform, ± 2 to 5 degrees, at elevated temperatures (>400 K) where heating is dominated by the flow tube walls and the mullite arrays. Although the apparatus is capable of temperatures up to 1500 K, experimental considerations as described below limited the upper temperature to 700 K for these studies.

Alkali atoms are generated by heating the pure metal in a 25 mm diameter cylindrical silver plated monel oven to a temperature sufficient to obtain a vapor pressure of 10^{-6} to 10^{-4} torr within the oven. The oven is mounted on the end of a movable 13 mm od alumina tube concentric to the main flow tube. The vapor is entrained in a flow of carrier gas and introduced into the flow tube in one of two configurations. For the kinetic measurements with O₂, the oven is placed at a fixed position upstream of the multichannel arrays and the alkali vapor is introduced into the main flow through a 10 cm length of 19 mm diameter silver tubing which passes through the center of the arrays. In the second configuration, the oven is placed downstream of the arrays and is movable throughout the reaction zone to determine the loss of alkali atoms on the reactor walls. The oven temperature is controlled with resistive heating elements independent of the flow tube heaters. Initial alkali atom concentrations in the reaction zone are maintained at less than 10^{10} cm⁻³ by adjusting the oven temperature and the carrier gas flow rate through the oven.

The alkali atoms are detected by laser induced fluorescence at the downstream end of the flow tube. A Molelectron DL14 nitrogen pumped dye laser is used to excite the $4s\ ^2S_{1/2} \rightarrow 5p\ ^2P_{3/2}$ transition at 404.4 nm for potassium or the $3s\ ^2S_{1/2} \rightarrow 3p\ ^2P_{3/2}$ transition at 589.0 nm for sodium. Fluorescence is collected using a gated phototube and a computer controlled data acquisition system.³⁰ The signals are averaged over 100 laser pulses after subtracting for nonfluorescent background contributions and normalizing for pulse to pulse fluctuations in laser intensity. Although no direct calibration of the fluorescence signal was attempted, estimates of

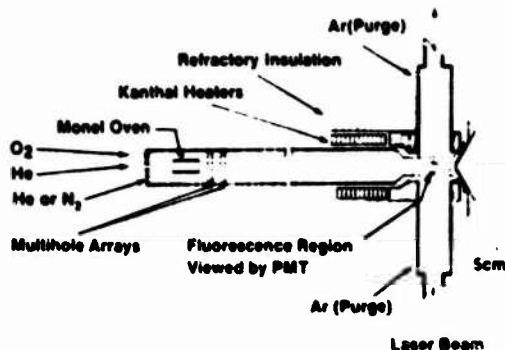


FIG. 1. Schematic view of the high temperature flow reactor.

sensitivity from known phototube and integrator response, measured laser power, and atomic transition probabilities indicate a detection limit for Na of 10^4 cm^{-3} and for K of 10^6 cm^{-3} using these transitions.

Molecular oxygen is added through a movable loop injector at distances from 10 to 60 cm upstream of the detection region. O_2 flow rates are measured with a calibrated thermal conductivity mass flow meter. The kinetic measurements are conducted under pseudo-first order conditions with $2 \times 10^{14} < [\text{O}_2] < 7 \times 10^{15} \text{ cm}^{-3}$, in large excess compared to the alkali metal atom concentration, yet always $< 5\%$ of the total gas concentration. First order rate constants are determined for a fixed O_2 concentration by recording the change in alkali atom concentration as a function of O_2 injector distance.

Corrections for both axial and radial diffusion and wall removal are made using the procedure outlined by Brown.³¹ This method is based on a numerical solution of the continuity equation including diffusion, first order chemical reaction and wall removal in a cylindrical tube with fully developed laminar flow. A multiplicative correction factor, obtained for each set of experimental conditions, is used to relate the observed decay to the true first order rate constant. This correction factor is dependent on the wall removal rate constant, k_w , and the binary diffusion coefficient for the alkali atom in the carrier gas. Values for k_w are determined in separate experiments at each pressure and temperature by observing the change in atom concentration at the detection point while varying the source oven position. The loss of atoms to the wall was found to be diffusion limited for all the conditions used in this study, implying a surface accommodation coefficient $\gamma > 0.1$. The observed wall loss rate under these conditions may therefore be used to determine the diffusion coefficient³² which is then used to determine the correction factor for the reactive flow analysis. The correction factors obtained by this method were in the range $k_{\text{true}}/k_{\text{obs}}$ from 1.52 to 1.86, with most lying between 1.60 and 1.65. Under the flow conditions of these experiments, the ratio of reaction to diffusion times is not unlike those encountered in ion-molecule reactions,³¹ which also exhibit correction factors on the order of 1.6.

Results and Discussion

Reaction rate constants of atomic sodium with O_2 were measured over the temperature range of 320–696 K for nitrogen as the third body collision partner, and over the range of 309–473 K in helium; for potassium, the corresponding temperature ranges were 308–720 K and 296–520 K, respectively. Room temperature measurements were also made in argon for both Na and K. Pressures at each temperature range from 1 to between 5 and 8 torr. Above

700 K, no reliable decays could be measured, because alkali atoms which had accumulated on the walls at lower temperatures began to effuse into the flow, interfering with the rate measurements.

Using the data for $\text{Na} + \text{O}_2 + (\text{He})$ as an example, we see in Fig. 2 that the first-order (logarithmic) decays of signal with reaction time are linear for over a factor of 100. Plots of a series of first-order rate constants (corrected for wall and diffusional effects) versus $[\text{O}_2]$ are illustrated in Fig. 3. Second-order rate constants derived from these are then plotted vs. total number density and the third-order rate constants are determined from the slopes of these plots. In most cases, these lines intersect the origin to within the statistical uncertainties of the fit ($\pm 10 \text{ s}^{-1}$). For $\text{Na} + \text{O}_2 + (\text{N}_2)$, a small positive intercept is observed at all temperatures. The cause for the intercept is unclear. An explanation sometimes given for such behavior is that the wall acts as a stabilizing third body and adds a pressure independent component to k^{II} . However, this explanation would appear unlikely in these experiments given the near unit efficiency for wall removal of all alkali species. An alternative explanation is that insufficient diffusional mixing of the injected O_2 could lead to underestimation of k^{II} at higher pressures, resulting in an apparent intercept

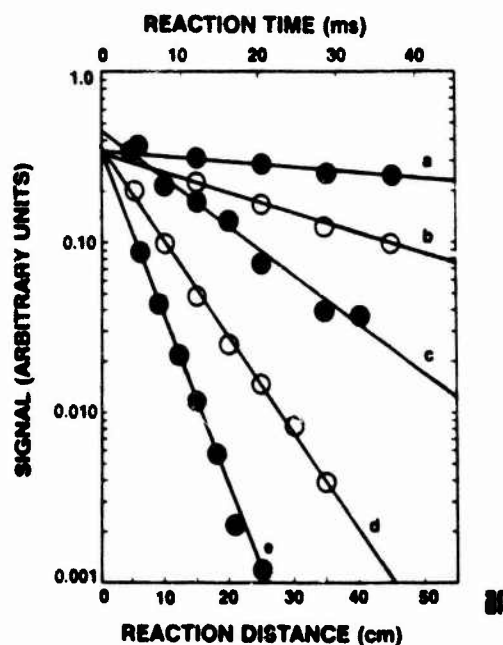


FIG. 2. Pseudo-first order decay of Na fluorescence signal vs. reaction distance for $M = \text{He}$ at 309 K and 5.05 torr. $[\text{O}_2] = 1.09$ (a), 3.36 (b), 7.29 (c), 14.3 (d), 26.6 (e), units of 10^{14} cm^{-3} . The estimated relative standard deviations for these points range from 1% to 4%.

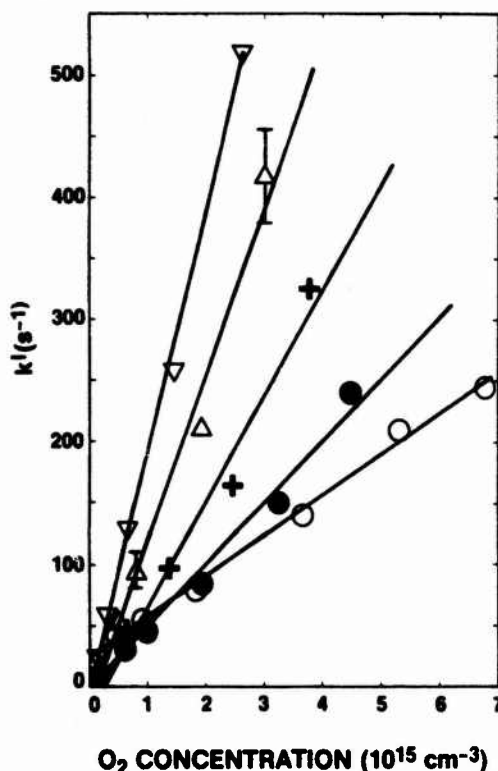


FIG. 3. Plots of first-order Na decay rates vs. $[O_2]$ for $M = He$ and $T = 309\text{--}335\text{ K}$. Total pressure (torr) = 1.05 (\circ), 1.51 (\bullet), 2.52 (+), 3.04 (Δ), 5.05 (∇). Each point has been corrected for the effects of diffusion and wall loss. Error bars correspond to $\pm 2\sigma$.

in the k^{II} vs. pressure plots. However, calculations of mixing length indicate that this effect should not be significant even at the highest pressure (5 torr) in these studies.

The three-body association rate constants as a function of temperature for various third body collision partners are shown for sodium in Fig. 4 and for potassium in Fig. 5. The data can be described by an expression of the form $k^{\text{III}}(T) = AT^{-n}$. The results of nonlinear least-square fits to this function are found in Table 1. For sodium in helium and nitrogen, and for potassium in helium, a simple T^{-1} representation could also be used. However, the results for potassium in nitrogen show a somewhat weaker temperature dependence, best represented by $T^{-0.56 \pm 0.20}$, although this difference is not significant within the statistical uncertainties of the data.

The expressed total experimental uncertainties, including allowance for systematic errors, can be estimated as the square root of the sum of the squared individual uncertainties due to a) flow velocity, temperature, pressure, and concentration

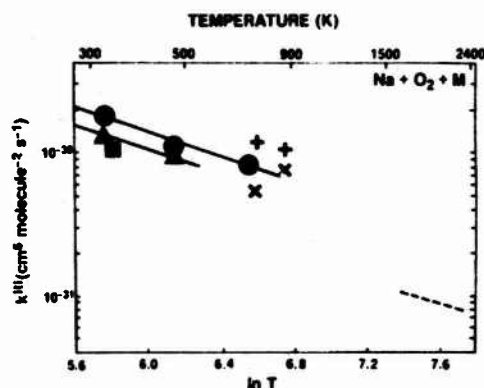


FIG. 4. Plot of $\ln k(T)$ vs. $\ln T$ for the reaction $Na + O_2 + M$, with $M = N_2$ (circles), He (triangles), and Ar (square) for this work. The solid lines are least-square fits to these data. The + and \times symbols represent data for $M = N_2$ and He , respectively from reference 25, and the dashed line ($M = \text{flame gases}$) is from reference 25.

calibration factors, 5%; b) the precision in determining the coefficient A in the expression for $k^{\text{III}}(T)$, 17%; and c) the uncertainty in the correction of observed first-order decays for wall removal and diffusional effects, 10%.

Table 1 also contains other determinations of k . Husain and Plane^{28,29} used a flash photolysis system to generate alkali atoms from KI and NaI and followed the decay of K and Na by atomic resonance absorption. They observed no temperature dependence over their limited temperature range (724 K and 844 K) for the $Na + O_2 + M$ reaction.

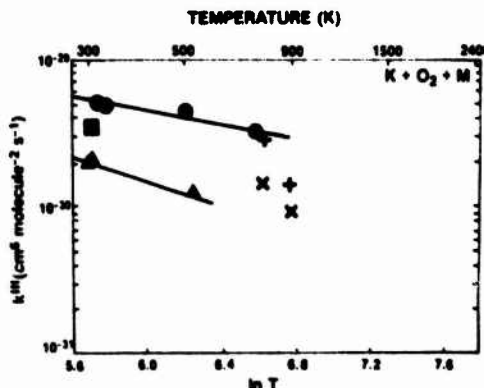


FIG. 5. Plot of $\ln k(T)$ vs. $\ln T$ for the reaction $K + O_2 + M$, with $M = N_2$ (circles), He (triangles), and Ar (square). The solid lines are least-square fits to these data. The + and \times symbols represent data for $M = N_2$ and He , respectively from reference 29.

TABLE I
Comparison of measured rate constants for $\text{Na} + \text{O}_2 + \text{M} \rightarrow \text{NaO}_2 + \text{M}$
and $\text{K} + \text{O}_2 + \text{M} \rightarrow \text{KO}_2 + \text{M}$

Reference	Alkali	Method	M	P (torr)	T(K)	k ($\text{cm}^6 \text{s}^{-1}$)
This work	Na	Fast Flow Reactor	N_2	0.8–8.0	320–700	$(1.9 \pm 0.4) \times 10^{-30} (T/300)^{-1.1 \pm 0.5}$
		Laser Induced Fluorescence	He	1.0–8.1	310–470	$(1.4 \pm 0.3) \times 10^{-30} (T/300)^{-0.9 \pm 0.5}$
			Ar	1.0–3.0	324	$(1.2 \pm 0.3) \times 10^{-30}$
Husain and Plane ²⁵	Na	Flash Photolysis Resonance Absorption	N_2	25–150	724	1.1×10^{-30}
					844	1.0×10^{-30}
			He	30–120	724	0.53×10^{-30}
					844	0.67×10^{-30}
Hynes et al. ²⁵	Na	Flame Studies with Laser Induced Fluorescence	$\text{H}_2\text{O}/\text{O}_2/\text{N}_2$ Mixtures	760	1650–2400	$2 \times 10^{-26} \text{T}^{-1}$
Bawn and Evans ¹⁶	Na	Diffusion Flame	N_2	4–25	533	4.6×10^{-30}
This work	K	Fast Flow Reactor	N_2	1.0–6.0	302–720	$(5.4 \pm 0.2) \times 10^{-30} (T/300)^{-0.96 \pm 0.20}$
		Laser Induced Fluorescence	He	1.0–6.0	296–520	$(2.0 \pm 0.5) \times 10^{-30} (T/300)^{-0.9 \pm 0.5}$
			Ar	1.6	300	$(3.5 \pm 1.0) \times 10^{-30}$
Husain and Plane ²⁹	K	Flash Photolysis Resonance Absorption	N_2	40–160	753	2.9×10^{-30}
					873	1.4×10^{-30}
			He	40–160	753	1.5×10^{-30}
					873	0.96×10^{-30}

A substantially larger variation with temperature was obtained for their $\text{K} + \text{O}_2 + \text{M}$ study although they arbitrarily fit their data to a T^{-1} dependence. The agreement between their values and the slightly extrapolated temperature dependent rate constants for both reactions from this work is satisfactory, especially considering the very different methods employed. This comparison is shown in Figs. 4 and 5.

Hynes et al.²⁵ have studied the $\text{Na} + \text{O}_2 + \text{M}$ reaction in experiments using laser induced fluorescence to measure Na and OH profiles under fuel lean conditions in $\text{H}_2/\text{O}_2/\text{N}_2$ flames. A detailed kinetic model assuming reasonable values for rate constants for the reactions interconnecting the species Na, NaO_2 , NaO and NaOH is used to determine the best fit to the observations. Their optimum value of $k[\text{Na} + \text{O}_2 + \text{M}]$, assuming a T^{-1} temperature dependence, is shown in Fig. 4, and is lower by about a factor of 4 compared to the extrapolated fit from this work. Part of this difference may be explained by the different identities of M (N_2 , O_2 , H_2O mixtures) in their flame studies. Hynes et al.²⁵ also explain the discrepancy between their result and the earlier flame studies,^{17–19} which obtained a lower value for $k[\text{Na} + \text{O}_2 + \text{M}]$ by

nearly three orders of magnitude. The earlier works had incorrectly attributed the global disappearance of Na to reaction with O_2 , while in fact the Na concentration follows that of atomic hydrogen, whose decay is controlled by reaction with O_2 to form HO_2 . A similar explanation has been proposed by Jensen.²⁴

The much earlier diffusion flame studies^{15, 16} correctly identified the $\text{Na} + \text{O}_2 + \text{M}$ reaction to be fast for a three body process. The later and more extensive study by Bawn and Evans¹⁶ obtained a value at 533 K which is higher by a factor of 3 than this study. They also observed a fall-off behavior for their second order rate constant with pressure above about 10 torr and present their results in terms of an energy transfer mechanism using a Lindemann-type expression to interpret their data. This fall-off behavior was not observed by Husain and Plane²⁵ who show linear plots of k'' versus pressure from 25 to 150 torr. Their effective bimolecular rate at 150 torr and 724 K for the $\text{Na} + \text{O}_2 + (\text{N}_2)$ reaction of $2.2 \times 10^{-12} \text{cm}^3 \text{s}^{-1}$ is nearly equal to the high pressure limit inferred by Bawn and Evans of $3 \times 10^{-12} \text{cm}^3 \text{s}^{-1}$. It thus appears that the pressure dependence observed by Bawn and Evans

may have been an artifact of their experimental diffusion flame technique. No curvature was observed in our lower pressure $P \leq 8$ torr conditions of this study and under these conditions, the recombination reaction appears to be in its low pressure, third order, limit.

In this limit, the recombination rate constant can best be calculated using unimolecular rate theory,³⁴ in which second-order rate constants for unimolecular decomposition are related through the equilibrium constant to the third order (low pressure) association rate constants. The unimolecular rate constants are obtained using simplified equations of Troe based on RRKM theory.³⁵⁻³⁶ The recombination rate constant can be expressed as the product of a strong collision rate constant $k_{rec,0}^*$ and a weak collision deactivation efficiency term β_c .

$$k_{rec} = k_{rec,0}^* \beta_c \quad (1)$$

In effect, β_c is a term expressing the efficiency by which $(NaO_2)^*$ is stabilized upon collision. In the absence of detailed state-to-state energy transfer rates, β_c is an adjustable parameter which depends on the average change in internal energy of the transition state complex per collision, $\langle \Delta E \rangle$, so that

$$\frac{\beta_c}{1 - \beta_c^{1/2}} = \frac{\langle \Delta E \rangle}{F_E RT} \quad (2)$$

F_E is a correction term for the energy dependence of the density of states in the transition complex. Using a value of 163 kJ mole^{-1} for the $Na-O_2$ bond energy,²⁵ Patrick and Golden³⁷ have calculated k_{rec}^* for $Na + O_2 + (He)$ at 300 and 700 K. The computations result in $k_{rec,0}^*$ (300 K) = $7.5 \times 10^{-30} \text{ cm}^6 \text{ s}^{-1}$ for $M = He$. Thus, a value of $\beta_c = 0.18$ is required to reproduce the experimental result. The average energy transferred per collision is 0.8 kJ mole^{-1} . At 700 K, $k_{rec,0}^* = 4.2 \times 10^{-30} \text{ cm}^6 \text{ s}^{-1}$, suggesting a value of $\beta_c = 0.09$ if $\langle \Delta E \rangle$ is assumed to be independent of temperature. Extrapolation of the experimental value for helium to 700 K results in an observed $\beta_c = 0.14$, in good agreement, considering the simplified assumptions of this approach.

This unimolecular approach has been shown to be fairly reliable in calculating termolecular association rate constants for a variety of species.¹¹⁻¹⁶ The values of β_c for $M = N_2$ and Ar tend to lie in the range of 0.1-0.5. The calculations for $Na + O_2$ in helium agree quite well with these numbers, given that one might expect helium to be somewhat less efficient than N_2 in quenching the excited intermediate. For the similar reaction $H + O_2 + (N_2)$, the calculations also perform well, giving $\beta_c = 0.08$, even though the rate constant for this reaction, $5.9 \times 10^{-12} \text{ cm}^6 \text{ s}^{-1}$ at 300 K,¹⁶ is approx-

imately 30 times slower than the corresponding sodium reaction.

In extrapolating our measured rate constants to higher pressures, it is important to understand the fall-off behavior as the reaction mechanism goes from its low pressure third order limit to its high pressure second order limit. A method for calculating the fall-off parameter based on RRKM theory has been developed by Luther and Troe.³⁹ Using their approach, the bimolecular rate constant in the transition region may be calculated as^{34,38}

$$k^{II} = \frac{k_x k_0 [M]}{k_x + k_0 [M]} F^{1/2} \cdot \{ \log_{10} [k_0 [M] / k_x] \}^{-1} \quad (3)$$

where k_x and k_0 are the high pressure and low pressure limiting rate constants, respectively. The broadening parameter, F , is dependent on the molecular structure of the adduct and typically is on the order of 0.6 for small molecules.³⁴ The Patrick and Golden calculation for NaO_2^* gives $F = 0.5$.³⁷

In order to assess the fall-off behavior, the association rate k_x may be estimated from the dynamics of the $Na + O_2$ encounter. Alkali atom reactions are often described in terms of their ionic character which leads to very fast reaction rates via an electron jump mechanism.⁴⁰ Ionic forces in the alkali-oxygen associations, however, are not as dominant as in other alkali atom reaction mechanisms. Although the approaching species do adiabatically transfer from the incident covalent potential surface to an ionic surface (electron jump mechanism), the crossing distance (r_c) is relatively small as compared with alkali-halogen systems and the overall association rate is dominated by the dispersion interaction on the covalent potential surface. This is illustrated by comparing the rate constant based on the product of the mean collision velocity and the electron jump cross section (modified to account for the dispersion and angular momentum terms in the covalent potential function),⁴¹ to a rate constant computed solely from a close collision model,⁴² in which all collisions surmounting the angular momentum barrier of a Cr^{-6} potential contribute to the rate. For $Na + O_2$ at 300 K, an electron jump rate constant ($r_c = 2.6 \text{ \AA}$) is $1.5 \times 10^{-10} \text{ cm}^3 \text{ s}^{-1}$, while the close collision constant is $5.9 \times 10^{-10} \text{ cm}^3 \text{ s}^{-1}$. Thus, it appears that the rate of intermediate complex formation for reaction (2) is governed by long range dispersion forces, as found in most covalent systems. Once formed, however, these intermediates are certainly $(alkali)^+ O_2^-$ ion pairs.²² In either case, the association rate constant is expected to be fast with a value for $k_x > 10^{-10} \text{ cm}^3 \text{ s}^{-1}$.

Using a value for $k_x = 2 \times 10^{-10} \text{ cm}^3 \text{ s}^{-1}$, Eq. (3) may be used to estimate the ratio of the observed rate constant, k_{obs} , to the true third order low pressure limit, k_0 . At the maximum density in

our studies, $1.6 \times 10^{17} \text{ cm}^{-3}$, one obtains $k_{\text{obs}}/k_0 = 0.93$ which indicates that our experiments are essentially in the low pressure limit. For the conditions of Husain and Plane²⁸ (150 torr, 724 K), this same calculation would predict $k_{\text{obs}}/k_0 = 0.87$. For the combustion conditions with $P = 760 \text{ torr}$, $T = 2000 \text{ K}$ applicable to the Hynes et al. study,²⁵ one obtains $k_{\text{obs}}/k_0 = 0.89$. Thus, the large value for k_x would indicate that both of these studies are also essentially in the low pressure limit with regard to the recombination reaction.

Acknowledgments

The authors would like to thank Dr. F. Kaufman for many helpful discussions, and Drs. D. Golden and R. Patrick for performing association rate calculations for sodium. The technical assistance of W. Goodwin is greatly appreciated. This work was supported by the Air Force Geophysics Laboratory under Contract Number F19628-83-C-0010, by the Army Research Office under Contract Number DAAG29-81-C-0024, and by the Chemical Manufacturers Association under Contract Number FC82-401.

REFERENCES

- FRIEDMAN, R. AND LEVY, J. B.: *Comb. Flame* 7, 195 (1963).
- WOLFHARD, H. G., GLASSMAN, I. AND GREEN, L., JR.: *Prog. in Aeronautics and Astronautics* 15, 419, Academic Press, 1964.
- McHALE, E. T.: *Comb. Flame* 24, 277 (1975).
- YUSEFIAN, V., MAY, I. W. AND HEIMERL, J. M.: "An Algebraic Criterion for the Prediction of Secondary Muzzle Flash—A Progress Report," 18th JANNAF Combustion Meeting, CPIA Publication 347, Vol. II, 63, Jet Propulsion Laboratory, Pasadena, CA, October, 1981.
- JENSEN, D. E. AND JONES, G. A.: *Comb. Flame* 41, 71 (1981).
- REID, W. T.: *External Corrosion and Deposits*, Elsevier, New York, 1971.
- ELSTON, C., ESSENHUGH, R. H., COHN, A., AND STEWART, G. W.: *Coal Fired Gas Turbine Workshop Report*, Electric Power Research Institute, Palo Alto, CA (1984).
- STEARNS, C. A., KOHL, F. J., AND RONNER, D. E.: *Proceedings of the NACE International Conference on High Temperature Corrosion*, San Diego, CA (March, 1981).
- LIU, S. C. AND REID, G. C.: *Geophys. Res. Lett.* 6, 283, (1979).
- KOLB, C. E. AND ELGIN, J. B.: *Nature* 263, 458 (1976).
- CHAPMAN, S.: *Astrophys. J.* 90, 309 (1939).
- SZE, N. D., KO, M. C. W., SWIDER, W. AND MURAD, E.: *Geophys. Res. Lett.* 9, 1187 (1982).
- MURAD, E., SWIDER, W., AND BENSEN, S. W.: *Nature* 289, 273 (1981).
- SILVER, J. A., STANTON, A. C., ZAHNISER, M. S., AND KOLB, C. E.: *J. Phys. Chem.* 88, 3123 (1984).
- HABER, F. AND SACHSSE, H.: *Z. Physik. Chem. Bodenstein-Festband*, 831 (1931).
- BAWN, C. E. H. AND EVANS, A. G.: *Trans. Faraday Soc.* 33, 580 (1937).
- KASKAN, W. E.: *Tenth Symposium (international) on Combustion*, p. 41, The Combustion Institute, 1965.
- CARABETTA, R. AND KASKAN, W. E.: *J. Phys. Chem.* 72, 2483 (1962).
- McEWAN, M. J. AND PHILLIPS, L. F.: *Trans. Faraday Soc.* 62, 1717 (1966).
- DOUGHERTY, G. J., McEWAN, M. J. AND PHILLIPS, L. F.: *Comb. Flame* 21, 253 (1973).
- HERM, R. R. AND HERSHBAUGH, D. R.: *J. Chem. Phys.* 52, 5783 (1970).
- ALEXANDER, M. H.: *J. Chem. Phys.* 69, 3502 (1978).
- FIGGER, H., SCHREPP, W., AND ZHU, X.: *J. Chem. Phys.* 79, 1320 (1983).
- JENSEN, D. E.: *J. Chem. Soc. Faraday Trans. 1* 78, 2835 (1982).
- HYNES, A. J., STEINBERG, M. AND SCHOFIELD, K.: *J. Chem. Phys.* 80, 2585 (1984).
- KRAMER, S. D., LEHMANN, B. E., HURST, G. S., PAYNE, M. G., AND YOUNG, J. P.: *J. Chem. Phys.* 76, 3614 (1982).
- GROSSMAN, L. W., HURST, G. S., KRAMER, S. D., PAYNE, M. G., AND YOUNG, J. P.: *Chem. Phys. Lett.* 50, 207 (1977).
- HUSAIN, D. AND PLANE, J. M. C.: *J. Chem. Soc. Faraday Trans. II*, 78, 163 (1982).
- HUSAIN, D. AND PLANE, J. M. C.: *J. Chem. Soc. Faraday Trans. II*, 78, 1175 (1982).
- GERSH, M. E., SILVER, J. A., ZAHNISER, M. S., KOLB, C. E., BROWN, R. G., GOZEWISKI, C. M., KATTELIS, S. AND WORSHOUD, J. C.: *Rev. Sci. Instr.* 52, 1213 (1981).
- BROWN, R. L.: *J. Res. NBS* 83, 1 (1978).
- SILVER, J. A.: *J. Chem. Phys.* (accepted for publication, 1984).
- FERGUSON, E. E., FEHSENFELD, F. C. AND SCHMETTERKOPF, A. L.: *Adv. Atomic Mol. Phys.* 5, 1 (1969).
- PATRICK, R. AND GOLDEN, D. M.: *Int. J. Chem. Kinet.* 15, 1189 (1983).
- TROE, J.: *J. Chem. Phys.* 66, 4745 (1977).
- TROE, J.: *J. Chem. Phys.* 66, 4758 (1977).
- PATRICK, R. AND GOLDEN, D. M.: *SRI International*, private communication.
- BALECH, D. L., COX, R. A., HAMPSON, JR., R. F., KERR, J. A., TROE, J., AND WATSON, R. T.: *J. Chem. Phys. Ref. Data* 9, 295 (1980).
- LUTHER, K. AND TROE, J.: *Seventeenth Sym-*

- posium (International) on Combustion, p. 535. The Combustion Institute, 1979.
40. LEVINE, R. D. AND BERNSTEIN, R. B.: *Molecular Reaction Dynamics*, Oxford Press, 1974.
41. GISLASON, E. A.: *Alkali Halide Vapors* (P. Davidovits and D. L. McFadden, Ed.), Chap. 13, p. 415, Academic Press, 1979.
42. JOHNSTON, H. S.: *Gas Phase Reaction Rate Theory*, p. 144 and 253, Ronald Press, 1966.

COMMENTS

A. Fontijn, *Rensselaer Polytechnic Institute, USA*.
You mentioned some work you did on the temperature dependence of reactions of NaOH and NaCl (e.g., with H). How were the reactants generated in these experiments?

Authors' Reply. We have recently completed a study of rate constant measurement for the reactions of $\text{NaOH} + \text{HCl} \rightarrow \text{NaCl} + \text{H}_2\text{O}$, and $\text{NaO} + \text{HCl} \rightarrow \text{NaCl} + \text{OH}$.¹ Both alkali reactants are formed from the gas phase reaction of atomic sodium and hydrogen peroxide. Measurement of the

alkali products was done by converting the alkali molecule to atomic sodium in the detection zone (by addition of excess atomic hydrogen) and detection using laser induced fluorescence.

REFERENCE

1. J. A. SILVER, A. C. STANTON, M. S. ZAHNISER, AND C. E. KOLB, "Gas Phase Reaction Rate of Sodium Hydroxide with Hydrochloric Acid," *J. Phys. Chem.* **68**, 3123 (1964).

SECTION 3

DETERMINATION OF THE ABSOLUTE RATE CONSTANTS FOR
THE ROOM TEMPERATURE REACTIONS OF ATOMIC
SODIUM WITH OZONE AND NITROUS OXIDE

Prepared by

Joel A. Silver* and Charles E. Kolb
Aerodyne Research, Inc.
Center for Chemical and Environmental Physics
45 Manning Road
Billerica, MA 01821

October 1985

*Present address: Southwest Sciences, Inc.
1570 Pacheco Street, Suite E-11
Santa Fe, NM 87501

DETERMINATION OF THE ABSOLUTE RATE CONSTANTS FOR THE ROOM TEMPERATURE
REACTIONS OF ATOMIC SODIUM WITH OZONE AND NITROUS OXIDE

Joel A. Silver* and Charles E. Kolb
Center for Chemical and Environmental Physics
45 Manning Road, Billerica, MA 01821

ABSTRACT

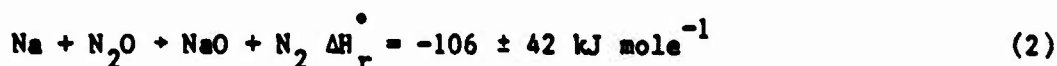
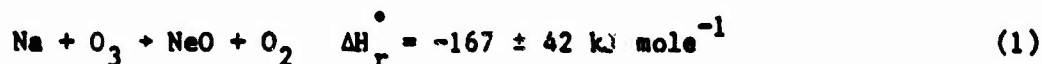
The reaction of atomic sodium with ozone is important in describing the chemistry of the lower thermosphere and upper mesosphere, and is directly related to the observed sodium D-line emissions at 589 nm in these regions of the atmosphere. We report a room temperature rate constant of this reaction to be $(3.1 \pm 0.4) \times 10^{-10} \text{ cm}^3 \text{ molecule}^{-1} \text{ s}^{-1}$. The rate constant for the $\text{NaO} + \text{O}_3$ reaction is determined to be about $2 \times 10^{-10} \text{ cm}^3 \text{ molecule}^{-1} \text{ s}^{-1}$, with 0.7 ± 0.2 of the products being $\text{NaO}_2 + \text{O}_2$, and the remainder $\text{Na} + 2\text{O}_2$. We have also measured the rate constant for $\text{Na} + \text{N}_2\text{O} \rightarrow \text{NaO} + \text{N}_2$ to be $(7.7 \pm 0.9) \times 10^{-13} \text{ cm}^3 \text{ molecule}^{-1} \text{ s}^{-1}$ at 295 K. The impact of the reactions with ozone on the mesospheric chemistry of alkali metals of meteoric origin is discussed.

*Present address: Southwest Sciences, Inc.
1570 Pechaco Street, Suite E-11
Santa Fe, NM 87501

INTRODUCTION

The reaction of atomic sodium with ozone is of fundamental importance in understanding the chemistry of ablated meteor metals in the lower thermosphere and upper mesosphere. It is the major sink for atomic sodium above 85 km and knowledge of its rate constant is critical for modeling the 70-95 km layer and in understanding the processes leading to the sodium D-line Chapman emissions.¹⁻¹⁵ Despite these significant modeling efforts, prior to 1982 almost no kinetic data existed for most of the reactions used in these models. The earlier models utilized rate constants which were estimated from analogy with atomic hydrogen reactions. In 1976, Kolb and Elgin¹⁶ pointed out that the alkali metal atom reaction rates are often much faster than the analogous hydrogen reactions, due to long-range "electron-jump" processes.¹⁷ However, it has only been in the last few years that direct measurements of alkali rate constants have been made to confirm these suggestions.¹⁸⁻²⁵

In this paper we report room temperature measurements of the rate constants for the reactions of atomic sodium with ozone and nitrous oxide,



We also present information on the approximate rate constant and product branching ratio for the reaction of sodium monoxide with ozone,



These and other recent results will help to provide a clearer picture of the chemistry of meteor metals in the mesosphere.

EXPERIMENTAL

Rate constant determinations are made in a fast-flow reactor, which is illustrated in Figure 1 and has been described in detail elsewhere.^{18,26} Briefly, the flow reactor is a 7.26-cm-diameter, 120-cm-long alumina tube, with four perpendicular side arms at the tube exit which permit optical detection of the flow species. Helium carrier gas is added at the entrance of the flow tube through mullite multichannel arrays which laminarize the flow. Gas volumetric flow rates are determined with calibrated thermal conductivity type mass flow meters. A calibrated MKS Baratron Model 310-BHS capacitance manometer (0.8% accuracy) is used to measure pressure.

Alkali atoms are generated by heating a 1 g sample of metallic sodium in a 2.5-cm-diameter cylindrical monel oven to a temperature commensurate with attaining a vapor pressure of 10^{-6} to 10^{-4} torr within the oven. The oven is enclosed in a 4-cm-diameter water-cooled sheath to prevent heating of the main flow carrier gas. The sodium vapor is entrained in a small flow of helium and introduced into the flow tube, where dilution by the carrier gas in the main flow tube restricts the sodium concentration in the reaction zone to no more than 10^{10} cm^{-3} .

Ozone is generated just before each experiment in a commercial ozonator (Welsbach Model T-408) and collected on silica gel at 196 K. It is then pumped on for a few hours to remove any remaining O_2 . It is eluted into the flow tube quartz injector with a controlled flow of helium. The ozone flow rate is determined by UV absorption at 253.7 nm (using a Hg pen lamp and interference filter) in a 1.00-cm-long stainless steel cell. The partial pressure is measured using Beer's law and the absorption cross section of $1.15 \times 10^{-17} \text{ cm}^2$.²⁷ This calculation uses a cell temperature about 7°C above room temperature, due to heating of the cell by the lamp. The total pressure in the cell, typically 700 - 760 torr, is measured with a Validyne pressure transducer. There are negligible losses of ozone during transport, via Teflon tubing, to the flow tube, in the 2-meter-long quartz injector, or along a 72 cm length of the flow tube. This was ascertained by a series of calibrations in which a second absorption system was set up to measure O_3 partial pressures in the flow reactor detection zone. This system consisted of a mercury resonance lamp (Spectroline), with the 253.7 nm line isolated by a 0.074 m monochromator (PTR Optics), and measured by a photodiode using phase-sensitive detection. After correction for differing path lengths, flows, etc., the O_3 concentration in the flow tube matched that in the cell to within 10%, over all flow conditions used during the actual rate experiments.

Detection of atomic sodium was accomplished in two ways, either by resonance lamp fluorescence with phase sensitive detection, or by laser-induced fluorescence using a gated integrator. At the low levels of atomic sodium reaching the detection region optical trapping is not a problem. In both cases, the data were fed to an IBM X/T computer for on-line collection and analysis.

All rate measurements are performed with O_3 or $N_2O \gg Na$, ensuring pseudo-first order kinetic conditions. Reaction times were varied from approximately 3 - 40 ms for the ozone reaction and 1 - 30 ms for the nitrous oxide reaction. Data analysis and corrections for wall loss and diffusion effects were made as described in previous alkali reaction studies.^{19,28}

The purities of chemicals used in these experiments are as follows: sodium metal, 99.95% (Alfa); helium for O_3 and Na flows, 99.998%; helium for main flow, 99.995%; oxygen, 99.99%; hydrogen chloride, 99.99%; nitrous oxide, 99.0%; and carbon monoxide, 99.8%.

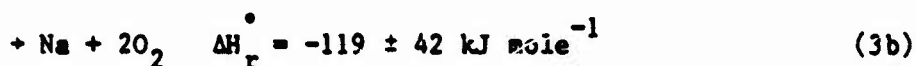
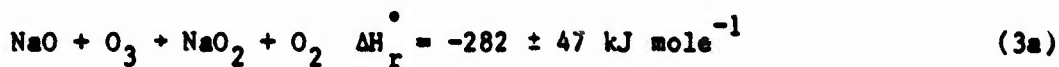
RESULTS

Na + O_3

The reaction of atomic sodium with ozone forms sodium monoxide as a product,



However, the NaO subsequently reacts with ozone, to produce either NaO_2 or to reform atomic sodium,



If the branching to 3b is significant, the observed decays of sodium would not be linear (on a semilog plot of signal versus reaction time), and a more complicated data analysis would be required.

We suppressed this possible complication by adding hydrogen chloride along with the main carrier flow in concentrations exceeding that of O_3 by a factor of 100. The reaction of NaO with HCl produces nonreactive NaCl,¹⁸



so that the observed semilog decays of atomic sodium become linear and result only from reaction 1.

Decays of Na for seven concentrations of ozone covering the range of $4.04\text{--}36.3 \times 10^{12} \text{ cm}^{-3}$ are shown in Figure 2. These were made for pressures of 1.95–2.31 torr and flow velocities of 1380–1635 cm s^{-1} at 293 K. These plots are linear for over four orders of magnitude of sodium concentration. The first order decay rates obtained from the slopes of the lines, corrected for diffusion and wall loss (with factors ranging from 1.66 to 1.90), are plotted versus the corresponding O_3 concentration in Figure 3. A least-squares fit to the slope of this line, weighted by the uncertainties in each point, results in a rate constant value of $(3.1 \pm 0.4) \times 10^{-10} \text{ cm}^3 \text{ molecule}^{-1} \text{ s}^{-1}$ for reaction 1. The uncertainty expressed includes precision errors (one standard deviation), as well as estimated errors in accuracy.

Our Na + O_3 results are in good agreement with recent measurements by Hussein et al.²¹ who measured this rate constant to be $4 (+4, -2) \times 10^{-10} \text{ cm}^3 \text{ molecule}^{-1} \text{ s}^{-1}$ at 500 K using atomic resonance spectroscopy following pulsed

irradiation. However, they did not take into account any effects of the $\text{NaO} + \text{O}_3$ reaction, so that their result can be considered only qualitatively correct. Our results are a factor of two smaller than that measured by Ager and Howard,²⁵ using very similar experimental techniques. The reason for this discrepancy is unclear.

A series of measurements were also made without adding HCl . We attempted to fit the observed curvature in these decays with a model containing reactions 1, 3a, and 3b. The analytic solution for $[\text{Na}]$ is a sum of two exponential decays,²⁹

$$[\text{Na}(x)] = ae^{-bx} + ce^{-dx},$$

where

a, b, c , and d are algebraic combinations of k_1 , k_{3a} , and k_{3b} , and $x = [\text{O}_3]t$. Sodium profiles (as measured at the detector) from this calculation are plotted as a function of $[\text{O}_3]t$ in Figure 4, along with the experimental data taken without HCl . The values used for the rate constants are those uncorrected for diffusion effects, as we are trying to fit raw data. However, these corrections are straightforward, since they are approximately independent (1.66-1.90 for this data) of the magnitude of the observed reaction rate in the situation of unit wall loss and fast radial diffusion.²⁸ We also assume that the wall loss rate and diffusion corrections are the same for all of the molecular sodium species in the calculation. One set of solutions is shown in Figure 4, using the measured value of k_1 and a value of k_3 equivalent to $2 \times 10^{-10} \text{ cm}^3 \text{ molecule}^{-1} \text{ s}^{-1}$. The curves illustrate how the decay varies as a

function of k_{3a}/k_3 . Although the fit for $k_{3a}/k_3 = 0.7$ is good, the shapes of the curves vary with k_3 . As k_3 is decreased, the curves break away from the $k_{3b} = 0$ curve (e) at larger values of $[O_3]t$, and flatten out more rapidly for corresponding values of k_{3a}/k_3 . Given the approximations in this calculation, the scatter in our data, and the ambiguity in fitting these curves, we conclude that k_3 is approximately $2 \times 10^{-10} \text{ cm}^3 \text{ molecule}^{-1} \text{ s}^{-1}$ and that $k_{3a}/k_3 = 0.7 \pm 0.2$.

NaO + N₂O

The reaction of atomic sodium with nitrous oxide is much slower than with ozone. Furthermore, nonlinearities in the semilog plots of signal versus reaction time are not observed, demonstrating then the reaction of NaO with N₂O does not have a significant atomic sodium product channel. Thirteen sodium decays were measured (of which, for clarity, seven are shown in Figure 5) for a nitrous oxide concentration range of $3.97 - 95.4 \times 10^{13} \text{ cm}^{-3}$. The flow velocity for these experiments was either 840 or 1240 cm s^{-1} , at corresponding pressures of 1.52 and 2.23 torr. The overall results were the same for both operating conditions. The corrected first order decays obtained from these lines (with correction factors ranging from 1.62 to 1.82) are plotted versus $[N_2O]$ in Figure 6. The resultant rate constant for this reaction is $k_2 = (7.7 \pm 0.9) \times 10^{-13} \text{ cm}^3 \text{ molecule}^{-1} \text{ s}^{-1}$ at 295 K. This is in excellent agreement with an extrapolation to room temperature of results of Husein and Marshall.²⁴ Their value of $k_2 = (1.9 \pm 0.3) \times 10^{-10} \exp(-12.5 \pm 0.6 \text{ kJ/mole/RT}) \text{ cm}^3 \text{ molecule}^{-1} \text{ s}^{-1}$, was measured over the temperature

range of 349 - 917 K. This also agrees with a room temperature result of $(8.2 \pm 1.5) \times 10^{-13} \text{ cm}^3 \text{ molecule}^{-1} \text{ s}^{-1}$ of Ager and Howard.²⁵

DISCUSSION

The results of this work confirm that the $\text{Na} + \text{O}_3$ reaction rate constant approaches the gas kinetic limit, agreeing remarkably well with $3.3 \times 10^{-10} \text{ cm}^3 \text{ molecule}^{-1} \text{ s}^{-1}$ predicted by Kolb and Elgin¹⁶ using an electron-jump model. Unlike ozone, N_2O is an 18-electron closed shell molecule and despite a large exothermicity, exhibits a moderate activation energy,²⁴ leading to a lower value for the room temperature rate constant. This activation energy might be explained by the increase of reactive cross section with increasing vibrational excitation, in correlation with the increasing stability of a bent N_2O^- structure as predicted by Walsh's rules, as previously observed with reactions of N_2O with Ba and Sm.³⁰⁻³²

The fate of neutral sodium as it enters the mesosphere is illustrated in Figure 7. Above 85 km, it reacts primarily with ozone to form NaO , which subsequently reacts with atomic oxygen to produce both ground state and electronically excited sodium atoms. This latter process leads to the observed D-line emission of sodium at 589 nm.¹ Below 85 km, the termolecular recombination with O_2 dominates, forming NaO_2 . This molecule can react with atomic oxygen to form NaO , which is rapidly converted to NaOH by reaction with H_2O .²⁵ It is still uncertain whether NaOH is the major alkali species below 70 km, or if both NaO_2 and NaOH are significant. This depends on the rate constant for $\text{NaO}_2 + \text{O} \rightarrow \text{NaO} + \text{O}_2$, and on the photolysis rates for NaO , NaO_2 and NaOH , which have not yet been directly measured.

In conclusion, we have confirmed that the reaction of ozone with atomic sodium at room temperature is near its gas kinetic limit, strengthening the recent model predictions for the partitioning of alkali species in the mesosphere and upper stratosphere. Although much remains to be done, our understanding of atmospheric chemical cycles involving metals of meteoric origin has significantly improved in the past few years.

ACKNOWLEDGEMENTS

We gratefully acknowledge the many contributions of Dr. Mark Zahniser, Warren Goodwin, and the late Dr. Frederick Kaufman, as well as helpful discussions with Drs. William Swider, Edmond Murad, and Charles Gallagher of the Air Force Geophysics Laboratory.

This work was supported by the Air Force Geophysics Laboratory under Contract No. F19628-83-C-0010.

REFERENCES

1. S. Chapman, *Astrophys. J.*, 1939, 90, 309.
2. J.E. Blamont and T.M. Donahue, *J. Geophys. Res.*, 1964, 69, 4093.
3. W.J. Baggaley, *Nature (London)*, 1975, 257, 567.
4. W.J. Baggaley, *Nature (London)*, 1977, 267, 376.
5. S.C. Liu and G.C. Reid, *Geophys. Res. Lett.*, 1979, 6, 283.
6. E. Murad and W. Swider, *Geophys. Res. Lett.*, 1979, 5, 929.
7. E.S. Richter and C.F. Sechrist, Jr., *Geophys. Res. Lett.*, 1979, 6, 183;
J. Atmos. Terr. Phys., 1979, 41, 579.
8. W. Swider, *Geophys. Res. Lett.*, 1985, 12, 589.
9. D.M. Simonich, B.R. Clemensha, and V.W.J.H. Kirchoff, *J. Geophys. Res.*,
1979, 84, 1543.
10. M.A. Hapgood, *Nature (London)*, 1980, 286, 582.
11. V.W.J.H. Kirchoff, B.R. Clemensha, and D.M. Simonich, *J. Geophys. Res.*,
1981, 86, 6892; *J. Geophys. Res.*, 1983, 88, 442.
12. N.D. Sze, K.W. Ko, W. Swider, and E. Murad, *Geophys. Res. Lett.*, 1982, 9,
1187.
13. V.W.J.H. Kirchoff, *Geophys. Res. Lett.*, 1983, 10, 721.
14. L. Thomas, M.C. Isherwood, and M.R. Bowman, *J. Atmos. Terr. Phys.*, 1983,
45, 587.
15. D.M. Hunten, *Space Sci. Rev.*, 1967, 6, 493.
16. C.E. Kolb and J.B. Elgin, *Nature (London)*, 1976, 263, 488.
17. D.R. Herschbach, *Adv. Chem. Phys.*, 1966, 10, 319.

18. J.A. Silver, A.C. Stanton, M.S. Zahniser, and C.E. Kolb, J. Phys. Chem. 88, 1984, 3123.
19. J.A. Silver, M.S. Zahniser, A.C. Stanton, and C.E. Kolb, 20th Symposium (International) on Combustion, The Combustion Institute, Pittsburgh, 1984, 605.
20. J.A. Silver and C.E. Kolb, J. Phys. Chem., submitted for publication, 1985.
21. D. Husain, P. Marshall, and J.M.C. Plane, J. Chem. Soc. Chem. Commun., 1985, 1216.
22. D. Husain and J.M.C. Plane, J. Chem. Soc. Faraday Trans. 2, 1982, 78, 163.
23. D. Husain, P. Marshall, and J.M.C. Plane, J. Chem. Soc. Faraday Trans. 2, 1985, 81, 301.
24. D. Husain and P. Marshall, Comb. Flame, 1985, 60, 81.
25. J.W. Ager and C.J. Howard, University of Colorado, Boulder (private communication), 1985.
26. M.E. Gersh, J.A. Silver, M. Zahniser, C.E. Kolb, R.G. Brown, C.M. Gozewski, S. Kallelis, and J.C. Wormhoudt, Rev. Sci. Instrum., 1981, 52, 1213.
27. W.B. DeMore and O. Raper, J. Phys. Chem., 1964, 68, 412.
28. J.A. Silver, J. Chem. Phys., 1984, 81, 5125.
29. N.M. Rodiguin and E.N. Rodiguina, Consecutive Chemical Reactions, Van Nostrand, New York, 1964.
30. D.J. Wren and M. Manzinger, J. Chem. Phys., 1975, 63, 4557.
31. D.J. Wren and M. Menzinger, Faraday Discuss. Chem. Soc., 1979, 67, 97.
32. A. Yokozaki and M. Menzinger, Chem. Phys., 1977, 20, 9.

FIGURE CAPTIONS

1. Illustration of fast flow reactor in which these rate constant measurements were made.
2. Pseudo first-order decays for the $\text{Na} + \text{O}_3$ reaction in the presence of hydrogen chloride. $[\text{O}_3] = 5.04$, (\circ), 5.34 (\bullet), 8.64 (\square), 17.2 (\blacksquare), 17.3 (\triangle), 21.8 (\blacktriangle), 36.3 (\diamond); units of 10^{11} cm^{-3} .
3. Dependence of corrected pseudo-first-order rate constant on O_3 concentration at 293 K.
4. Plot of computed curves for observed Na decay as a function of $[\text{O}_3]t$ for a variety of values of k_{3a}/k_3 . This calculation uses $k_1 = 3.1 \times 10^{-10} \text{ cm}^3 \text{ molecule}^{-1} \text{ s}^{-1}$, and $k_2 = 2 \times 10^{-10} \text{ cm}^3 \text{ molecule}^{-1} \text{ s}^{-1}$.
 $k_{3a}/k_3 = \text{a) } 0; \text{ b) } 0.5; \text{ c) } 0.7; \text{ d) } 0.9; \text{ e) } k_{3b} = 0$.
5. Pseudo-first-order decays for the $\text{Na} + \text{N}_2\text{O}$ reaction. $[\text{N}_2\text{O}] = 3.97$ (\circ), 10.8 (\bullet), 24.0 (\square), 35.5 (\blacksquare), 48.7 (\triangle), 61.2 (\blacktriangle), 95.4 (\diamond); units of 10^{13} cm^{-3} .
6. Dependence of corrected pseudo-first-order rate constant on N_2O concentrations at 295 K.
7. Schematic Diagram for Mesospheric Sodium Chemistry.

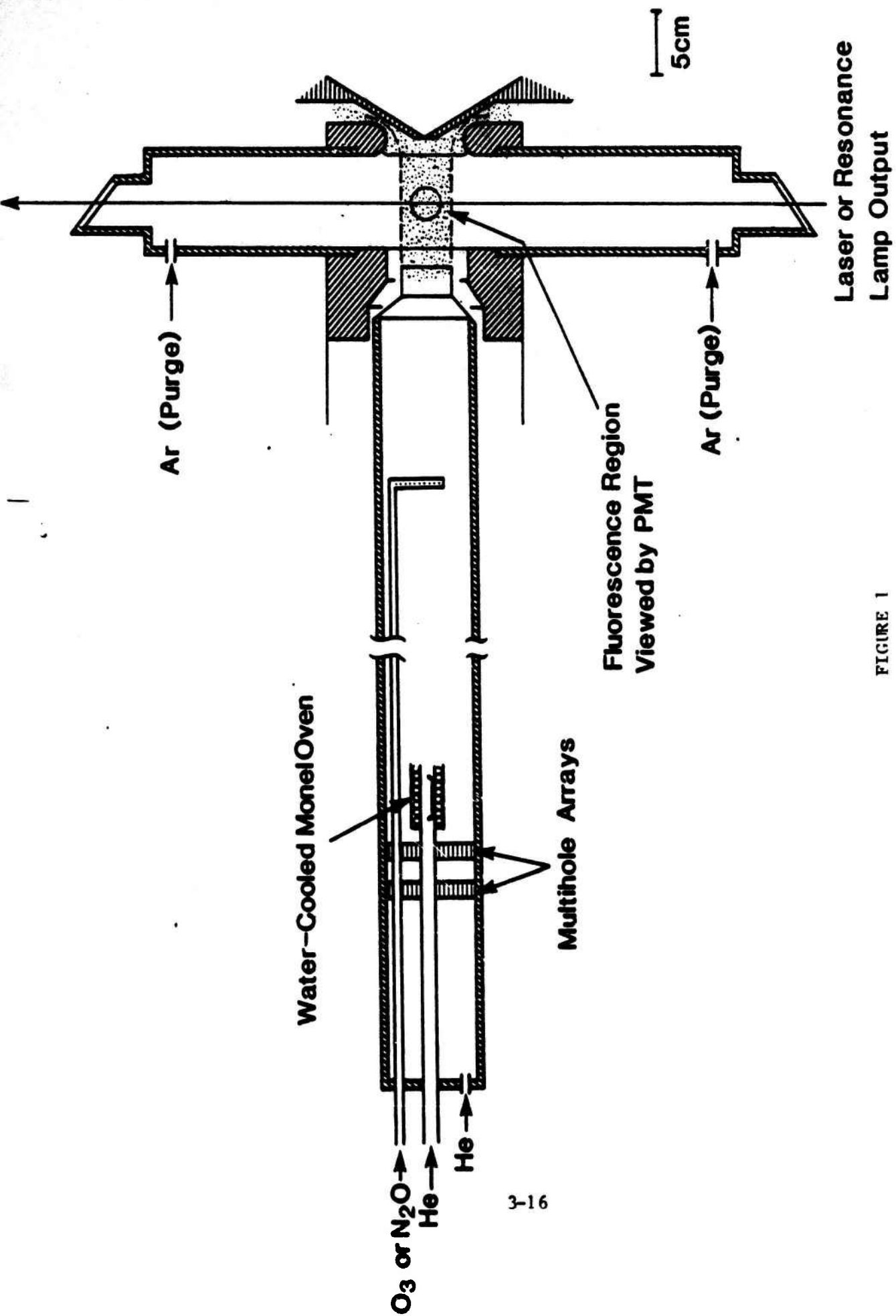


FIGURE 1

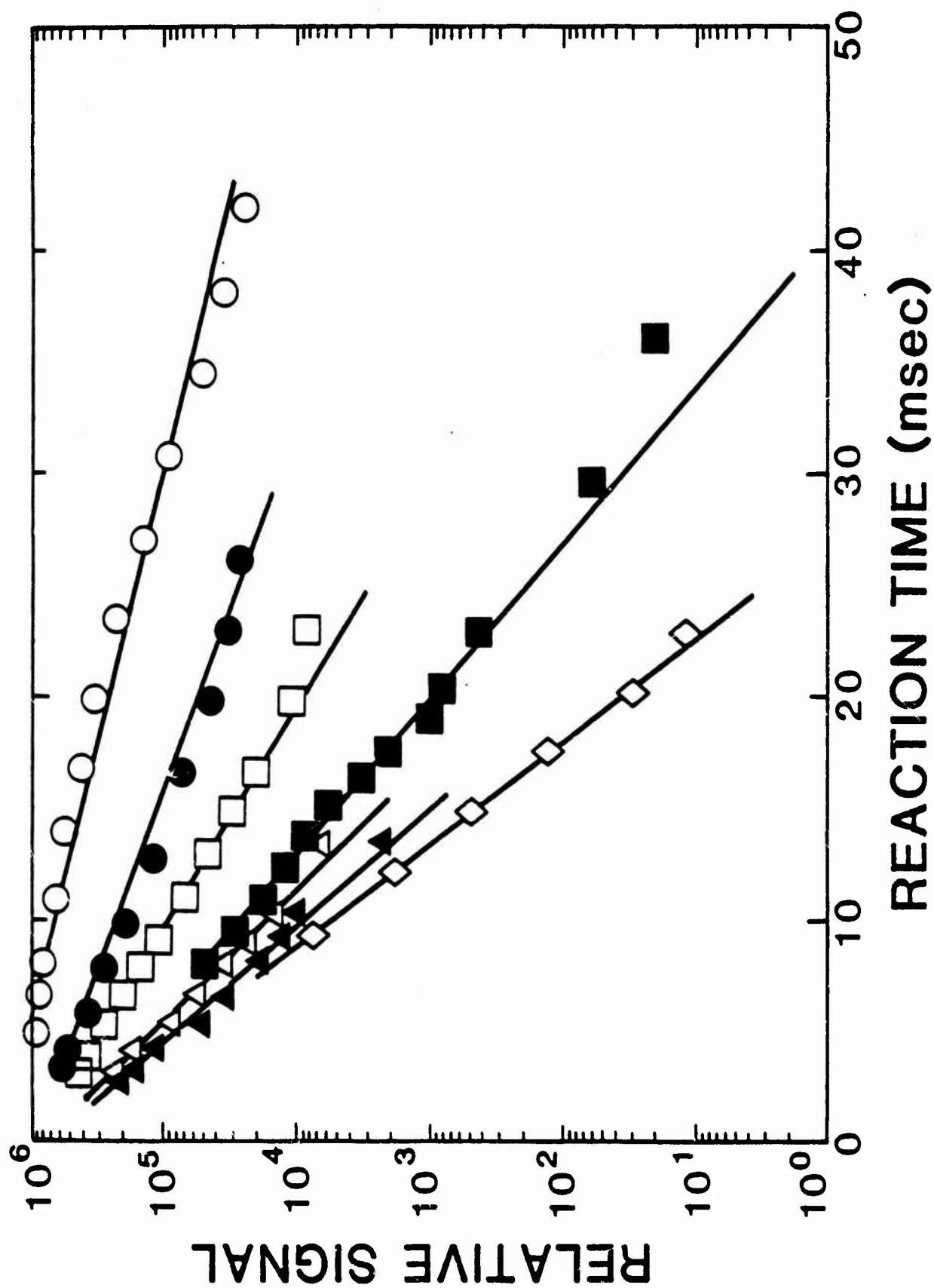


FIGURE 2

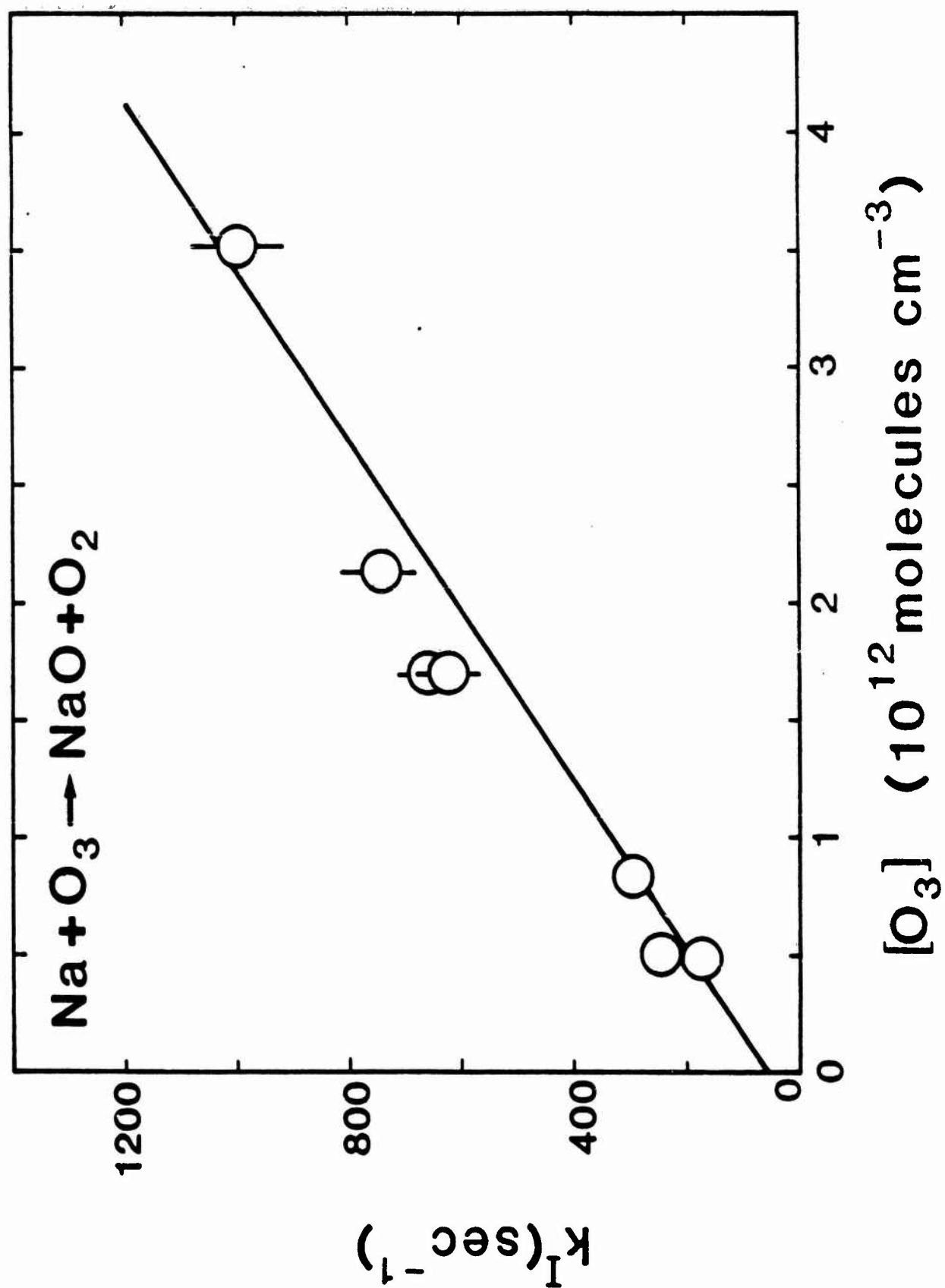


FIGURE 3

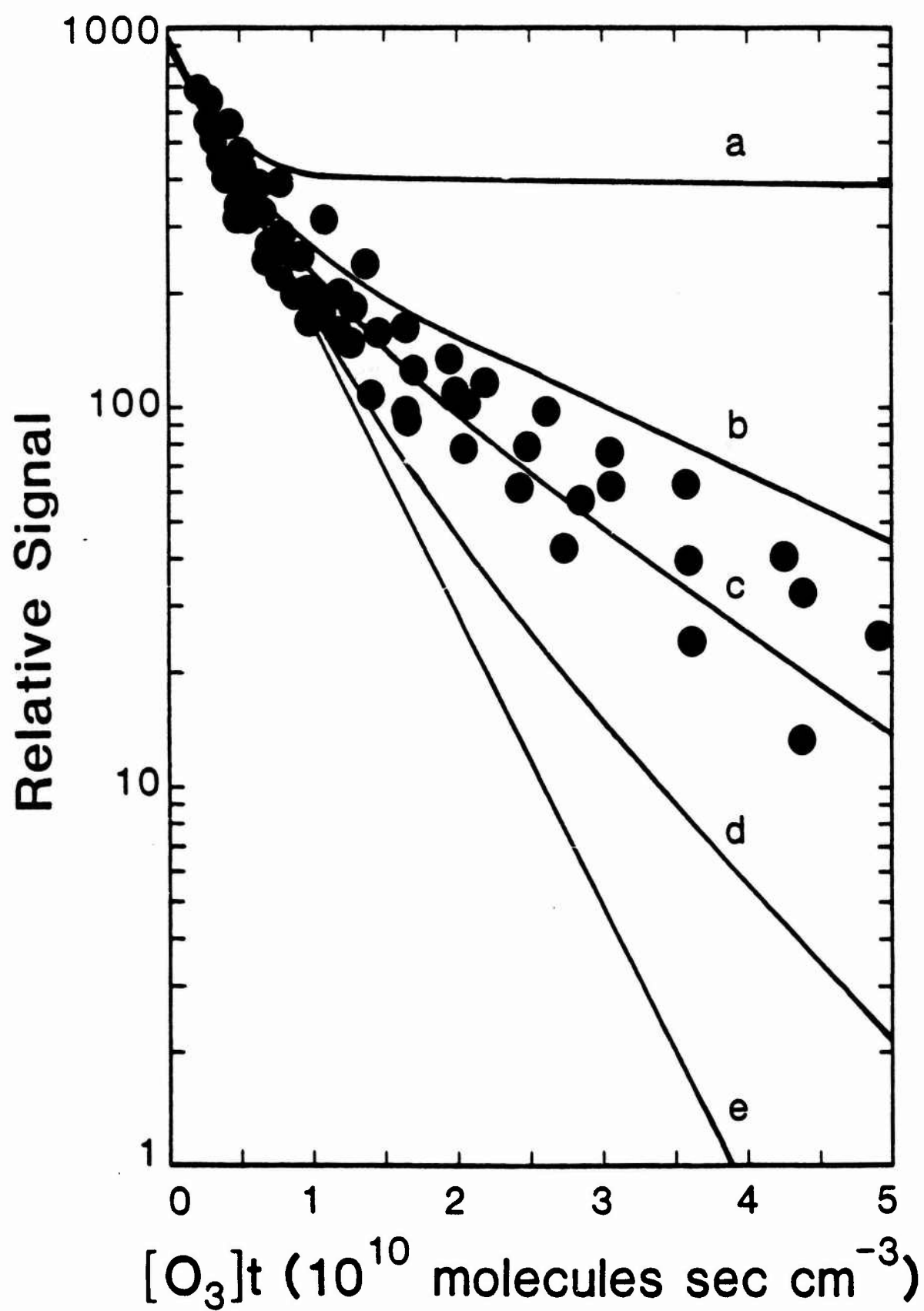


FIGURE 4

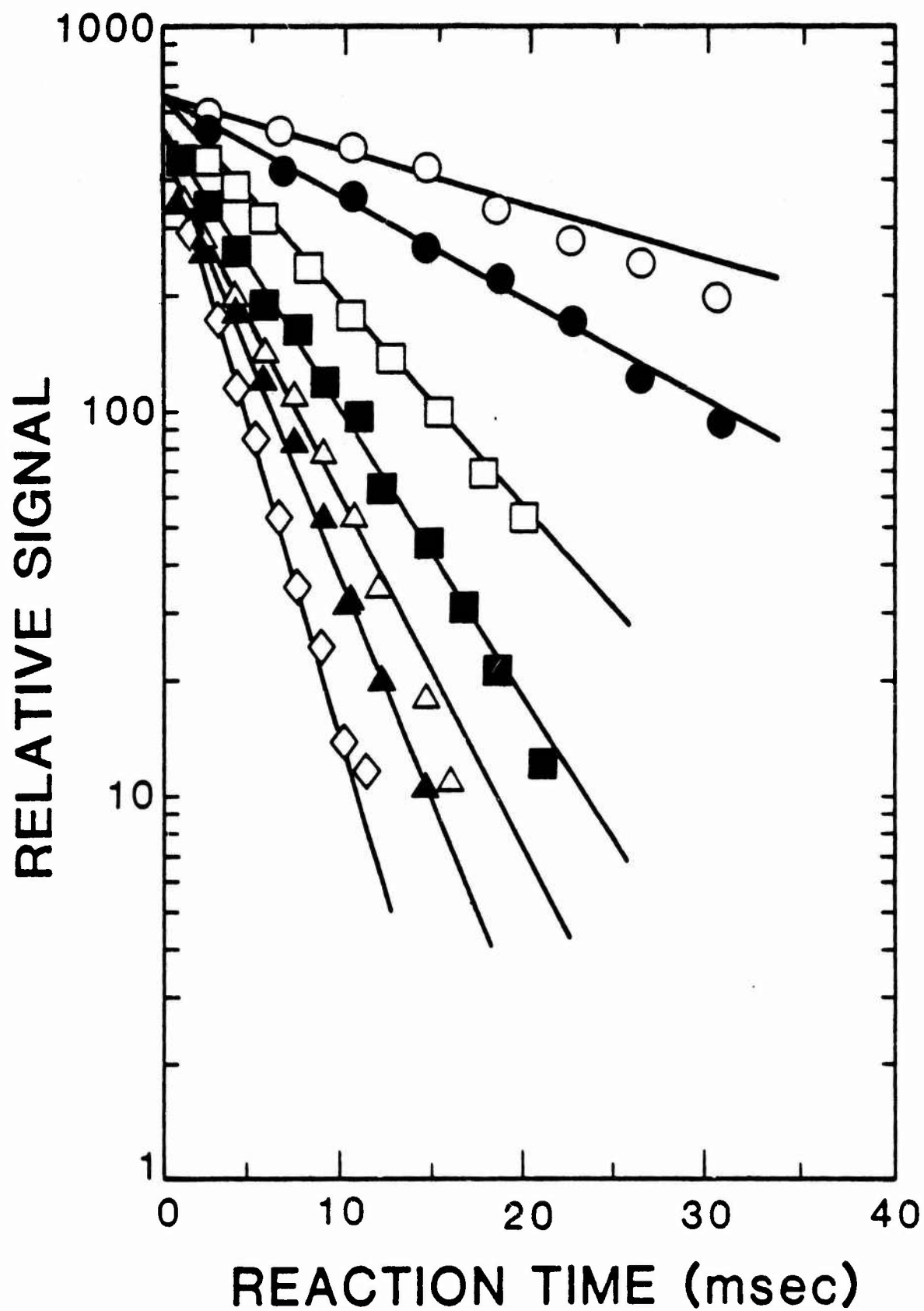


FIGURE 5

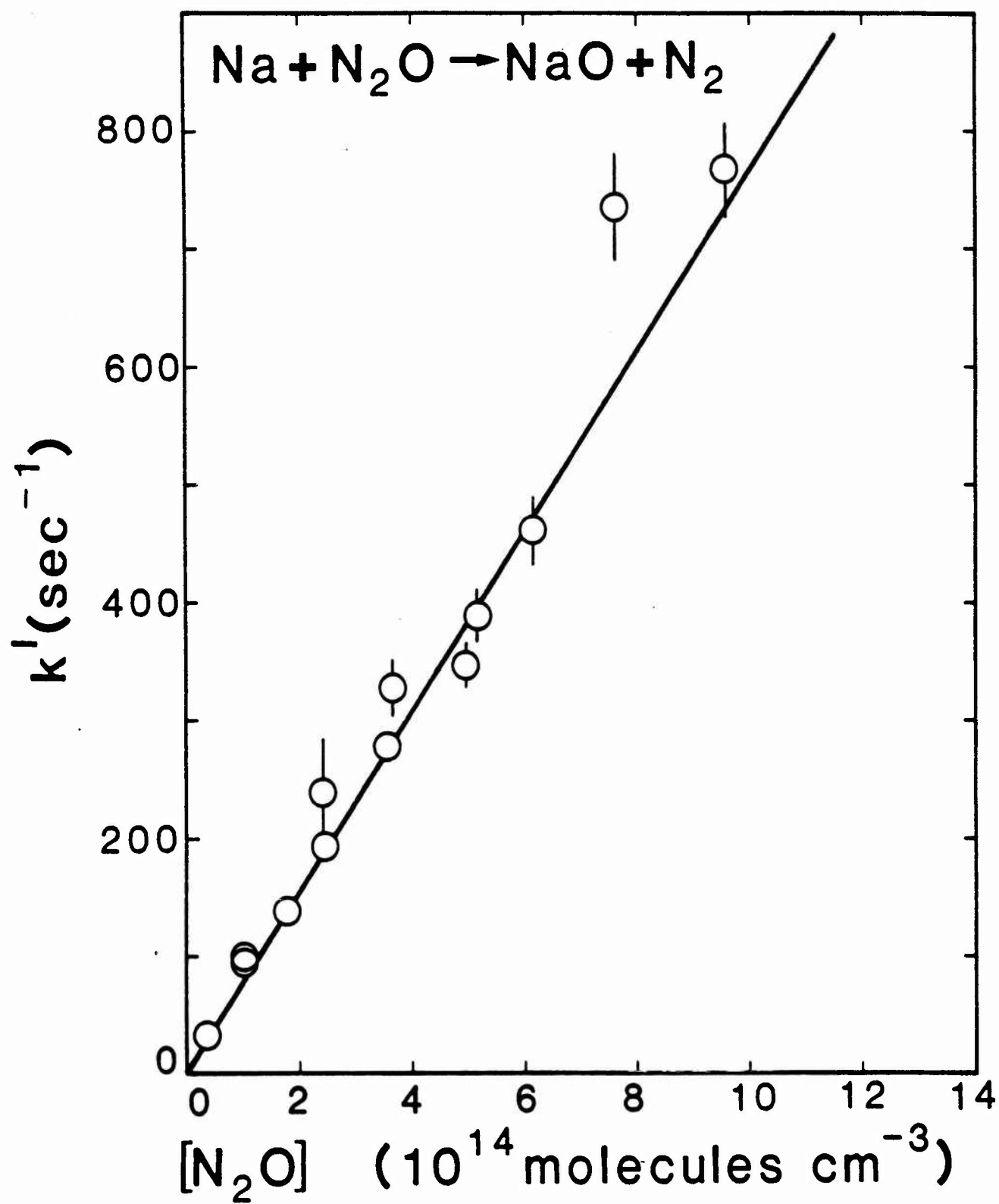


FIGURE 6

METEORS

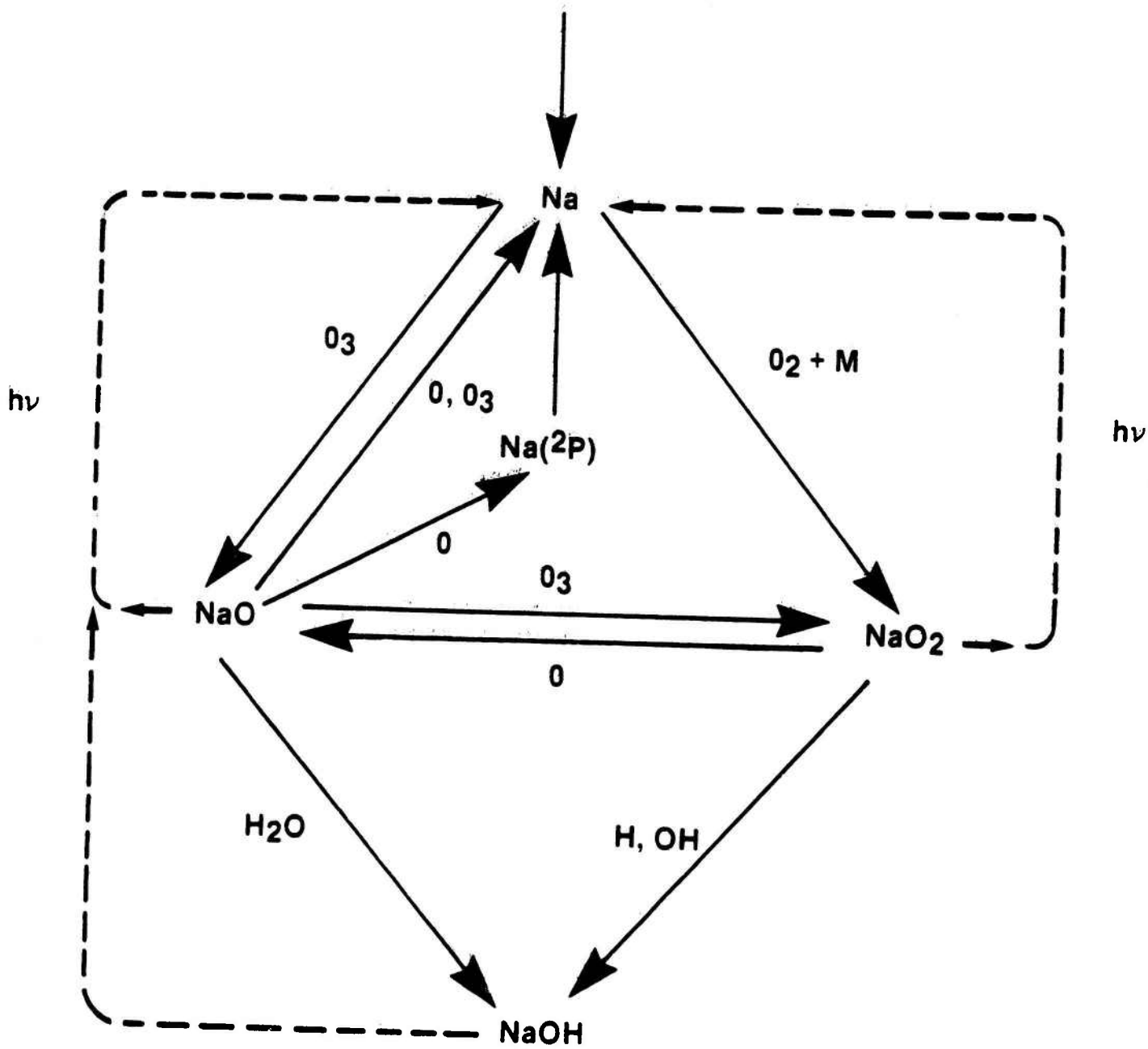


FIGURE 7

SECTION 4

GAS-PHASE REACTION RATE OF SODIUM HYDROXIDE
WITH HYDROCHLORIC ACID

Reprinted from The Journal of Physical Chemistry, 1984, 88, 3123.
Copyright © 1984 by the American Chemical Society and reprinted by permission of the copyright owner.

The U.S. Government is authorized to reproduce and sell this report.
Permission for further reproduction by others must be obtained from
the copyright owner.

Gas-Phase Reaction Rate of Sodium Hydroxide with Hydrochloric Acid

J. A. Silver,* A. C. Stanton, M. S. Zahniser, and C. E. Kolb

Center for Chemical and Environmental Physics, Aerodyne Research, Inc., Billerica, Massachusetts 01821

(Received: February 7, 1984)

The reactions of metallic species introduced into the atmosphere by meteor ablation may play a significant role in stratospheric chemistry. In particular, it has been suggested that the reaction of NaOH with HCl might affect the concentration of odd chlorine, thus having an impact on the ozone balance. This paper describes the first measurement of this reaction rate constant. At 308 K, we find that $k = (2.8 \pm 0.9) \times 10^{-10} \text{ cm}^3 \text{ molecule}^{-1} \text{ s}^{-1}$. As a result of the methods developed to perform this measurement, we have also determined estimates of the following room temperature rate constants in units of $\text{cm}^3 \text{ molecule}^{-1} \text{ s}^{-1}$: $k(\text{NaO} + \text{HCl} \rightarrow \text{NaCl} + \text{OH}) \approx 2.8 \times 10^{-10}$, $k(\text{NaOH} + \text{H} \rightarrow \text{Na} + \text{H}_2\text{O}) > 4 \times 10^{-12}$, $k(\text{NaCl} + \text{H} \rightarrow \text{Na} + \text{HCl}) \approx 5 \times 10^{-14}$, and $k(\text{Na} + \text{H}_2\text{O}_2) \approx 6.9 \times 10^{-11}$, where approximately 0.6 of the reactions produce NaOH + OH, with the remainder forming NaO + H₂O.

Introduction

Metallic elements volatilized during meteor entry into the Earth's upper atmosphere play a significant role in the structure of the D and E regions of the ionosphere,¹⁻² and, at least in the

case of sodium, the visible day and nightglow emissions from the mesosphere and lower thermosphere.³⁻⁵ Recently, it was suggested

(1) E. Murad, *J. Geophys. Res.*, **83**, 5525 (1978).

(2) T. L. Brown, *Chem. Rev.*, **73**, 645 (1973).

(3) J. E. Blamont and T. M. Donahue, *J. Geophys. Res.*, **69**, 4093 (1964).

(4) D. M. Hunten, *Space Sci. Rev.*, **6**, 493 (1967).

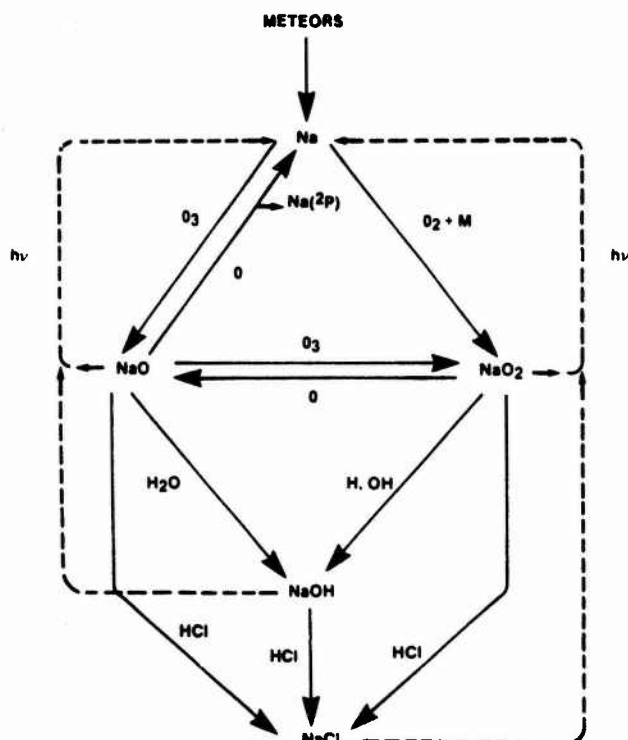


Figure 1. Schematic diagram of atmospheric sodium chemistry

that sodium and other meteor metals may be important in stratospheric chemistry by affecting ozone reduction by the catalytic chlorine cycle.⁶⁻⁸

The influx of meteor metals into the upper atmosphere has been estimated⁹ to be 3.5×10^6 kg yr⁻¹, with a sodium abundance of 2% leading to a calculated sodium flux of 1.2×10^4 atoms cm⁻² s⁻¹. Other estimates of sodium flux run as high as 2×10^4 cm⁻² s⁻¹.¹⁰ The flux of other metallic species such as Mg, Ca, Al, Si, and Fe will be as much as 10 times higher and speculative concerns about their influence on upper atmospheric homogeneous and heterogeneous chemistry have been published.^{1-2,7-8,10}

Unfortunately, all attempts to model the role of volatilized meteor metals (particularly sodium) in the mesosphere and stratosphere^{3-4,7,9-15} have suffered from an almost total lack of measured rate constants. All such models start with the oxidation of sodium or other metallic species in reaction with atmospheric O, O₂, or O₃. However, the only measured chemical rate constants currently available for any alkali meteor metal oxidation reactions are those for the three-body recombination reactions of alkali atoms (Na, K) with O₂.¹⁶⁻¹⁸

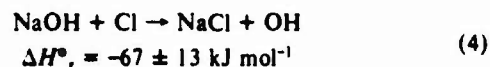
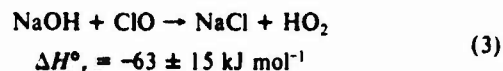
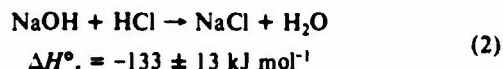


In fact, until 2 years ago, even this reaction was thought to be ~1000 times slower¹⁹⁻²⁰ than the value found in the more recent measurements.

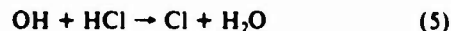
From the recent modeling work^{7-8,10,13,21-22} and comparison of these models with atmospheric measurements,^{12,14-15} neutral sodium is believed to be transformed via a series of chemical reactions involving NaO and NaO₂ intermediates to NaOH. A survey of the relevant literature^{6-8,10,13} provides a fairly complete list of possible neutral sodium reactions of importance, and a simplified schematic diagram of these reactions is shown in Figure 1.

Neutral sodium appears in a range between 110- and 70-km altitude. As shown in Figure 1, the main removal mechanisms are by reaction with O₂ or O₃, the latter used by Chapman²³ to explain the Na nightglow. We have recently completed temperature-dependent measurements of the reaction rates with O₂ in our laboratory which show that this reaction proceeds with a fast three-body rate constant of 1.9×10^{-30} cm⁶ s⁻¹ with N₂ as the third body at 300 K.¹⁸ This leads us to believe that most of the Na in the lower mesosphere is converted to NaO₂, since the three-body recombination rate with O₂ exceeds even a gas kinetic two-body rate with O₃ below 80 km. Since none of the remaining rates have ever been measured, the rest of the mechanism (as proposed by various models) is speculative. However, the dominant sodium species which leave the mesosphere and enter the stratosphere are probably NaOH and/or NaO₂.

The fate of NaOH is very uncertain. Indeed, only in the past few years has NaOH been recognized as a major reaction product. Ferguson⁶ suggested that it forms NaOH cluster ions of the form H⁺(NaOH)_n(H₂O)_m, which either may be rained out from the troposphere or removed in the stratospheric aerosol layer. In a recent paper by Murad et al.,⁸ it was proposed that the reactions of metal hydroxides (and superoxides) with chlorine compounds between 40 and 70 km may have an impact on the depletion of stratospheric ozone. In the case of sodium, the exothermic bimolecular reactions



might be expected to proceed rapidly and act as a sink for Cl, given that NaCl can readily polymerize and condense via heterogeneous nucleation.⁸ Murad et al. calculated that if k_2 were $\sim 10^{-11}$ cm³ molecule⁻¹ s⁻¹, then the reaction of NaOH with HCl would be comparable to the major recognized Cl regeneration mechanism



While previously published studies have viewed NaCl as a potential sink for stratospheric chlorine,⁷⁻⁸ more recent analyses by Rowland²⁴ indicate that photolysis of NaCl may in fact release free Cl. Given the potentially large J values (photolysis rates) for this process,²⁴ reactions 2-4 could effectively supplement reaction 5 as a release mechanism for Cl from the inactive HCl stratospheric reservoir and thereby determine the extent to which ozone might be depleted by chlorine compounds in the stratosphere. However,

(5) (a) V. W. J. H. Kirchhoff, B. R. Clemesha, and D. M. Simonich, *J. Geophys. Res.*, **84**, 1323 (1979); (b) D. R. Bates and P. C. Ojha, *Nature (London)*, **286**, 790 (1980).

(6) E. E. Ferguson, *Geophys. Res. Lett.*, **5**, 1035 (1978).

(7) E. Murad and W. Swider, *Geophys. Res. Lett.*, **6**, 929 (1979).

(8) E. Murad, W. Swider, and S. W. Benson, *Nature (London)*, **289**, 273 (1981).

(9) E. S. Richter and C. F. Sechrist, Jr., *J. Atmos. and Terr. Phys.*, **41**, 579 (1979); *Geophys. Res. Lett.*, **6**, 183 (1979).

(10) S. C. Liu and G. C. Reid, *Geophys. Res. Lett.*, **6**, 283 (1979).

(11) (a) W. J. Baggaley, *Nature (London)*, **257**, 567 (1975); (b) *ibid.*, **297**, 376 (1977); (c) M. A. Hapgood, *ibid.*, **286**, 582 (1980).

(12) V. W. J. H. Kirchhoff, B. R. Clemesha, and D. M. Simonich, *J. Geophys. Res.*, **86**, 6892 (1981).

(13) N. D. Sze, M. K. W. Ko, W. Swider, and E. Murad, *Geophys. Res. Lett.*, **9**, 1187 (1982).

(14) V. W. J. H. Kirchhoff, *Geophys. Res. Lett.*, **10**, 721 (1983).

(15) L. Thomas, M. C. Isherwood, and M. R. Bowman, *J. Atmos. Terr. Phys.*, **45**, 587 (1983).

(16) D. Husain and J. M. C. Plane, *J. Chem. Soc., Faraday Trans. 2*, **78**, 163, 1175 (1982).

(17) A. J. Hynes, M. Steinberg, and K. Schofield, *J. Chem. Phys.*, **80**, 2585 (1984).

(18) J. A. Silver, M. S. Zahniser, A. C. Stanton, and C. E. Kolb, *Symp. (Int.) Combust. [Proc.]*, 20th, accepted for publication.

(19) R. Carabetta and W. E. Kaskan, *J. Phys. Chem.*, **72**, 2483 (1968).

(20) M. J. McEwan and L. F. Phillips, *Trans. Faraday Soc.*, **62**, 717 (1966).

(21) C. E. Kolb and J. B. Elgin, *Nature (London)*, **263**, 488 (1976).

(22) D. M. Simonich, B. R. Clemesha, and V. W. J. H. Kirchhoff, *J. Geophys. Res.*, **84**, 1543 (1979).

(23) S. Chapman, *Astrophys. J.*, **90**, 309 (1939).

(24) F. S. Rowland and P. J. Rogers, *Proc. Natl. Acad. Sci. U.S.A.*, **79**, 2737 (1982).

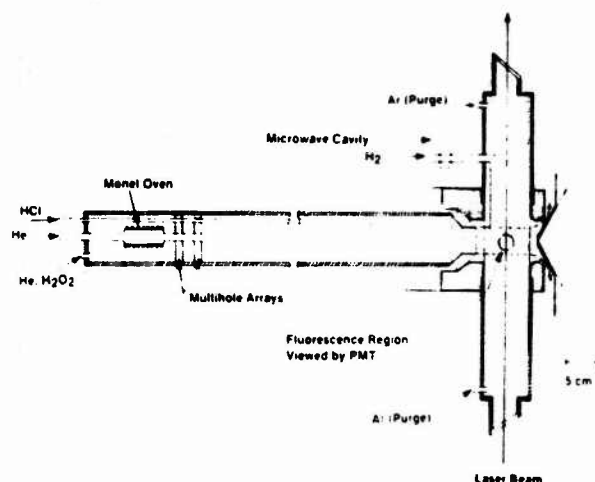


Figure 2. Schematic view of the flow tube

to understand fully the role of alkali species in the atmosphere. We must also consider the effects of NaO_2 and NaOH photodissociation on these processes.^{13,25}

The purpose of this study is to provide a direct experimental rate measurement of the reaction $\text{NaOH} + \text{HCl} \rightarrow \text{NaCl} + \text{H}_2\text{O}$, which serves as a starting point for understanding the stratospheric role of sodium and other meteoric metals. Only by obtaining accurate, directly measured rate constants can we hope to understand atmospheric metal chemistry, and, in particular, how this chemistry affects the ozone balance.

Experimental Section

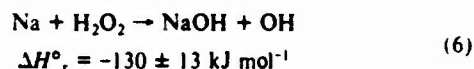
Very little gas-phase research has been done on alkali hydroxides because they are difficult to vaporize,²⁶ are extremely corrosive,²⁷ and readily dimerize in the gas phase.²⁸ In addition, there are no established detection techniques sensitive enough to allow kinetic analyses of alkali hydroxide reactions. With this in mind we have taken an indirect approach for producing and detecting NaOH , i.e., chemical production of NaOH by the reaction of atomic sodium with hydrogen peroxide, and detection of NaOH by chemical conversion back to atomic sodium, which is then observed by laser-induced fluorescence.

The measurements were performed in the Aerodyne high-temperature fast-flow reactor, which is fully described in ref 29 and whose relevant features are illustrated in Figure 2. Briefly, a 7.26-cm-diameter, 120-cm-long alumina tube is used, fitted with Kanthal heater elements which can radiatively heat the tube over the temperature range 294–1500 K. Four perpendicular alumina side arms at the tube exit permit detection of flow species by a variety of optical techniques, including laser- or resonance lamp-excited fluorescence, infrared absorption (either broad band or high resolution), and observation of chemiluminescence. Gas temperatures are obtained with chromel–alumel or shielded W–5% Re–W–26% Re thermocouples.³⁰ Extensive calibrations indicate the temperature can be measured with an accuracy of ± 10 K over the entire operating range of the reactor for flow Reynolds numbers below 500; for the current experiments they are typically below 50. The gas is pumped by a Kinney KMBD 1602 mechanical pump and Roots blower with an effective pumping speed of 450 L s^{-1} . The helium carrier gas is added at the entrance of the flow tube through mullite multichannel arrays which laminarize the flow. These are ~ 2.5 -cm upstream of the outlet of

the reactant inlet tube and 78 cm from the detection region. This allows sufficient distance (18 cm) for the helium flow to mix with the reactants and develop a parabolic velocity profile before reaching the reaction zone. Gas volumetric flow rates are determined with calibrated thermal conductivity type mass flow meters. Flow speeds can be varied from 4 to 100 m s^{-1} . A calibrated MKS Baratron Model 310-BS1110 capacitance manometer (0.8% accuracy) is used to measure pressure.

Alkali atoms are generated by heating the sample in a 2.5-cm-diameter cylindrical monel oven to a temperature commensurate with attaining a vapor pressure of that species of 10^{-6} to 10^{-4} torr within the oven. The oven is silver plated to resist alkali corrosion.²⁷ The vapor is entrained in a flow of inert carrier gas and introduced into the flow tube through a 10-cm section of 19-mm o.d. silver tubing. The sodium vapor is further diluted by the carrier gas in the main flow tube so that the sodium concentration within the reaction zone is always less than 10^{10} cm^{-3} . For wall removal rate measurements the entire oven assembly may be placed downstream of the mullite arrays as a movable source. Since the oven is heated, it warms the main carrier gas flow slightly. Axial temperature surveys in the reaction region show that the final flow temperature profile is uniform at a value of 308 K.

Sodium hydroxide is produced via the reaction

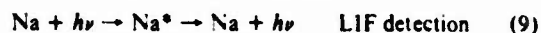
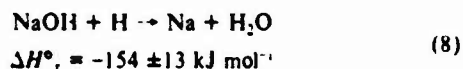


The H_2O_2 is added upstream of the mullite arrays with the main carrier gas. An all glass and teflon inlet system is used to prevent decomposition of H_2O_2 between its reservoir and the flow tube. Flow rates of H_2O_2 are determined by entraining the vapor in a measured helium flow at a known total reservoir pressure, where

$$\text{H}_2\text{O}_2 \text{ flow} = (P_{\text{H}_2\text{O}_2}/P_{\text{total}})(\text{He flow through system}) \quad (7)$$

The partial pressure of H_2O_2 at 25 °C is 2.0 torr.

Detection of NaOH is accomplished by converting it back to atomic sodium in the detection region, where the sodium is measured by laser-induced fluorescence (LIF). This conversion is accomplished by injecting an excess of atomic hydrogen into the flow 2-cm upstream of the LIF detector.



The hydrogen atoms, produced by microwave discharge of pure molecular hydrogen, are introduced through a teflon-lined 6-mm-diameter tube. With the mean flow velocity of 1000 cm s^{-1} , the reaction time of hydrogen in the detector (t_d) is 2 ms. The atomic hydrogen concentration is estimated to be $2 \times 10^{14} \text{ cm}^{-3}$, by measuring the H_2 flow rate and assuming that 10% of the H_2 passing through the discharge dissociates,³¹ with no recombination³² or loss on the inlet tube walls.³¹

A Moletron DL14 nitrogen pumped dye laser is used for laser-induced fluorescence detection of Na. The laser-induced fluorescence data acquisition system and manipulation of data have been detailed elsewhere.¹¹ However, it should be noted that fluorescence is usually averaged over 100 laser pulses, accounting for nonfluorescent background signals and for pulse-to-pulse fluctuations in laser intensity. The combined signal-to-noise ratio for these measurements generally exceeds 25.

Purities of the chemicals used in these experiments are as follows: sodium metal, 99.95% (Alfa); helium, 99.995% (Northeast Cryogenics); hydrogen, 99.995% (Air Products); nitrogen, 99.998% (Northeast Cryogenics); and hydrogen chloride, 99.99% (Northeast Cryogenics). Hydrogen peroxide, obtained

(25) F. S. Rowland and Y. Makide, *Geophys. Res. Lett.*, **9**, 473 (1982).
(26) "JANAF Thermochemical Tables", The Dow Chemical Company, Midland, MI, 1970.

(27) N. Acquista and S. Abramowitz, *J. Chem. Phys.*, **51**, 2911 (1969).
(28) R. C. Schoonmaker and R. F. Porter, *J. Chem. Phys.*, **28**, 454 (1958).

(29) M. E. Gersh, J. A. Silver, M. S. Zahniser, C. E. Kolb, R. G. Brown, C. M. Gozewski, S. Kallelis, and J. C. Wormhoudt, *Rev. Sci. Instrum.*, **52**, 1213 (1981).

(30) A. Fontijn and W. Felder, *J. Phys. Chem.*, **83**, 24 (1979).

(31) W. E. Jones, S. D. MacKnight, and L. Teng, *Chem. Rev.*, **73**, 407 (1973).

(32) D. W. Trainor, D. O. Ham, and F. Kaufman, *J. Chem. Phys.*, **58**, 4599 (1973).

(33) J. A. Silver and C. E. Kolb, *J. Phys. Chem.*, **86**, 3240 (1982).

TABLE I: Typical Experimental Conditions

temp. K	308
flow velocity, m s ⁻¹	10.0
press., torr	2.0
[Na], cm ⁻³ (initial)	≤ 10 ¹⁰
[H ₂ O ₂], cm ⁻³	1.3 × 10 ¹³
[HCl], cm ⁻³	(1–4) × 10 ¹²
[H], cm ⁻³	2 × 10 ¹⁴

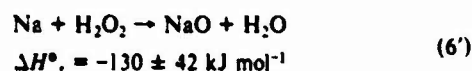
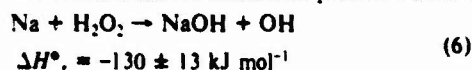
as a 90% (by weight) solution from FMC Corp., is purified by vacuum distillation. Titration with potassium permanganate indicates a resulting purity on the order of 99%. This corresponds to a purity in the vapor phase of ~93%, with the balance being water vapor.

Rate measurements are made with one reactant in excess of the other (detected) reactant, thus ensuring pseudo-first-order kinetic conditions. Reaction times are varied by changing the injector position at fixed total flow velocity and pressure. Corrections for both axial and radial diffusion and wall removal are made with the procedure outlined by Brown.³⁴ This method is based on a numerical solution of the equations describing diffusion and reaction in a flow tube. It assumes that Poiseuille flow exists and provides ranges for k , k_w (wall removal), and D (diffusion coefficient) for which the solutions have been shown to be valid. Wall removal rates of the measured species are determined in separate experiments by varying the oven position. The observed wall removal rate, as well as the reaction rate, is corrected for diffusion effects. Diffusion constants for alkali atoms and hydroxides were obtained from wall removal measurements in the instance where the observed disappearance of the species is diffusion limited.³⁵ At 308 K, $D(\text{Na-He}) = 0.50 \text{ atm cm}^2 \text{ s}^{-1}$ and $D(\text{NaOH-He}) = 0.47 \text{ atm cm}^2 \text{ s}^{-1}$.

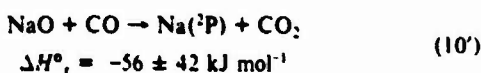
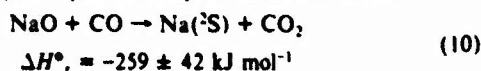
An important aspect of the data analysis is the ability to ensure that secondary reactions have no effect on the concentration of the species being monitored. This could dramatically affect the accuracy of the rate measurements. The effects of secondary reactions are determined by modeling the reactions occurring in the flow tube. This is done with the Aerodyne PACKAGE code,³⁶ a kinetic modeling program which numerically integrates the differential rate equations for a specified set of reactions. Backward reaction rates determined from the JANAF thermochemical tables and the forward rates are included, to ensure that accuracy is maintained.

Results

Na + H₂O₂ Reaction. The NaOH formation rate was measured by directly observing the disappearance of sodium, with H₂O₂ in known excess. The reaction has two exothermic product channels



so what is measured by monitoring Na disappearance is the total reaction rate. However, one can add excess CO (~2 × 10¹⁵ cm⁻³), which rapidly and quantitatively converts NaO to Na³⁷⁻³⁸



(34) R. L. Brown, *J. Res. Natl. Bur. Stand.*, **83**, 1 (1978)

(35) J. A. Silver, manuscript in preparation.

(36) V. Yousefian, M. H. Weinberg, and R. Haines, "PACKAGE: A Computer Program for Calculation of Partial Chemical Equilibrium/Partial Finite Chemical Rate Controlled Composition of Multiphased Mixtures Under One Dimensional Steady Flow", Aerodyne Research, Inc., Report No. ARJ-RR-177, Feb 1980.

(37) C. P. Fenimore and J. R. Kelso, *J. Am. Chem. Soc.*, **72**, 5045 (1950)

(38) R. C. Benson, C. B. Barger, and R. E. Walker, *Chem. Phys. Lett.*, **35**, 161 (1975)

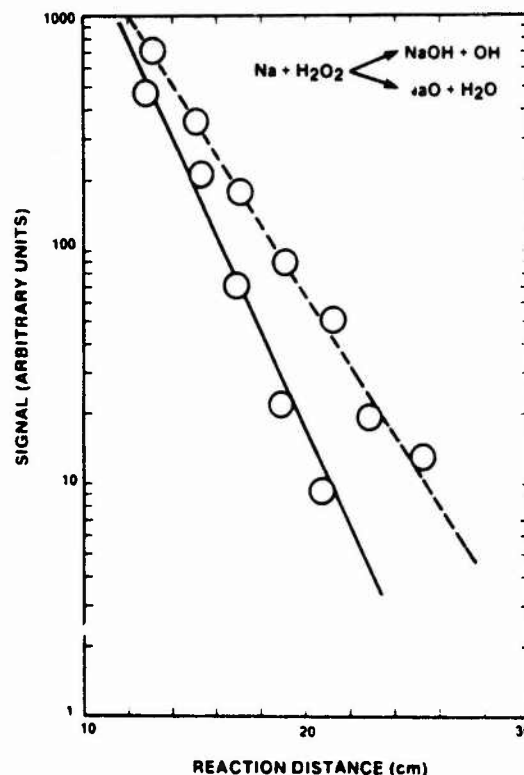
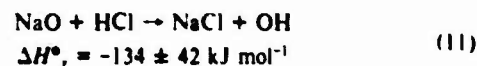


Figure 3. Pseudo-first-order decays for Na + H₂O₂ reaction. The solid line is the total reaction rate; the dashed line is the rate for branching to NaOH only (CO added).

Although the value for k_{10} has not been measured, indirect estimates from ref 37 imply $k_{10} \geq 10^{-11} \text{ cm}^3 \text{ molecule}^{-1} \text{ s}^{-1}$. The large amount of CO added is required to ensure that all of the NaO cycles back to Na on a time scale much shorter than the time required for reaction 6 to occur.

A rate measurement with CO present results in the production rate for only the NaOH branch. The results of these measurements are shown in Figure 3. Experimental conditions are given in Table I. The rate constant for both channels is $k_{6+6'} = (6.9 \pm 3.0) \times 10^{-11} \text{ cm}^3 \text{ molecule}^{-1} \text{ s}^{-1}$, and the fraction in the NaOH product channel is 0.61 ± 0.10 . The major uncertainty in the rate constants k_6 and k_6' is the H₂O₂ concentration, which is not directly measured but is obtained as indicated earlier.

An independent determination of the product branching ratio for reaction 6 is obtained by observing the hydroxyl radical via laser-induced fluorescence at 308.6 nm. When Na reacts with H₂O₂, only the NaOH product channel produces OH. However, when excess HCl is added to the NaO and NaOH product mixture, additional OH is formed by the reaction



Thus a measurement of the amounts of OH produced before and after addition of HCl provides the relative amounts of NaOH and NaO originally formed from Na + H₂O₂. The observed NaOH product fraction by this method is 0.60 ± 0.10 , in excellent agreement with the value obtained from the rate measurements.

NaOH + HCl Reaction. In the presence of excess CO, the reaction of sodium with hydrogen peroxide produces only NaOH. With this reaction used as a source for NaOH, a series of rate measurements were made for the reaction of NaOH with HCl. First-order decays were linear for more than a factor of 10 in fluorescence signal, with the HCl concentrations ranging from 1×10^{12} to $4 \times 10^{12} \text{ cm}^{-3}$. The results of these experiments are shown in Figure 4, and the rate constant for this reaction is $k_7 = (2.8 \pm 0.9) \times 10^{-10} \text{ cm}^3 \text{ molecule}^{-1} \text{ s}^{-1}$. The uncertainty expressed includes estimated precision errors at a 95% confidence level, as well as estimated errors in accuracy.

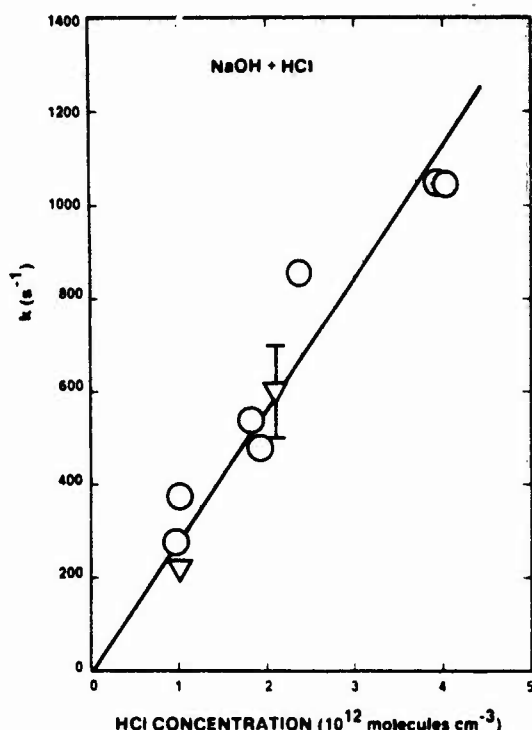
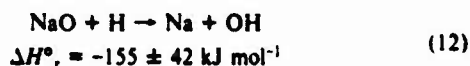


Figure 4. First-order reaction rates vs. $[HCl]$ for the reactions of NaOH (NaO) + HCl: (O) without CO added; (▽) with CO added.

Separate measurements were also made without adding CO. In this case NaO, in addition to NaOH, is present and reacts with HCl (reaction 11), complicating the analysis. Furthermore, the detection scheme, based on conversion to Na by addition of atomic hydrogen, would not appear to distinguish between NaO and NaOH, since Na atoms are also produced in the reaction



Thus, without CO, the decrease in signal upon addition of HCl is due to both reactions 2 and 11, weighted by the branching ratio from reaction 6,6'. The results, however, show the same decay with and without added CO (see Figure 4), implying that both NaO and NaOH react with HCl at approximately the same rate. This observation is reasonable if one considers the hydroxyl group on NaOH to act as a quasi-atom in respect to its chemical behavior given identical exothermicities for both reactions.

Separate OH measurements confirm that atomic hydrogen reacts with NaO as well as with pure NaOH. Although we could not measure the NaO + HCl rate constant directly, the observation that (1) OH is formed in the NaO + H reaction (proving the existence of NaO), (2) OH is also formed upon addition of HCl to NaO, and (3) the decay rates with added HCl are identical both with or without CO, imply that NaO reacts with HCl at approximately the same rate as NaOH with HCl.

Detector Corrections and Modeling. Although the plots of $\ln(\text{signal})$ vs. reaction time are linear over the first order of magnitude decrease in signal, at longer times they flatten out at a value typically a few percent of the initial (zero reaction time) signal (Figure 5). This effect can be attributed to an additional component to the Na signal from the reaction



For the case with CO present, sodium formed in the detection region by addition of atomic hydrogen has two sources. NaOH and NaCl, the amount of each depending on the extent to which the NaOH + HCl \rightarrow NaCl + H₂O reaction has gone to completion. The rate equation for the formation of sodium in the detector is

$$d[\text{Na}]/dt = k_8[\text{NaOH}]_d[\text{H}] + k_{11}[\text{NaCl}]_d[\text{H}] \quad (14)$$

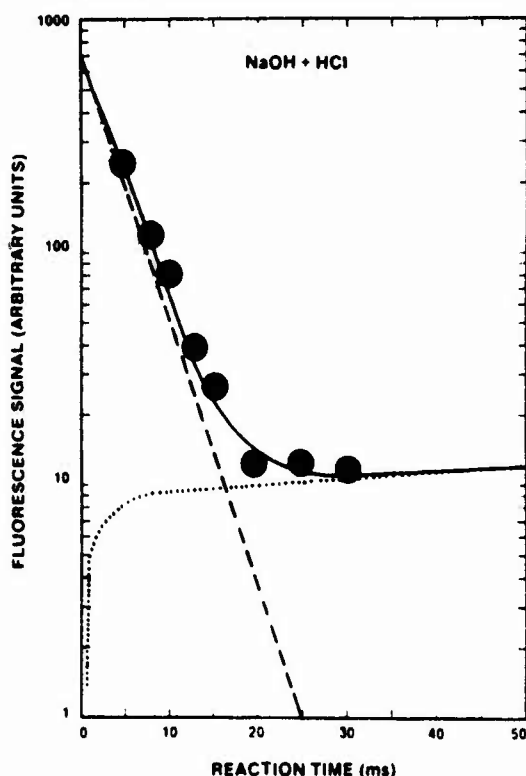


Figure 5. Typical decay of fluorescence signal vs. reaction time for NaOH + HCl, showing contribution to total detected sodium (—) from NaOH (---) and NaCl (.....). Circles are experimental data.

where the d subscript indicates the concentration at the entrance to the detector zone. Integrating over the detector reaction time (t_d), assuming excess hydrogen, we obtain

$$[\text{Na}] = [\text{NaOH}]_d(1 - e^{-k_8[\text{H}]t_d}) + [\text{NaCl}]_d(1 - e^{-k_{11}[\text{H}]t_d}) \quad (15)$$

If no HCl is added, the observed LIF signal arises solely from NaOH. We have observed that this signal (after correcting for differences in diffusion and wall removal between Na and NaOH) is identical with that arising from only sodium (i.e., without H₂O₂ added). This means that, within the available detector reaction time, all of the NaOH is converted to sodium, with an estimated error of 20%. This sets a lower limit to $k_8[\text{H}]t_d$. Given $t_d = 2$ ms and $[\text{H}] \approx 2 \times 10^{14} \text{ cm}^{-3}$, this requires that $k_8 \geq 4 \times 10^{12} \text{ cm}^3 \text{ molecule}^{-1} \text{ s}^{-1}$. The accuracy of t_d is ± 0.5 ms. If less than 10% of the H₂ is dissociated (it is unlikely to be higher under our operating conditions), then k_8 is faster than the stated limit.

This value for k_8 is in reasonable agreement with a value of $1 \times 10^{12} \text{ T}^{1/2}$ ($1.7 \times 10^{11} \text{ cm}^3 \text{ molecule}^{-1} \text{ s}^{-1}$ at 300 K) which is used by Hynes et al.¹⁷ in fitting their flame data over a wide range of conditions, and also with $2 \times 10^{11} e^{-4000/T}$ (1.4×10^{12} at 300 K), which is used in various atmospheric models.^{10,13} The former value is claimed to be accurate to within a factor of two at flame temperatures, and the latter is only an estimate. We are planning to perform direct measurements of this reaction in the near future.

Now if we measure the reaction rate of NaOH + HCl, at short reaction times the decay in signal is logarithmic because $[\text{NaOH}]_d > [\text{NaCl}]_d$, and only the first term in eq 15 is significant. At long reaction times, $[\text{NaCl}]_d > [\text{NaOH}]_d$ and the second term becomes dominant (Figure 5). If $k_{11} = k_8$, we would never observe a decay in $[\text{Na}]$ since both terms in eq 15 would always have the same sum. However, the fact that an initial decay is observed with a later leveling of signal shows that $k_{11} \ll k_8$ and, from the relative value of the signal where it levels off, we can estimate k_{11} .

To determine k_{11} , we modeled this reaction system using the conditions in Table II and rate set in Table III. This rate set is more extensive than the above discussion implies because there could be secondary reactions between the excess H₂O₂ and the sodium formed in the detector, as well as other minor OH, H,

TABLE II: Initial Conditions Used in Chemical Model

temp, K	308
flow velocity, m s ⁻¹	10.0
press., torr	2.0
[Na], cm ⁻³ (initial)	10 ¹⁰
[H ₂ O ₂], cm ⁻³	1.3 × 10 ¹³
[HCl], cm ⁻³	1.93 × 10 ¹²
[H] _a , cm ⁻³	2 × 10 ¹³ –1 × 10 ¹⁵
[H ₂] _a , cm ⁻³	10 ¹⁵ –10 ¹⁶
[H ₂ O], cm ⁻³	7 × 10 ¹¹
t _{run} , ms	0–25
t _d , ms	0.5–4.0

TABLE III: Reaction Rate Set Used for Modeling Na Chemistry^a

reaction	k, cm ³ molecule ⁻¹ s ⁻¹	ref
Na + H ₂ O ₂ → NaOH + OH	6.9 (–11)	b
NaOH + HCl → NaCl + H ₂ O	2.8 (–10)	b
NaOH + H → Na + H ₂ O	1.0 (–10)–1.0 (–14)	b
NaCl + H → Na + HCl	1.0 (–10)–1.0 (–14)	b
Na + HO ₂ → NaOH + O	1.0 (–10)	est
2HO ₂ → H ₂ O ₂ + O ₂	1.6 (–12)	39
O + H ₂ O ₂ → OH + HO ₂	1.0 (–11)e ^{-2500/T}	40
OH + H ₂ O ₂ → H ₂ O + HO ₂	2.96 (–12)e ^{-164/T}	41
H + H ₂ O ₂ → H ₂ + HO ₂	2.13 (–12)e ^{-1400/T}	42
H + H ₂ O ₂ → OH + H ₂ O	2.76 (–12)e ^{-1400/T}	42
H ₂ + OH → H + H ₂ O	7.7 (–12)e ^{-2100/T}	40
H ₂ + O → H + OH	1.6 (–11)e ^{-4570/T}	40
OH + HO ₂ → H ₂ O + O ₂	8.0 (–11)	40
H + HO ₂ → 2OH	3.2 (–11)	40
H + HO ₂ → H ₂ + O ₂	1.4 (–11)	40
H + HO ₂ → H ₂ O + O	9.4 (–13)	40
O + HO ₂ → O ₂ + OH	8.0 (–11)e ^{-500/T}	40
2OH → O + H ₂ O	1.8 (–12)	40
HCl + OH → H ₂ O + Cl	6.6 (–13)	40

^aNo three-body rates were used because the system is at low pressure. ^bThis work.

etc. reactions. This model also includes the undissociated hydrogen, and the water impurity (~7%) in the H₂O₂. We systematically varied k_9 , k_{13} , [H], [H₂O₂], and t_d . The results show that all secondary reactions have little effect (<5%) on the calculated sodium densities and that the variations of Na with [H₂O₂] and [H₂] are small, in reasonable agreement with additional experiments. The value for k_{13} which best fits the experimental data is $(8 \pm 3)/[H]$, which leads to value of k_{13} in the range 1×10^{-14} to 5×10^{-13} cm³ molecule⁻¹ s⁻¹, with a best estimate of 5×10^{-14} cm³ molecule⁻¹ s⁻¹. In light of the small exothermicity for this reaction, this value is not unreasonable. If the rate constant is expressed in the Arrhenius form, $k = Ae^{-E/RT}$, this would correspond to only a 21 kJ mol⁻¹ barrier, even with a gas kinetic preexponential term.

Discussion

The reaction rate constant of HCl with NaOH is found to be in its gas kinetic limit. Given the large exothermicity, absence of obvious steric effects, and the fact that reactant and product states correlate on a singlet potential energy surface, one might not consider this surprising. On the other hand, the strong covalent HCl bond must be broken during the reaction with an efficiency approaching unity. One can calculate a rate constant for this reaction using simple close collision theory.⁴¹ This procedure assumes that the attractive portion of the intermolecular potential varies as C/r^6 , where C depends on the dipole moments and static polarizabilities of the reactants,⁴⁴ and r is the intermolecular

distance. The total effective potential energy curve at large r is this attractive portion plus a centrifugal term which accounts for orbital angular momentum. The rate of close collisions is identified as applying to collisions with total energy sufficient to surmount the orbital angular momentum barrier in this effective potential energy curve. If it is assumed that all close collisions react, and that there is no activation energy, the rate constant calculated for NaOH + HCl is 1.8×10^{-10} cm³ molecule⁻¹ s⁻¹, in good agreement with the measured value.

Few gas-phase reactions of alkali molecules have been studied, none involving alkali hydroxides. The alkali-hydroxide bond is ionic in character, so that (OH) is a closed-shell species, not dissimilar to its isoelectronic and isobaric analogue, F⁻. Thus, in absence of data on NaOH, we can use available information on NaF and other alkali halides to try to understand the properties of the alkali hydroxides. There have been a number of molecular beam scattering measurements of alkali halides with other alkali halides or hydrogen halide molecules.⁴⁵ As a class, they all imply the existence of a strong collision complex. In the case of CsCl + KI → CsI + KCl, the reaction proceeds without any activation energy (despite being four-centered) and has a large total cross section.⁴⁶ This has been explained by the large ionic character of both species and by the fact that alkali halide dimers have large binding energies in the geometry of a cyclic planar rhomboid.⁴⁵ This ion-pair intermediate formulation has also been invoked in describing the BaI₂ + HCl reaction,⁴⁷ where, for large alkaline earths such as barium, we can treat BaI₂ as (BaI)⁺I⁻. What we can draw from these comparative systems is that a gas kinetic rate constant without any activation barrier is a reasonable expectation for this system. In the extrapolation of the measured rate data to lower temperatures characteristic of the stratosphere, one would not expect any great dependence on temperature for the reaction rate.

The importance of reaction 2 in stratospheric ozone chemistry may be estimated by comparing the Cl regeneration rates from HCl via reaction with OH with regeneration rates from reaction with NaOH followed by photolysis of NaCl. Estimates of stratospheric NaCl photolysis rates by Rowland and Rogers²⁴ are in the range from 10⁻² to 10⁻³ s⁻¹. At 40 km, the meteoric sodium is partitioned among the species NaOH, NaO₂, and NaO. Estimates of total stratospheric sodium concentrations by Liu and Reed¹⁰ are on the order of 5×10^4 cm⁻³. If all of the meteoric sodium were in the form of NaOH at 40 km, our measurement of k_2 would give a first-order rate constant for Cl formation of 1.4×10^{-4} s⁻¹, providing that J_{NaCl} is in the range estimated by Rowland and Rogers. This is a factor of ~20 faster than the first-order rate constant for Cl regeneration from OH + HCl of 6×10^{-6} s⁻¹, based on an OH concentration of 10⁷ cm⁻³ and the value $k_4(250\text{ K}) = 5.7 \times 10^{-13}$ cm³ molecule⁻¹ s⁻¹.⁴⁸ Although the partitioning of total sodium among NaOH, NaO, and NaO₂ requires a more detailed knowledge of rate constants for the processes shown in Figure 1, this calculation demonstrates that, even if only 5% is in the form of NaOH, regeneration of Cl from HCl via alkali chemistry would be comparable to regeneration by the OH reaction.

This simple computation leads us to two conclusions. First, our results for this and the other alkali reactions described show that meteoric metal reactions may have a potentially significant impact on our understanding of chemistry in the mesosphere and upper stratosphere. The large values of the sodium rate constants measured in this study emphasize this possibility. Secondly, it clearly motivates the need for further investigation of this chem-

(39) S. P. Sander, M. Peterson, R. T. Watson, and R. Patrick, *J. Phys. Chem.*, **86**, 1236 (1982).

(40) D. L. Baulch, R. A. Cox, P. J. Crutzen, R. F. Hampson, Jr., J. A. Kerr, J. Troe, and R. T. Watson, *J. Phys. Chem. Ref. Data*, **11**, 327 (1982).

(41) U. C. Sridharan, B. Reimann, and F. Kaufman, *J. Chem. Phys.*, **73**, 1286 (1980).

(42) R. F. Hampson, U.S. Department of Transportation, Report No. FAA-EE-80-17, 1980.

(43) H. S. Johnston, "Gas Phase Reaction Rate Theory", Ronald Press, New York, 1966, Chapter 9.

(44) J. O. Hirschfelder, C. F. Curtiss, and R. B. Bird, "Molecular Theory of Gases and Liquids", Wiley, New York, 1964.

(45) R. R. Herm in "Alkali Halide Vapors", P. Davidovits and D. I. McFadden, Ed., Academic Press, New York, 1979, Chapter 6, and references therein.

(46) W. B. Miller, S. A. Safran, and D. R. Herschbach, *J. Chem. Phys.*, **56**, 3581 (1972).

(47) A. Freedman, R. Behrens, Jr., T. P. Parr, and R. R. Herm, *J. Chem. Phys.*, **65**, 4739 (1976).

(48) M. S. Zahniser, F. Kaufman, and I. Anderson, *Chem. Phys. Lett.*, **27**, 507 (1974).

istry, via detailed models, additional laboratory measurements of reaction rate constants and photolysis cross sections, and direct measurement of molecular sodium concentration profiles in the upper atmosphere.

Acknowledgment. The authors thank Drs. F. Kaufman, M. McElroy, and E. Murad for their helpful discussions and insights.

and W. Goodwin for his excellent technical assistance. This work was supported by the Chemical Manufacturers Association under Contract No. FC82-401, by the Air Force Geophysics Laboratory under Contract No. F19628-83-C-0010, and by the Army Research Office under Contract No. DAAG29-81-C-0024.

Registry No. NaOH, 1310-73-2; HCl, 7647-01-0

SECTION 5

GAS-PHASE REACTION RATE OF SODIUM SUPEROXIDE
WITH HYDROCHLORIC ACID

Prepared by

J.A. Silver* and C.E. Kolb
Center for Chemical and Environmental Physics
Aerodyne Research, Inc.
45 Manning Road
Billerica, MA 01821

Prepared for

Journal of Physical Chemistry

October 1985

*Present address: Southwest Sciences, Inc.
1570 Pacheco St., Suite E-11
Santa Fe, NM 87501

GAS-PHASE REACTION RATE OF SODIUM SUPEROXIDE WITH HYDROCHLORIC ACID

J.A. Silver* and C.E. Kolb
Center for Chemical and Environmental Physics
Aerodyne Research, Inc.
45 Manning Road
Billerica, MA 01821

ABSTRACT

Metal compounds originating from meteor ablation may be an additional mechanism for the release of free chlorine from HCl in the stratosphere. For the alkali metals, and sodium in particular, catalytic chemical pathways have been postulated which describe these processes. A critical step in this mechanism is the reaction of NaO_2 with HCl. We have measured the rate constant for this reaction in a fast-flow reactor at 295 K and find it to be $(2.3 \pm 0.4) \times 10^{-10} \text{ cm}^3 \text{ molecule}^{-1} \text{ s}^{-1}$. The implication of this result on stratospheric ozone chemistry is discussed.

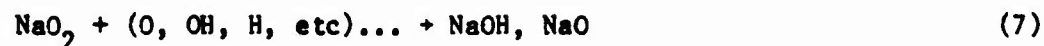
Present address: Southwest Sciences, Inc.
1570 Pacheco St., Suite E-11
Santa Fe, NM 87501

INTRODUCTION

In the past few years, a number of experimental rate constant measurements have been completed¹⁻⁵ which support the contention that alkali metals originating from meteor ablation may have a significant role in determining the extent to which ozone might be depleted by chlorine compounds in the upper stratosphere.⁶⁻⁷ This would be accomplished by the sodium catalyzed release of free chlorine from the inactive HCl stratospheric reservoir at a rate comparable to the major recognized reaction



The chemistry of alkali metals in the lower thermosphere and upper stratosphere has been discussed elsewhere,^{1,8-14} and will only be highlighted here. Metals (in particular, sodium) volatilized during meteor entry into the earth's atmosphere are oxidized and enter the upper stratosphere as a mixture of NaO_2 , NaO , and NaOH . The suggested catalytic cycle for release of free chlorine comes as a result of the reaction of these species with HCl, and their subsequent regeneration on a time scale comparable to that of reaction 1.



Recent kinetic measurements on reactions 3, 4, and 6 indicate that these proceed rapidly.¹⁻⁴ Estimates of the photolysis rates of NaCl,⁷ based on high temperature absorption cross section measurements,¹⁵ are also relatively fast ($10^{-2} - 10^{-3} \text{ s}^{-1}$), so that the potential rate limiting step(s) to this process is the conversion of NaO₂ to NaCl, either directly through reaction 2, or indirectly via step 7 and reactions 3 and 4. If the overall rate constant for Cl formation of either of these is comparable to that for reaction 1 ($k_1 \cdot [\text{OH}] \approx 10^{-6} \text{ s}^{-1}$), then the presence of alkali metals may indeed impact stratospheric ozone levels.

The purpose of this study is to provide a measurement of the rate constant for the direct path, i.e., the reaction of NaO₂ + HCl → NaCl + HO₂. The results of this measurement should help confirm whether or not meteor metals could play a significant role in stratospheric ozone chemistry.

EXPERIMENTAL SECTION

The fast-flow reactor and experimental techniques used in these experiments have been fully described in previous papers.^{1,16} Briefly, the flow reactor is a 7.26-cm-diameter, 120-cm-long alumina tube with four perpendicular side arms at the tube exit which permit optical detection of the reactive species. Helium carrier gas is added at the entrance of the flow tube through mullite multichannel arrays which laminarize the flow. Gas volumetric flow rates are determined with calibrated thermal conductivity type mass flow meters. Flow rates of hydrogen chloride are determined by diverting the flow into a calibrated volume, and then measuring the rate of pressure increase. A calibrated MKS Baratron Model 310-BSH10 capacitance manometer (0.8% accuracy) is used to measure pressure.

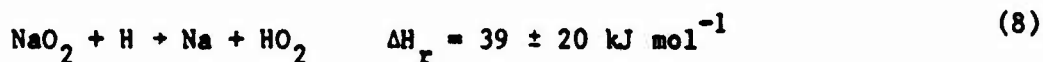
Sodium atoms are generated by heating the sample in a 2.5-cm-diameter cylindrical monel oven to a temperature commensurate with attaining a vapor pressure of that species of 10^{-6} to 10^{-4} torr within the oven. The oven is enclosed in a 4-cm-diameter water-cooled sheath to prevent heating of the main flow carrier gas. The vapor is entrained in a flow of inert carrier gas and introduced directly into the flow tube. The sodium vapor is further diluted by the carrier gas in the main flow tube so that the sodium concentration within the reaction zone is always less than 10^{10} cm^{-3} .

Sodium superoxide is produced via the termolecular reaction



where $M = \text{He}$ and $k_5(\text{He}) = 1.4 \times 10^{-30} \text{ cm}^6 \text{ s}^{-1}$ at 295 K.² Molecular oxygen ($\sim 10^{15} \text{ cm}^{-3}$) is added to the carrier gas in the flow tube and reacts rapidly under the conditions present (2.07 torr, 295 K), so that conversion of Na to NaO_2 is essentially complete before reaching the region where HCl is injected into the flow.

Detection of NaO_2 is accomplished by converting it back to atomic sodium in the detection region, where it is measured by resonance fluorescence. This conversion is done by injecting an excess of atomic hydrogen into the flow 2-cm upstream of the detection volume.



The hydrogen atoms, produced by microwave discharge of pure molecular hydrogen, are introduced through a 6-mm-diameter quartz tube, whose inner walls are coated with syrupy phosphoric acid. With the mean flow velocity of 920 cm s^{-1} , the reaction time of hydrogen in the detector (t_d) is $\sim 2 \text{ ns}$. The atomic hydrogen concentration is estimated to be $2 \times 10^{14} \text{ cm}^{-3}$, by measuring the H_2 flow rate and assuming that 10% of the H_2 passing through the discharge dissociates, with no recombination¹⁷ or loss on the inlet tube walls.¹⁸

Resonance fluorescence is accomplished using a 25-Watt Spectroline sodium resonance lamp and phase-sensitive detection techniques. The data are fed directly into an IBM/XT computer for processing. Purities of the chemicals used in these experiments are as follows: sodium metal, 99.95% (Alfa); helium, 99.995% (Northeast Cryogenics); oxygen 99.993% (Northeast Cryogenics); hydrogen, 99.995% (Air Products); and hydrogen chloride 99.99% (Northeast Cryogenics).

Rate measurements are made with $[\text{HCl}] \gg [\text{NaO}_2]$, thus ensuring pseudo-first-order kinetic conditions. Reaction times were varied from 1 to 15 ms by changing the injector position. Data analysis and corrections for wall loss and diffusion effects were performed as described in our previous work on the reactions of NaO and NaOH with HCl^{1,19}. The diffusion coefficient for NaO₂ in helium was estimated to be $0.3 \text{ cm}^2 \text{ s}^{-1}$ at 1 atm, but in fact, the correction for diffusion was quite insensitive to this value (i.e., less than one percent difference if $0.4 \text{ cm}^2 \text{ s}^{-1}$ was used).

RESULTS

Decay of NaO₂ for seven concentrations of HCl covering the range $1.02 - 41.9 \times 10^{11} \text{ cm}^{-3}$ are shown in Figure 1. The first order decay rates obtained from the slopes of these lines and corrected for diffusion effects are plotted versus the corresponding HCl concentration in Figure 2. A least-squares fit to the slope of this line, weighted by the uncertainties in each point, results in a value of the rate constant for this reaction of $(2.3 \pm 0.4) \times 10^{-10} \text{ cm}^3 \text{ molecule}^{-1} \text{ s}^{-1}$. The uncertainty expressed in this expression

includes precision errors (one standard deviation), as well as estimated errors in accuracy.

In previous measurements of this type,¹ corrections to the data were required to account for the reaction of NaCl product with the atomic hydrogen titrant,



We had estimated the rate constant for this reaction as $5 \times 10^{-14} \pm 1$ cm³ molecule⁻¹ s⁻¹. In these experiments, the decays were observed for reaction times varying between one and fifteen milliseconds, and under these conditions, reaction 10 has insufficient time to proceed enough to require any data corrections.

DISCUSSION

Similar to NaO and NaOH, NaO₂ reacts with HCl with a rate constant near its gas kinetic limit. Although the first two reactions are considerably exothermic (133 ± 13 kJ mole⁻¹ and 134 ± 42 kJ mole⁻¹, respectively), the last is most probably barely exothermic by 19 ± 21 kJ mole⁻¹. Since the NaO₂ bond is strongly ionic,²⁰ one might explain its reactivity with HCl in a manner similar to that given for NaOH and NaO,¹ for the alkaline earth dihalides with Cl₂ and HCl,²¹ and for cesium halides with Cl₂ and ICl.²² In all of these examples, large dipole-dipole and dipole-induced dipole interactions provide strong long-range forces which lead to the formation of an ion-pair adduct, allowing a facile exchange reaction. In this case the adduct would likely be

$\text{Na}^+(\text{HOOC}\text{Cl})^-$. Although the $(\text{HOOC}\text{Cl})^-$ species has not been observed, it is analogous to the $(\text{HOOH})^-$ ion, which has indirectly been shown to exist, although its exact structure is unknown.²³

Demonstration of a nearly gas kinetic reaction rate constant for $\text{NaO}_2 + \text{HCl}$ supports the possibility that a sodium catalyzed Cl regeneration mechanism can be fast enough to compete with the $\text{OH} + \text{HCl}$ reaction in the upper stratosphere. Estimates of total stratospheric sodium concentrations by Liu and Reid²⁴ are on the order of $5 \times 10^5 \text{ cm}^{-3}$. If most of the sodium is in the form of NaOH , NaO_2 , or NaO , then the measured rate constants for reactions 2-4 result in a first-order rate constant for Cl release of $\sim 1 \times 10^{-4} \text{ s}^{-1}$, much larger than the 10^{-6} s^{-1} required for competition with reaction 1. Given the results of this work, and a recent study of room temperature NaCl photolysis rates,²⁵ the rate limiting step for the mechanism given by reactions 2-7 may be the photolysis of NaCl , so that it is probable that only ~ 1 -10% of the daytime molecular sodium is in the above molecular forms. Even at this level, this Cl release mechanism could be competitive with reaction 1.

One must also consider both homogeneous and heterogeneous loss mechanisms for gas phase alkali, which are all poorly understood. Homogeneous losses could include NaCl polymerization²⁶ and ionization/cluster formation,²⁷ while heterogeneous losses might include condensation onto small particulates²⁸ or liquid droplets at lower altitudes. The degree of alkali loss at the present time is uncertain, but if only 10% of the stratospheric alkali is left unscavenged, then the catalytic release of free chlorine by ablated meteor metals could still be significant on the upper stratospheric ozone balance.

ACKNOWLEDGEMENTS

The authors gratefully acknowledge the many insightful discussions with and the contributions of the late Dr. Fred Kaufman, and will miss him greatly. This work was supported by the Fluorocarbon Program Panel of the Chemical Manufacturers Association under Contract No. FC-84-494 and the Air Force Geophysics Laboratory under Contract No. F19628-83-C-0010, and the Army Research Office under Contract No. DAAG 29-81-C-0024.

REFERENCES

1. J.A. Silver, A.C. Stanton, M.S. Zahniser, and C.E. Kolb, J. Phys. Chem., 1984, 88, 3123.
2. J.A. Silver, M.S. Zahniser, A.C. Stanton, and C.E. Kolb, Symp. (Int.) Combust. [Proc.], 20th, 1984, 605.
3. D. Husain, P. Marshall, and J.M.C. Plane, J. Chem. Soc. Faraday Trans., 1985, 81, 301.
4. A.J. Hynes, M. Steinberg, and K. Schofield, J. Chem. Phys., 1984, 80, 2585.
5. J. Ager and C.J. Howard, U. Colorado, Boulder (Private Communication).
6. E. Murad, W. Swider, and S.W. Benson, Nature (London), 1981, 289, 273.
7. F.S. Rowland and P.J. Rogers, Proc. Natl. Acad. Sci. U.S.A., 1982, 79, 2737.
8. E. Murad, J. Geophys. Res., 1978, 83, 5525.
9. T.L. Brown, Chem. Rev., 1973, 73, 645.
10. J.E. Blamont and T.M. Donahue, J. Geophys. Res., 1964, 69, 4093.
11. D.M. Hunten, Space Sci. Rev. 1967, 6, 493.
12. (a) V.W.J.H. Kirchhoff, B.R. Clemesha, and D.M. Simonich, J. Geophys. Res., 1979, 84, 1323; (b) D.R. Bates and P.C. Ojha, Nature (London), 1980, 286, 790.
13. E.E. Ferguson, Geophys. Res. Lett., 1978, 5, 1035.
14. E. Murad and W. Swider, Geophys. Res. Lett., 1979, 6, 929.
15. P. Davidovits and D.C. Brodhead, J. Chem. Phys., 1967, 46, 2968.

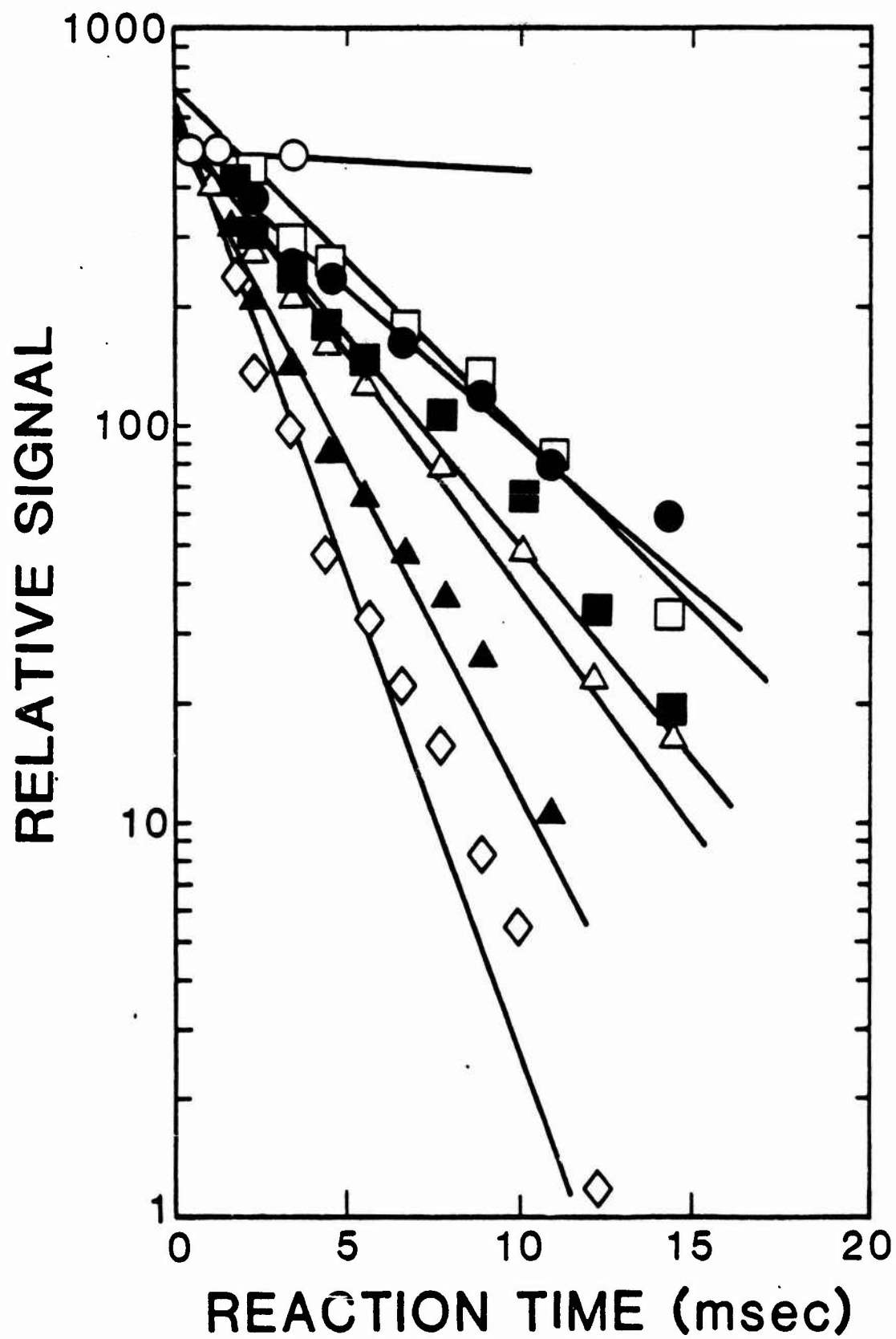
16. M.E. Gersh, J.A. Silver, M.S. Zahniser, C.E. Kolb, R.G. Brown, C.M. Gozewski, S. Kallelis, and J.C. Wormhoudt, *Rev. Sci. Instrum.*, 1981, 52, 1213.
17. D.W. Trainor, D.O. Ham, and F. Kaufman, *J. Chem. Phys.*, 1973, 58, 4599.
18. W.E. Jones, S.D. MacKnight, and L. Teng, *Chem. Rev.*, 1973, 73, 407.
19. J. Silver, *J. Chem. Phys.*, 1984, 81, 5125.
20. M.H. Alexander, *J. Chem. Phys.*, 1978, 69, 3502.
21. A. Freedman, R. Behrens, Jr., T.P. Parr, and R.R. Herm, *J. Chem. Phys.*, 1976, 65, 4739.
22. D.L. King and D.R. Herschbach, *Discuss. Faraday Soc.*, 1973, 55, 334.
23. F.C. Fehsenfeld and E.E. Ferguson, *J. Chem. Phys.*, 1974, 61, 3181.
24. S.C. Liu and G.C. Reid, *Geophys. Res. Lett.*, 1979, 6, 283.
25. J.A. Silver, D. Worsnop, A. Freedman, and C.E. Kolb, *J. Chem. Phys.*, in press, 1986.
26. J. Lamb and S. Benson, *J. Geophys. Res.*, in press, 1986.
27. A.C. Aiken, *Nature (London)*, 1981, 291, 638.
28. D.M. Hunten, R.P. Turco, and O.B. Toon, *J. Atmos. Sci.*, 1980, 37, 1342.

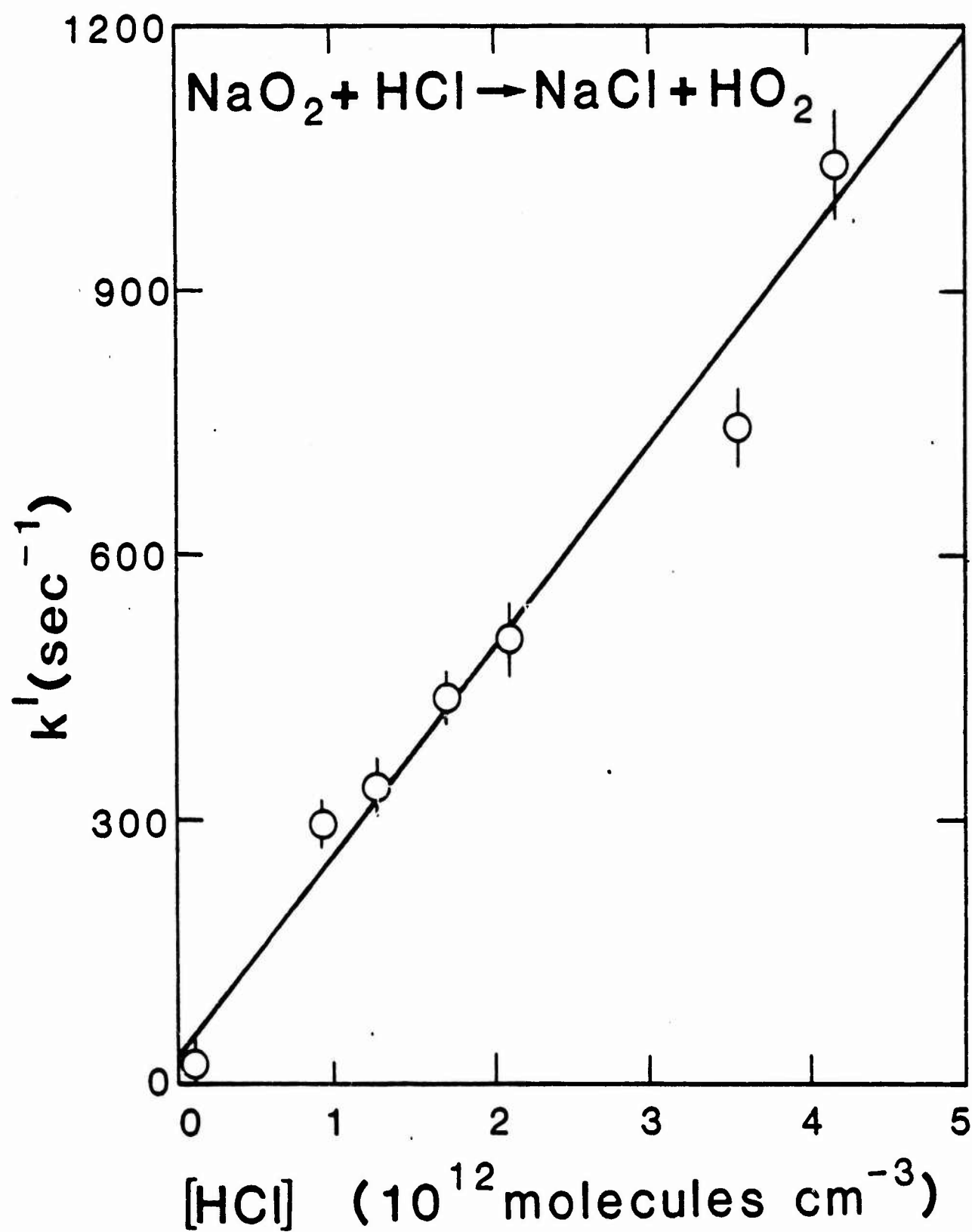
FIGURE CAPTIONS

Figure 1. Pseudo-first-order decays for $\text{NaO}_2 + \text{HCl}$ reaction.

$[\text{HCl}] = 1.02$ (\bigcirc), 9.21 (\bullet), 12.6 (\square), 17.0 (\blacksquare), 20.9 (\triangle),
 35.5 (\blacktriangle), 41.9 (\diamond); units of 10^{11} molecules cm^{-3}

Figure 2. Dependence of corrected pseudo-first-order rate constant on HCl concentration at 295 K.





SECTION 6

ABSOLUTE PHOTODISSOCIATION CROSS SECTIONS OF
GAS-PHASE SODIUM CHLORIDE
AT ROOM TEMPERATURE

Prepared by:

J.A. Silver*, D.R. Worsnop,
A. Freedman, and C.E. Kolb
Center for Chemical and Environmental Physics
Aerodyne Research, Inc.
45 Manning Road
Billerica, MA 01821

Prepared for:

The Journal of Chemical Physics

November 1985

*Present Address: Southwest Sciences, Inc.
1570 Pacheco St., Suite E-11
Santa Fe, NM 87501

ABSOLUTE PHOTODISSOCIATION CROSS SECTIONS OF GAS-PHASE SODIUM
CHLORIDE AT ROOM TEMPERATURE

Joel A. Silver*, Douglas R. Worsnop,
Andrew Freedman, and Charles E. Kolb
Center for Chemical and Environmental Physics
Aerodyne Research, Inc.
45 Manning Road
Billerica, MA 01821

ABSTRACT

Absolute photodissociation cross sections for gas phase NaCl are measured over the wavelength range of 189.7 to 359.8 nm at 300 K. Two well-resolved peaks are observed at 235 nm and 260 nm. The cross section also rises below 210 nm. These results are in good qualitative agreement with previous high temperature measurements and with cross sections computed from theoretically calculated potential surfaces. However, there are two significant differences, the width of the absorption peaks and to absolute magnitude of the cross sections. The importance of these measurements in understanding the photodissociative processes of ionic compounds and the implications for the role of NaCl in the stratospheric chemistry of chlorine compounds are discussed.

*Present Address: Southwest Sciences, Inc.
1570 Pacheco St., Suite E-11
Santa Fe, NM 87501

INTRODUCTION

The study of the optical spectra of gas phase alkali halides has a long and rich history,¹ having been pursued in flames,²⁻³ furnaces,⁴ shock tubes,⁵ and more recently, in room temperature cells⁶ and molecular beams.^{3,7-11} In conjunction with these experimental studies, the theory of photodissociation of alkali halides has received considerable attention.^{1,12-14}

Photodissociative processes for these systems are often approximated as one-electron charge transfers between a ground ionic state and excited covalent state. Measurement of the spectrally-resolved cross sections and determination of the relative probability of exciting parallel ($O^+ + \Sigma^+$) and perpendicular ($1 + {}^1\Sigma^+$) transitions lead to information about the shapes of the excited state potentials. Combined with product analysis, one can then learn how dissociation from the O^+ excited states is affected by the degree of adiabatic behavior in the exit channel when crossing the ionic ${}^1\Sigma^+$ potential curve.

The measurement of photodissociation cross section is also of interest in understanding the chemistry of alkali metals in the stratosphere. It has been suggested¹⁵⁻¹⁷ that sodium and other metals introduced into the atmosphere by meteor ablation may play a role in affecting ozone reduction by the catalytic chlorine cycle. One possible reaction sequence which demonstrates this mechanism is:





which leads to the net reaction



Rate constants for reactions 1 and 2 have been measured in our laboratory.¹⁸⁻¹⁹ Combining these results with photolysis rates based on the high temperature absorption measurements (1123-1223 K) of Davidovits and Brodhead,^{4,17} leads to the possibility that this mechanism could be comparable in magnitude to the major stratospheric Cl regeneration mechanism,



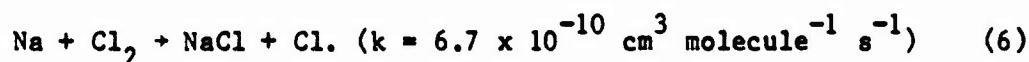
The rate limiting step of the sodium catalyzed mechanism (reactions 1-3) is reaction 3. Davidovits' absorption data include contributions from vibrationally excited states and possibly dimers, which will not contribute to photolysis at stratospheric temperatures near 260 K. Clearly, low temperature photodissociation cross section measurements are desirable.

In this paper we report measurements of the absolute cross section for photodissociation of NaCl at 300 K. Sodium chloride is produced by the gas phase reaction of atomic sodium with chlorine in a flow tube under dimer-free conditions and with over 80% of the NaCl in the ground vibrational state. The approach taken in these experiments does not require the knowledge of the absolute NaCl number density in the photolysis region, but rather uses a ratio technique to quantify the cross sections.

EXPERIMENTAL

Photodissociation Apparatus

Sodium chloride is generated in a flow tube by the fast bimolecular reaction of atomic sodium with excess chlorine,



Sodium atoms are generated by heating sodium metal in a 2-cm-diameter cylindrical stainless steel oven to ~ 510 K which produces a vapor pressure of $\sim 2 \times 10^{-3}$ torr within the oven. The vapor is entrained in a flow of helium, and carried through a heated 0.6-cm-diameter 40-cm-long stainless steel tube into the flow apparatus. This heated tube is wrapped with ~ 0.3 -cm-thick zirconia blanket insulation and enclosed in a water cooled jacket to prevent any heating of the main flow carrier gas. The sodium vapor is diluted by the carrier gas in the main flow so that the sodium or sodium chloride concentration within the photolysis zone is always less than 10^{10} cm^{-3} . Chlorine is mixed with the main carrier flow and its reaction with sodium is complete within a few centimeters of the sodium inlet orifice.

The flow apparatus is comprised of a small stainless steel tube 9.7 cm in diameter and approximately 50 cm long, with four perpendicular side arms at

the detection zone which permit photodissociation and detection of the flow species (Figure 1). The main flow of helium carrier gas is added at the entrance of the flow tube and a small purge flow of helium is introduced in each of the side arms to keep the optics clean. Gas volumetric flow rates are determined with calibrated thermal conductivity-type mass flow meters. Flow rates of chlorine are determined by diverting the flow into a calibrated volume and measuring the rate of pressure increase. A calibrated MKS Baratron capacitance manometer is used to measure pressure and a chromel-alumel thermocouple is used to determine the gas temperature. Experiments are performed with a flow velocity of 150 cm s^{-1} at a pressure of 2.1 torr.

Relative concentrations of atomic sodium are measured using laser-induced fluorescence of the $3s^2S_{1/2} - 3s^2P_{3/2}$ transition at 589.9 nm. The output of a nitrogen-pumped dye laser (Molelectron DL14) is transmitted to the experiment by a fiber optic line and is focussed in the photolysis region to a diameter of $0.380 \pm 0.005 \text{ cm}$. Fluorescence is detected by a photomultiplier located perpendicular to the laser path as shown in Figure 1. A 590 nm interference filter and optical baffles are used to reject spurious light from entering the PMT. A 1 cm diameter area of the photolysis region is imaged onto the phototube. The data are collected using a fast preamplifier and a gated integrator having a 60 ns acquisition gate width. The relative laser power in each pulse is monitored by a fast photodiode and is integrated and held until both the laser power and fluorescence signals are read into an IBM PC/XT computer for analysis.

Sodium chloride is photodissociated with a Raman-shifted excimer laser. The excimer laser (Questek) is equipped with unstable resonator optics and produces a beam with very low divergence. It uses either ArF or KrF with output pulse energies of 100-250 mJ. Its output is reflected by a dielectric-coated mirror into a Quanta Ray RS-1 Raman shifter. Using D₂, H₂, or a mixture of the two, both Stokes and anti-Stokes shifted wavelengths of the pump line are produced with pulse energies in the range .0023-4.4 mJ. This UV beam is focussed into the cell coaxial to the dye laser beam, with care taken to ensure that the UV beam diameter is equal to or slightly less than that of the dye laser. A BK-7 window (F1 in Figure 1) on the UV output side of the cell (visible input side) is used to absorb the UV light so that it cannot be refocussed into the fiber optic or interfere with the visible power measurements. A calibrated Scientech power meter is used to monitor the average UV power as it exits the photolysis cell. Corrections are made for transmittance of the output window and spectral response of the power monitor.

Triggering of both lasers and the time delay between them (variable from 0-10 ms in 10 ns increments) is controlled by a delay generator. The excimer is triggered at a frequency (30 Hz) twice that of the dye laser, so that any non-photodissociation related components of the signal are subtracted from the fluorescence of photodissociated sodium. The data acquisition system performs both these subtractions of background signals as well as normalization of the fluorescence to the power of each visible laser pulse. It then averages the corrected signals over a minimum of 100 pulses.

The purities of chemicals used in these experiments are as follows: sodium metal, 99.9% (Alfa); helium, 99.995% (Northeast Cryogenics); and chlorine, 99.5% (Northeast Cryogenics).

Experimental Procedure and Data Analysis

Photodissociation cross sections are measured using a probe-pump-probe approach. The first step consists of measuring the atomic sodium concentration with no chlorine present, $[Na]_0$, in the photolysis region using the visible dye laser. Excess molecular chlorine is then added at the upstream end of the flow tube, quantitatively converting all of the Na to NaCl in a distance much shorter than the 17 cm path between the sodium oven outlet and the photolysis region. The NaCl is then photodissociated with the UV laser and the product sodium ($[Na]_p$) detected with the visible laser approximately 200 ns later. This signal is related to the initial concentration of NaCl by

$$\frac{[Na]_p}{[NaCl]} = 1 - \exp[-I(\lambda)\sigma(\lambda)] \quad . \quad (7)$$

where $I(\lambda)$ is the ultraviolet laser photon fluence per pulse at wavelength λ , and $\sigma(\lambda)$ is the photodissociation cross section at this wavelength. Because $[NaCl] = [Na]_0$, we rewrite equation 7,

$$R = \frac{[Na]_p}{[Na]_0} = 1 - \exp[-I(\lambda)\sigma(\lambda)] \quad . \quad (8)$$

Since the detection techniques for measuring atomic sodium before and after the photolysis are identical, the ratio of their absolute concentrations in equation 8, defined as R, is equivalent to the ratio of their observed fluorescence signals. As a result, only $I(\lambda)$ need be measured absolutely.

This determination of $\sigma(\lambda)$ requires a few assumptions and clarifications. Since R depends exponentially on the UV photon flux, nonuniformities could introduce errors when using the spatially-averaged value of $I(\lambda)$. This is avoided by keeping the UV beam intensity low enough so that R is always less than 0.05. Accordingly, the exponential term can be expanded and rewritten as

$$\sigma(\lambda) = \frac{R}{I(\lambda)} \quad (9)$$

In this situation, R is linearly proportional to $I(\lambda)$, and the spatially-averaged value of R is independent of any intensity nonuniformities. We confirmed the linearity of the cross section by measuring R as a function of laser intensity for some of the more intense UV lines. A linear dependence of R on $I(\lambda)$ was observed at lower intensities, becoming nonlinear at the highest intensities. We always operated in the linear regime. The intensity profile of the visible laser beam is kept uniform to avoid nonlinearities in R.

The time delay between lasers is also critical. It must be small enough so that all of the sodium formed by dissociation is detected before reacting

with the remaining Cl_2 . To detect at least 98% of this sodium, and with Cl_2 concentrations on the order of $0.4\text{--}1.0 \times 10^{13} \text{ cm}^{-3}$, (large enough to react with Na in a distance much shorter than the distance from the oven to the photolysis region) the laser delay should be less than $3.0 \mu\text{s}$. On this time scale, the recoiling of photodissociated sodium will be thermalized. We measured the decrease in $[\text{Na}]_p$ as a function of delay time and observe a decay ($\tau \sim 100 \mu\text{s}$) commensurate with this secondary reaction with Cl_2 and with diffusion out of the detection region. On the other hand, it is desirable to have some delay so as to avoid any electronic interference or UV induced effects associated with the excimer pulse. Thus delays between 200 ns and $2.0 \mu\text{s}$ were used.

The most significant correction to the data arises in accounting for the different diffusivities of Na and NaCl. As mentioned above, Na emanating from the oven travels $\sim 17 \text{ cm}$ before being detected. When quantitatively converted to NaCl (in $1\text{--}2 \text{ cm}$), the NaCl then travels $\sim 15 \text{ cm}$ before detection. In our initial analysis above we have assumed that $[\text{NaCl}] = [\text{Na}]_0$ in the photolysis region. However, this is only approximately correct. Although true at the end of the narrow reaction zone, these species' axial concentrations will decay at different rates due to diffusion to and sticking on the reactor walls. A correction must therefore be made for the differing diffusivities of Na and NaCl. This is done according to the methods outlined in reference 21, using a measured diffusion coefficient for atomic sodium of $0.48 \text{ cm}^2 \text{ s}^{-1}$ at 1 atm and 300 K , and an approximate value for NaCl of $0.40 \pm 0.05 \text{ cm}^2 \text{ s}^{-1}$ at 1 atm .²² The underestimation of $[\text{NaCl}]$ in the photolysis region results in a reduction in R by a factor of $1.4 \pm .4$. This

systematic error affects only the absolute magnitude of the photodissociation cross section curve as a function of wavelength, but not the relative shape of the curve.

RESULTS

Room temperature photodissociation cross sections for gaseous NaCl were measured at 25 wavelengths in the range 189.9-359.8 nm. A plot of the results is shown in Figure 2. Error bars represent one standard deviation uncertainties in each point, excluding a systematic error of $\pm 30\%$ due to the correction for diffusion. This last uncertainty would have the effect of uniformly shifting the curve up or down. Table 1 lists the averaged data taken at each wavelength and illustrates the ability of this technique to accurately measure very small cross sections. Our results exhibit two distinct peaks and a rise in σ toward the shortest wavelengths. We do not observe any dissociation at energies below ~ 100 kcal mole⁻¹ (285 nm), which is consistent with the currently accepted value for the bond strength of 98 ± 2 kcal mole⁻¹.^{9,23}

As seen in Figure 2, the error bars for most points are less than 20%, except (unfortunately) at the center of the large peak at 234 nm. This point and the next two higher wavelength points were taken using very weak Raman-shifted lines (the latter two being combinations of Stokes and anti-Stokes lines),²⁴ so that there is a greater uncertainty in the absolute height of this peak as compared with the longer wavelength peak. For most points, the source of the error bars lies in the absolute UV power measurement and not in the determination of the ratio of $[\text{Na}]_p/[\text{Na}]_o$.

Table 1 - Measured Photodissociation Cross Sections for NaCl

Wavelength (nm)	Excimer Gas	Raman-Shifted Line ^a	Number of Measurements	Avg. Cross Section ^b (cm ²)
189.7	KrF	AS ₃ (H ₂)	2	6.12±1.44 (-18)
193.4	ArF	-	4	5.56±1.06 (-18)
203.1	KrF	AS ₃ (D ₂)	1	1.48±1.40 (-18)
205.3	ArF	S ₁ (D ₂)	1	9.06±1.48 (-19)
205.9	KrF	AS ₂ (H ₂)	2	8.96±0.60 (-19)
210.3	ArF	S ₁ (H ₂)	2	7.36±0.59 (-19)
216.3	KrF	AS ₂ (D ₂)	1	1.51±0.67 (-18)
218.7	ArF	S ₂ (D ₂)	2	4.63±1.76 (-19)
225.2	KrF	AS ₁ (H ₂)	4	1.46±0.08 (-18)
230.4	ArF	S ₂ (H ₂)	3	5.12±0.40 (-18)
231.2	KrF	AS ₁ (D ₂)	2	9.47±0.80 (-18)
234.0	ArF	S ₃ (D ₂)	2	1.30±0.30 (-17)
237.6	KrF	S ₁ (H ₂)+AS ₂ (D ₂) ^c	2	6.38±1.31 (-18)
241.4	KrF	AS ₁ (H ₂)+S ₁ (D ₂) ^c	2	6.74±0.72 (-18)
248.4	KrF	-	7	1.29±0.05 (-18)
251.6	ArF	S ₄ (D ₂)	1	2.51±1.19 (-18)
254.8	ArF	S ₃ (H ₂)	3	4.24±0.41 (-18)
260.2	KrF	AS ₁ (H ₂)+S ₂ (D ₂) ^c	1	4.33±0.50 (-18)
268.3	KrF	S ₁ (D ₂)	4	1.74±0.23 (-18)
277.0	KrF	S ₁ (H ₂)	6	4.00±0.47 (-19)
285.0	ArF	S ₄ (H ₂)	2	0 ±1.8 (-19)
291.8	KrF	S ₂ (D ₂)	2	8 ±1 (-21)
313.0	KrF	S ₂ (H ₂)	2	0 ±8 (-21)
319.6	KrF	S ₃ (D ₂)	1	0 ±9 (-21)
359.8	KrF	S ₃ (H ₂)	1	2.7 ±3.1 (-21)

- a Designation of Stokes or anti-Stokes line with gas used in the Raman-shift cell in parentheses. Gas cell pressures were 125 psig for H₂ and 250 psig for D₂.
- b Exponent in parentheses; error is one standard deviation uncertainty in precision.
- c These are combination Raman-shift lines in a 25% H₂:75% D₂ mixture at 250 psig total pressure.

DISCUSSION

The results presented in this work are in qualitative agreement with the earlier work of Davidovits and Brodhead.⁴ However, there are two significant differences: the resolution of the absorption peaks and the absolute magnitude of the cross sections. Gaseous alkali halides in the earlier work were produced in a heated reservoir and effused into a slightly warmer quartz absorption cell. For NaCl, cell temperatures were in the range of 1123-1223 K. At these temperatures, the first five vibrational levels account for over 90% of the population. One might expect broad absorption features since each excited vibrational state will dissociate over a different range of energies than for the ground vibrational state. In this work, NaCl is equilibrated with the flow carrier gas at 300 K, primarily populating only the ground and first excited vibrational states (83% and 14%, respectively), so that narrower peaks are not surprising.

The absolute magnitudes of the integrated cross sections for the data above 220 nm (see following discussion) calculated from the two sets of data pose a greater problem in that they differ by a factor of six. The quoted error bars on both experiments do not account for this discrepancy and one suspects that either or both experiments contain systematic errors. One possible explanation is the presence of NaCl dimers in the high temperature experiments. Davidovits and Brodhead determined their absorption cross sections assuming that NaCl monomer, calculated from tabulated vapor pressure curves, was the sole absorber in their cell. They also estimated the fraction of $(\text{NaCl})_2$ in their experiments to be 40%-60%. If these absorbed light to

form either $\text{Na} + \text{NaCl}_2$ or 2NaCl , the overall number density of absorbers would be larger and the reported cross section values lower.

No dimers are present in our experiments. Sodium chloride is formed by chemical reaction in a flowing carrier gas and there are insufficient collisions for dimerization to occur via termolecular recombination. Lamb and Benson²⁸ have calculated the rate constant for



to be $k = 10^{-28.5} \text{ cm}^6 \text{ molecule}^{-2}$ at 230 K. Assuming this value to be approximately the same at 300 K, less than .002 of the nascent NaCl dimerizes over the path between where it is formed and the photolysis volume.

Absorption in the ultraviolet has been observed for dimeric species such as $(\text{NO})_2$ and $(\text{N}_2\text{O})_2$.²⁶⁻²⁸ These absorptions occur in the same spectral region as absorptions of the monomer and, at least in the case for $(\text{NO})_2$, exhibits a large oscillator strength.²⁶ This suggests that it is possible for even a weakly bound dimer to exhibit a strong UV absorption cross section. On the other hand, Su and Riley did not observe any anomalous features in their time-of-flight recoil distributions of alkali halides, photodissociated at 266 nm, which suggest the presence of dimers.⁷⁻⁹ Oppenheimer and Berry did not observe any features attributable to dimers for matrix isolation measurements of LiI, NaBr, and NaI, where dimers would be expected to be present.²⁹ For NaCl, KI, RbBr, and LiBr, no absorption bands attributable to any species were observed.

The only other comparable alkali halide cross section measurement at room temperature is that for CsI by Grossman et al.⁶ The results are consistent with our measurements for NaCl. The spectral width for this $1-^1\Sigma^+$ transition (in Hund's case c notation) is narrower and the integrated cross section is a factor of two smaller than that reported by Davidovits and Brodhead.⁴ Furthermore, cesium iodide dimers are not expected to be present in either experiment.

Cross Section Calculations

The ionic ground electronic state for the lighter alkali halides is designated $X^1\Sigma^+$ (Hund's case a), and correlates to separated $M^+ + X^-$ ions. Excited molecular states correlating with neutral atoms $M + X$ are covalent, and for $Na(^2S) + Cl(^2P_J)$, are represented by Hund's case c angular momentum coupling as $\Omega = 0^+, 0^-, 1$, and 2 .^{1,30} Only $0^+ + ^1\Sigma^+$ (parallel) and $1 + ^1\Sigma^+$ (perpendicular) transitions are allowed. The potential curve for the ground electronic state of these molecules is fairly well represented by a modified Rittner potential, reproducing experimentally measured dissociation energies and anharmonic constants with reasonable accuracy (see Figure 3).³¹

The first few electronic excited state potentials are not well characterized. They are thought to be either repulsive or only slightly bound.^{1,4} Zeiri and Balint-Kurti¹⁴ have calculated the ground and first four excited electronic state potentials and associated transition dipole moments for a group of alkali halides using a semi-empirical valence-bond method, while excluding the effects of spin-orbit coupling. Within the framework of this Hund's case a approach, they find that the excited states

are all fairly repulsive (see Figure 3) and that use of the Franck-Condon approximation is invalid here as the transition dipole moments vary considerably with internuclear separation, r . Their excited state curves are labelled in ${}^1\Sigma^+$ (parallel) and ${}^1\Pi$ (perpendicular) notation.

In order to gain a clearer understanding of our results, we have calculated NaCl absorption cross section curves over the wavelength range 180-300 nm for comparison with our experimental data. We use the reflection approximation³² in which the electronic transition moment is calculated using a harmonic oscillator wavefunction for the ground electronic state, a δ -function for the upper repulsive state wavefunction, and Zeiri's transition dipole moments at each value of r . At 300 K, only $v=0$ and $v=1$ are sampled, so that the harmonic oscillator potential accurately represents the Rittner form (see insert in Figure 3). Small corrections for the displacement of higher vibrational levels from the equilibrium internuclear separation r_e , and for the effect of thermally-averaged rotational populations on the absorption wavelengths were also included in this calculation.

Figure 4 compares the calculated and experimental data. In all cases, the total integrated cross section for the sum of the A-X and B-X transitions for calculated curves have been normalized to that of the experimental curves. The dotted curve in Figure 4a shows absorption curve at 300 K calculated from the potentials of Zierl and Balint-Kurti.¹⁴ This curve, which does not match the experimental data (represented by the solid curve), is shifted to much shorter wavelengths and exhibits one broad peak. Transitions to both the A ${}^1\Pi$ and B ${}^1\Sigma^+$ states lie under this peak. Excitations to higher states lie further into the ultraviolet.

To better reproduce our experimental results, we varied the energies and shapes of the $A^1\Pi$, $B^1\Sigma^+$, $C^1\Pi$, and $D^1\Sigma$ states in a narrow region of ± 0.25 Å about $r_e = 2.36$ Å. This range corresponds to the values of r over which the square of the lowest five vibrational wavefunctions are important. For $v = 0$ and $v = 1$, only the region ± 0.10 Å about r_e contributes to σ , and the best fit to our data only senses this range of r . The results of this fit to our data are shown as the dashed curve in Figure 4a and results from lowering all four curves and flattening the A and B states in the region about r_e (Figure 3). These new curves are reasonable in light of the approximations made by Zeiri and Balint-Kurti.¹⁴ They state that no valence-bond structures corresponding to Rydberg states were included in their calculations, and the inclusion of these states would have made their calculated repulsive curves less repulsive.

The peaks at 235 nm and 260 nm in Figure 4a represent the B-X (parallel) and A-X (perpendicular) transitions, respectively. At wavelengths shorter than 220 nm, the C-X (and D-X) transition causes the cross section to rise, as observed in the data. We do not observe the peak absorption for this transition, so the shape and position of the $C^1\Pi$ data is less well determined than the A or B states. Nevertheless, the fact that this rise is seen at all near 200 nm strongly suggests that the $C^1\Pi$ state is bound, lying at energies which are equal to or slightly lower than the energy of its dissociation products, $Na(^2P) + Cl(^2P_J)$. This has been observed for this state in other alkali halides.²

The relative heights of the calculated peaks at room temperature agree qualitatively with the experimental data (normalized to total integrated cross section), suggesting that Zeiri's transition dipole moment calculations are approximately correct. Su and Riley measured the ratio of the parallel to total transition moments at 266 nm for a series of alkali halides using a molecular beam recoil velocity technique.⁷⁻⁹ They find that the amount of parallel character drops from about 60% for the iodides to less than 30% for alkali chlorides. This ratio for NaCl was determined to be 0.16 ± 0.02 .⁹ At the temperature of their source (1189 K), we calculate a ratio of 0.28.

Using the potentials which were fit to our room temperature data, we computed the absorption spectrum at 1123 K for comparison with the experiments of Davidovits and Brodhead.⁴ Despite the limitations of the calculation (and uncertainties in extending them to high temperatures), we see in Figure 4b that the agreement is remarkably good. The higher degree of structure in our calculations than were observed by Davidovits can be explained as arising from regions of r outside of $r_e \pm 0.10$ Å, so that small changes in the shapes of the potentials there would shift the absorption wavelengths and peak shapes for the excited vibrational states. Slightly steeper curves for $r < 2.2$ Å would tend to broaden the absorption peaks for the higher vibrational states and lead to a smoother overall absorption curve.

In comparing the calculated ratio of the parallel to perpendicular transition probabilities to those observed by Davidovits and Brodhead,⁴ Su and Riley,⁹ and ourselves, this ratio is systematically high. This suggests that

the B-X dipole transition moments of Zierl and Balint-Kurti¹⁴ are too large relative to those of the A-X transition.

In conclusion, photodissociation cross section measurements of NaCl at 300 K have resolved the A-X and B-X electronic transitions. From these spectra, more accurate potential curves for the $A^1\Pi$ and $B^1\Sigma^+$ electronic states have been derived in the region about the equilibrium internuclear distance of the NaCl ground state. The shape of the photodissociation spectrum is consistent with the photoabsorption spectrum of Davidovits and Brodhead,⁴ measured at 1123 K. However, the absolute magnitude of the integrated cross section in this work is about six times smaller than that of Davidovits. The most likely explanation is that the presence of dimers in the high temperature studies contributed to the observed absorption.

Stratospheric Photolysis of NaCl

The photolysis of NaCl is crucial in determining the extent to which alkali metals of meteoric origin affect the ozone balance in the upper stratosphere.¹⁵⁻¹⁷ Convoluting the measured total solar flux at 40 km (including albedo and scattering)³³ over our measured cross sections between 180 and 300 nm, we obtain a total photolysis rate J of $1.9 \pm 0.8 \times 10^{-4} \text{ s}^{-1}$. Based on our calculations for cross sections, the curve at stratospheric temperatures (~260 K) is nearly the same as our 300 K results. This number is a factor of ten smaller than that estimated by Rowland and Rogers¹⁷ using the high temperature data of Davidovits and Brodhead.⁴ The difference is due to two factors. First, the solar flux has a local minimum near 250 nm and falls off rapidly below 200 nm, offsetting much of the contributions of our

peaks near 190, and 235 nm (Figure 5). Second, the rapid rise in the solar flux above 270 nm overemphasizes excited vibrational state contributions to the cross section, which are absent at 40 km altitude (260 K).

Using $J = 1.9 \times 10^{-4} \text{ s}^{-1}$ and the measured rate constants for reactions 1 - 3,¹⁸⁻²⁰ the rate at which free chlorine is released from HCl at 40 km is $\sim 10^{-6} \text{ s}^{-1}$, where the photolysis of NaCl is the rate limiting step. This calculation assumes a total gas phase alkali concentration of $5 \times 10^5 \text{ cm}^{-3}$.³⁴ For comparison, the release rate of Cl for HCl by OH (i.e. $k_5 \cdot [\text{OH}]$) is $6.7 \times 10^{-6} \text{ s}^{-1}$, based on an OH concentration of 10^7 cm^{-3} and the value $k_5 (260 \text{ K}) = 6.7 \times 10^{-13} \text{ cm}^3 \text{ s}^{-1}$.³⁵ Thus we conclude that, depending on the altitude at which heterogeneous and homogenous removal processes of atmospheric alkali compounds dominate gas phase chemistry, meteoric alkali chemistry could be an additional and important source of free chlorine in the upper stratosphere. We are presently investigating the magnitudes of processes through which atmospheric alkali compounds might be removed from the gas phase.

ACKNOWLEDGEMENTS

The authors gratefully acknowledge helpful discussions with the late Professor Frederick Kaufman and the technical assistance of Warren E. Goodwin.

This work was sponsored by the Fluorocarbon Program Panel of the Chemical Manufacturers Association under Contract No. FC-84-494 and by the Air Force Geophysics Laboratory under Contract No. F19628-83-C-0010.

REFERENCES

1. R.S. Berry in Alkali Halide Vapors: Structure, Spectra and Reaction Dynamics, P. Davidovits and D.L. McFadden, Eds., Academic Press, N.Y., Chap. 3 (1979), and references therein.
2. N. Furuta, E. Yoshimura, H. Haraguchi, and K. Fuwa, *Spectrochimica Acta* 33B, 715 (1978), and references therein.
3. D.F. Dever, B. Cardelino, and J.L. Gole, *High Temperature Sci.* 18, 159 (1984).
4. P. Davidovits and D.C. Brodhead, *J. Chem. Phys.* 46, 2968 (1967).
5. A. Mandl in Alkali Halide Vapors: Structure, Spectra, and reaction Dynamics, P. Davidovits and D.L. McFadden, Eds., Academic Press, N.Y., Chap. 2 (1979).
6. L.W. Grossman, G.S. Hurst, M.G. Payne, and S.L. Allman, *Chem. Phys. Lett.* 50, 79 (1977).
7. T-M.R. Su and S.J. Riley, *J. Chem. Phys.* 71, 3194 (1979).
8. T-M.R. Su and S.J. Riley, *J. Chem. Phys.* 72, 1614 (1980).
9. T-M.R. Su and S.J. Riley, *J. Chem. Phys.*, 72, 6632 (1980).
10. N.J.A. Van Veen, M.S. DeVries, J.D. Sokol, T. Baller, and A.E. DeVries, *Chem. Phys.* 56, 81 (1981).
11. W.R. Anderson, B.M. Wilson, R.C. Ormerod, and T.L. Rose, *J. Chem. Phys.* 74, 3295 (1981).
12. P. Brumer and M. Karplus, *J. Chem. Phys.* 58, 3903 (1973).
13. R.N. Zare and D.R. Herschbach, *J. Mol. Spectrosc.* 15, 462 (1965).
14. Y. Zeiri and G.G. Balint-Kurti, *J. Mol. Spectrosc.* 99, 1 (1983).

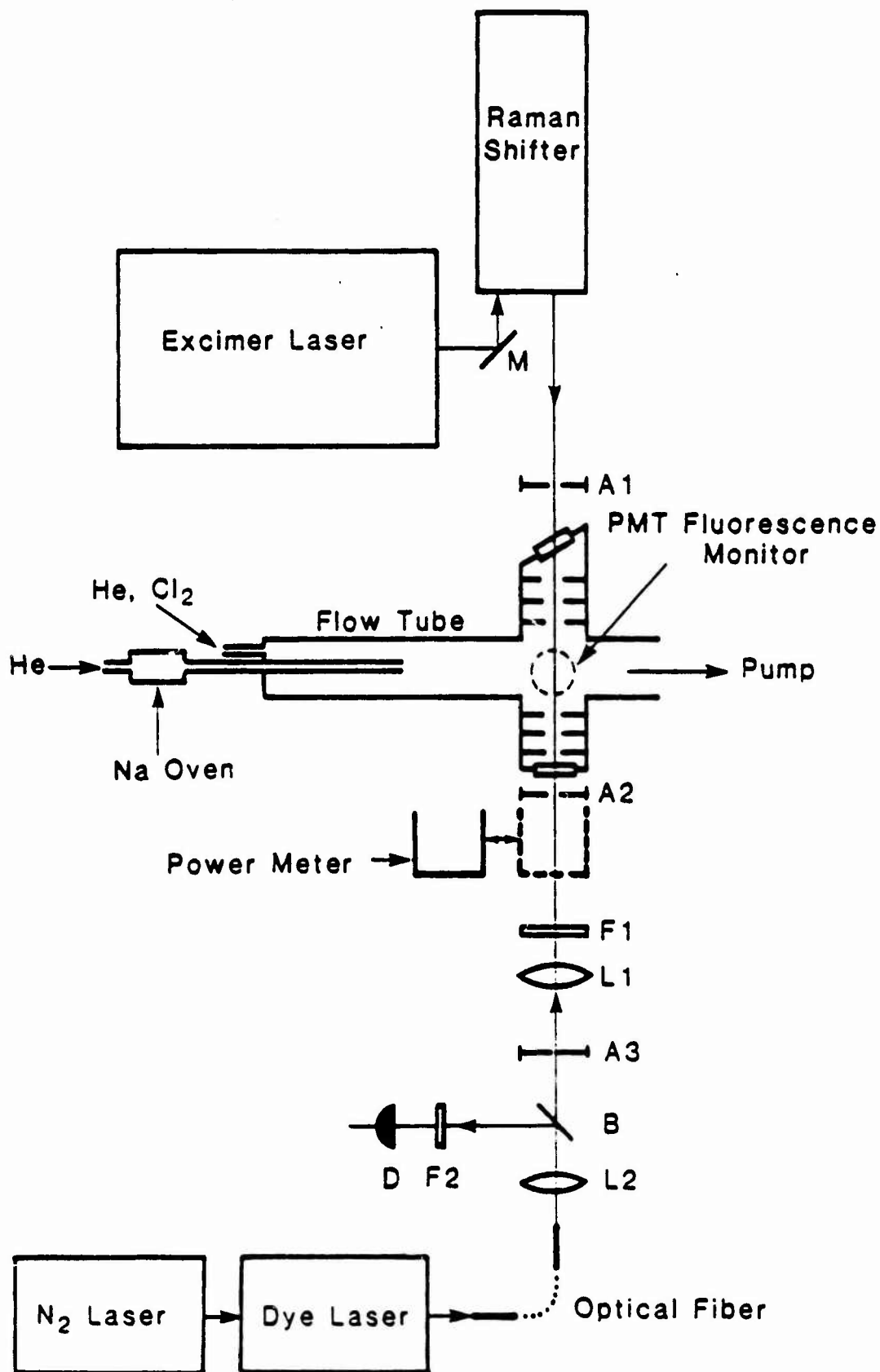
15. E. Murad and W. Swider, *Geophys. Res. Lett.* 5, 1035 (1978).
16. E. Murad, W. Swider and S. Benson, *Nature (London)* 289, 273 (1981).
17. F.S. Rowland and P.J. Rogers, *Proc. Natl. Acad. Sci. (USA)* 79, 2737 (1982).
18. J.A. Silver, M.S. Zahniser, A.C. Stanton, and C.E. Kolb, Twentieth Symposium (International) on Combustion, The Combustion Institute, 605, (1984).
19. J.A. Silver and C.E. Kolb, *J. Phys. Chem.*, in pres. (1986).
20. J.A. Silver, *J. Chem. Phys.*, in press (1986).
21. J.A. Silver, A.C. Stanton, M.S. Zahniser, and C.E. Kolb, *J. Phys. Chem.* 88, 3123 (1984).
22. J.A. Silver, *J. Chem. Phys.* 81, 5125 (1984).
23. B. deB. Darwent, Bond Dissociation Energies in Simple Molecules, NSRDS-NBS 31 (1970).
24. T.R. Loree, R.C. Sze, D.L. Barker, and P.B. Scott, *IEEE J. Quantum Electronics* QE-15, 337 (1979).
25. J.J. Lamb and S.W. Benson, submitted for publication (1985).
26. J. Billingsley and A.B. Callear, *Trans. Faraday Soc.* 67, 589 (1971).
27. O. Kajimoto, K. Honma and T. Kobayashi, *J. Phys. Chem.* 89, 2725 (1985).
28. K. Honma and O. Kajimoto, *Chem. Phys. Lett.* 117, 123 (1985).
29. M. Oppenheimer and R.S. Berry, *J. Chem. Phys.* 54, 5058 (1971).
30. G. Herzberg, Spectra of Diatomic Molecules, Van Nostrand, N.Y., 387-394 (1950).
31. J.E. Szymanski and J.A.D. Matthew, *Can. J. Phys.* 62, 584 (1984).

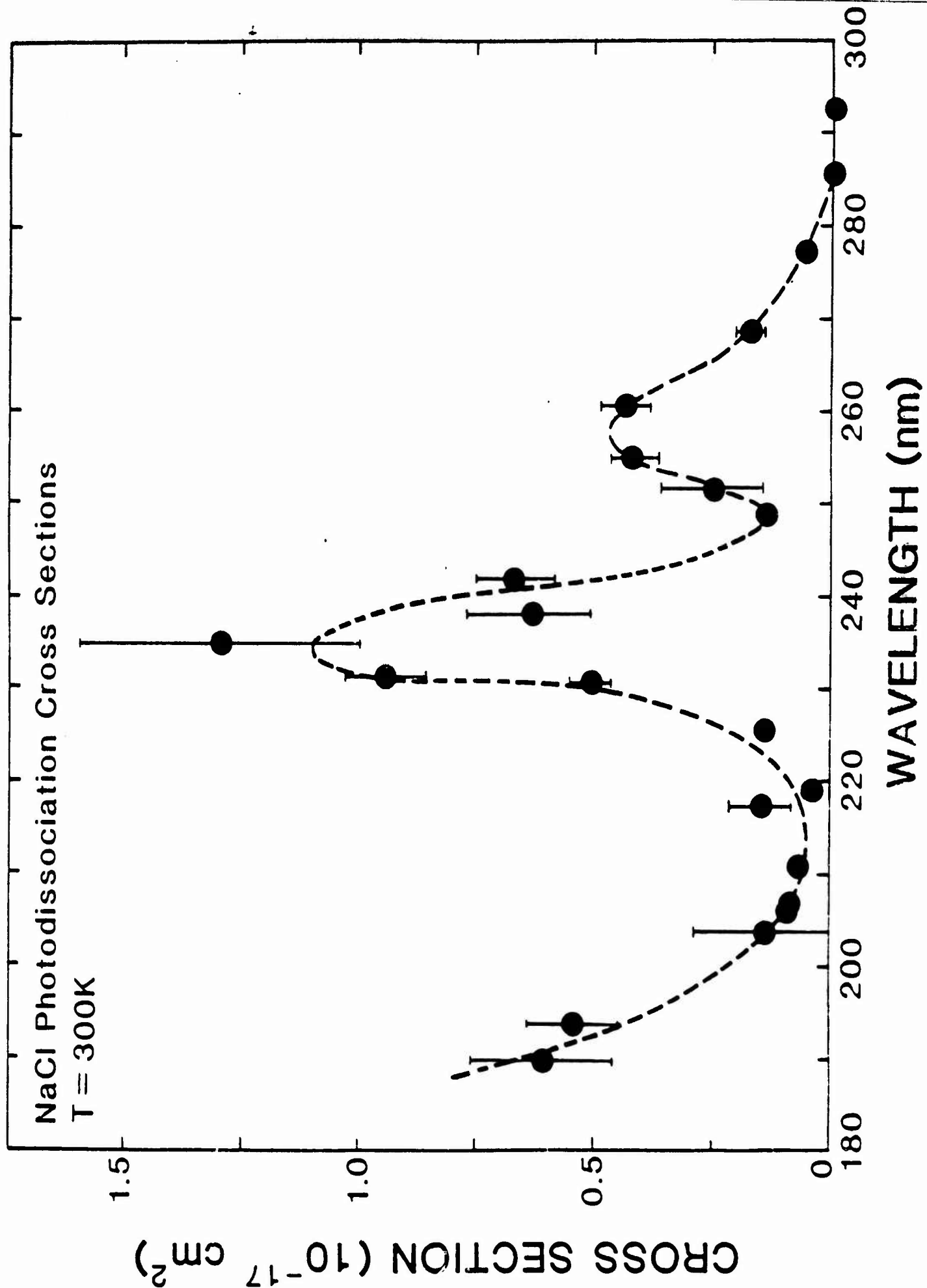
32. J.G. Winans and E.C.G. Stueckelberg, Proc. Natl. Acad. Sci. (USA) 14, 867 (1928).
33. J.R. Herman and J.E. Mentall, J. Geophys. Res. 87, 1319 (1982).
34. S.C. Liu and G.C. Reid, Geophys. Res. Lett. 6, 283 (1979).
35. W.B. DeMore, J.J. Margitan, M.J. Molina, R.T. Watson, D.M. Golden, R.F. Hampson, M.J. Kurylo, C.J. Howard, and A.R. Ravishankara, NASA Jet Propulsion Laboratory Publication, 85-37 (1985).

FIGURE CAPTIONS

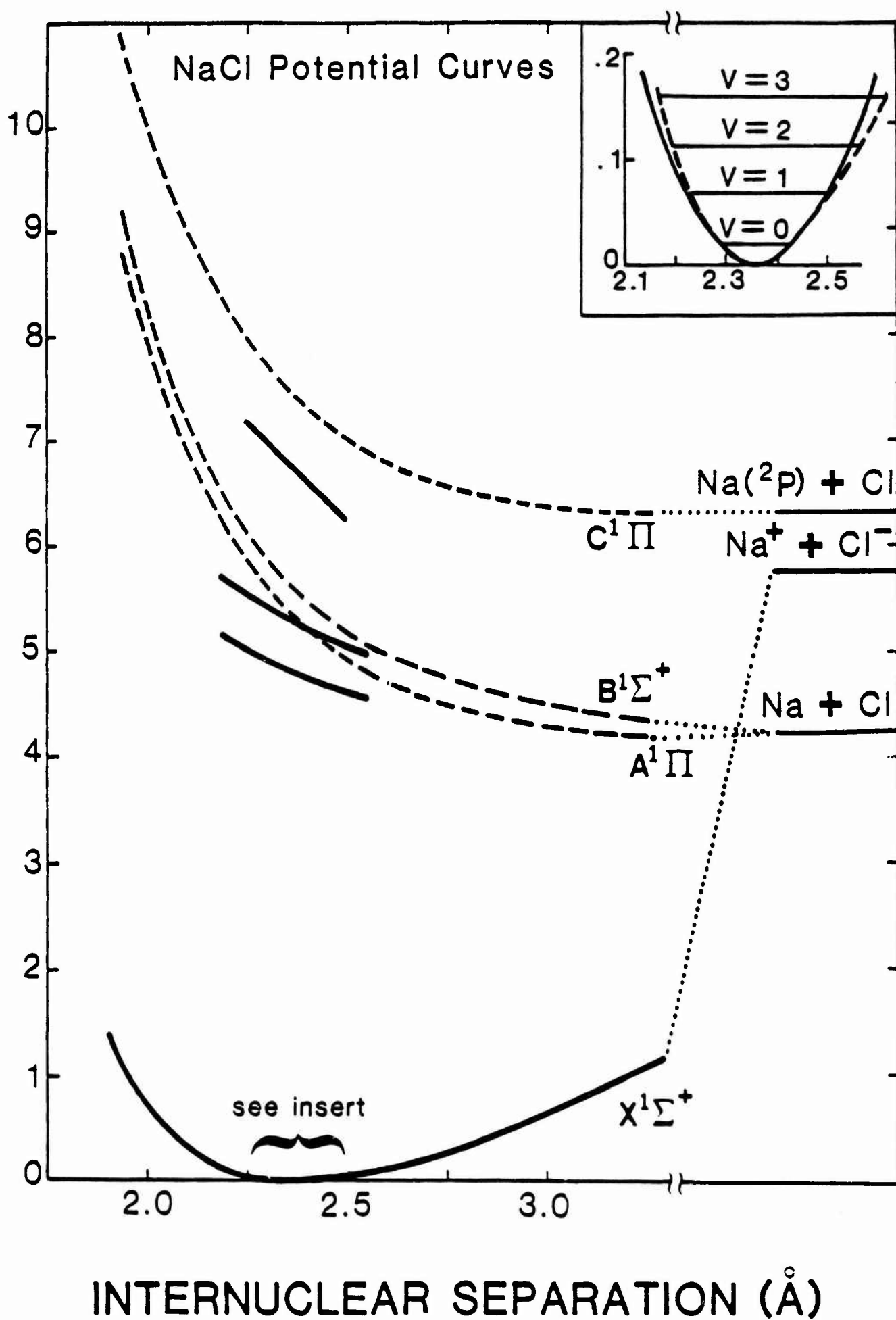
1. Schematic of the experimental apparatus for photodissociation of NaCl. Components are identified as follows: M = mirror; A1, A2, and A3 = apertures; F1 = BK-7 window acting as a UV absorbing filter; F2 = 590 nm interference filter; L1 and L2 = lenses; B = Quartz slide acting as a beamsplitter; D = fast UV photodiode detector.
2. Plot of experimental data versus wavelength of photodissociation cross sections for NaCl at 300 K. Error bars represent one standard deviation. A dashed curve is drawn through the points to highlight the shape of the data.
3. Potential curves used in the calculation of NaCl photodissociation cross sections. Dashed lines are the calculated curves of Zeiri and Balint-Kurti.¹⁴ Solid lines (for $A^1\Pi$, $B^1\Sigma^+$ and $C^1\Pi$) are derived as discussed in the text. The insert shows the lowest part of the $X^1\Sigma^+$ potential, and illustrates how the harmonic oscillator approximation (solid curve) compares with the Rittner potential (dashed curve)³¹ for the lower vibrational levels.
4. Plots of experimental data versus calculated cross section curves. a) 300 K data using representative experimental curve from Figure 1. b) 1123 K data of Davidovits and Brodhead.⁴ The computed curves have been normalized to have equal total integrated cross sections above 220 nm (sum of the A-X and B-X transitions).
5. Plot of the calculated photolysis rate of NaCl as a function of wavelength at 40 km altitude.

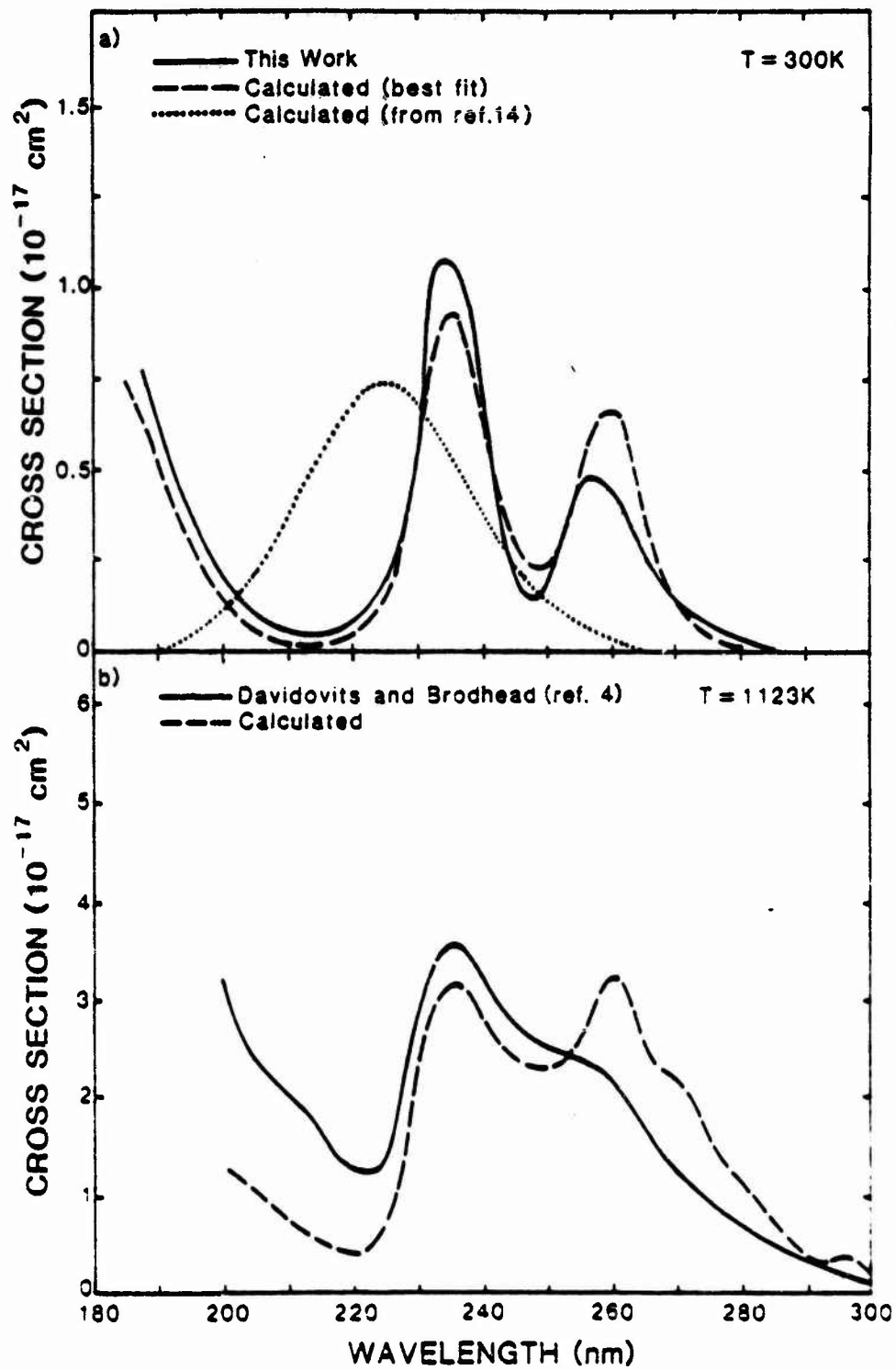
OPTICAL LAYOUT FOR MEASUREMENT OF PHOTODISSOCIATION CROSS SECTIONS

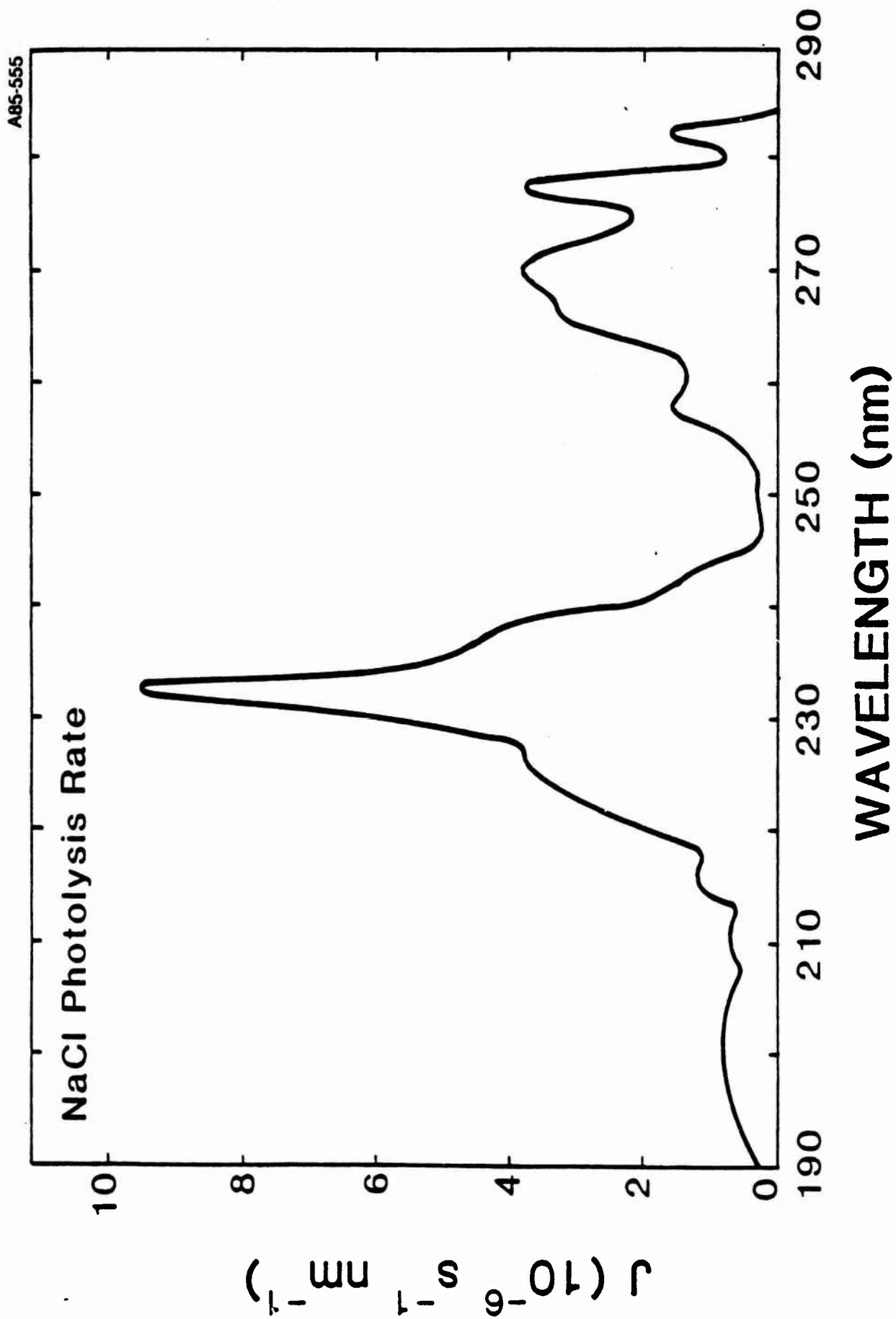




POTENTIAL ENERGY (eV)







7. RATE CONSTANT FOR THE REACTION OF NaOH WITH CO₂

7.1 Introduction

In addition to the chemical oxidation reactions of sodium involving oxyhydrogenic species, Murad et al.¹ suggested that reactions with CO₂ might also be important in both the mesosphere and upper stratosphere. At higher altitudes, the reaction



may serve as an additional sink for sodium. With CO₂ abundances of $>10^8 \text{ cm}^{-3}$ at 100 km and increasing at lower altitudes, this reaction could control the fate of Na even if k_1 were small. Near 40 km, the reaction



might augment or supplant the NaO, NaO₂, and NaOH reactions with HCl as sources for NaCl is the catalytic Cl release mechanism.

The goal of this task was to measure a room temperature rate constant for reaction 1 at a pressure of a few torr to estimate the importance of CO₂ in the chemistry of atmospheric sodium. Detection of NaOH in these experiments was to be accomplished using infrared diode laser absorption of the ν_1 transition (Na-OH stretch vibrational mode). Within the constraints of time and resources allocated for this task, we were unable to locate the ν_1 mode and were therefore unable to perform the rate measurements. A brief description of the steps taken in performing these measurements follows.

7.2 Formation of Gas Phase Sodium Hydroxide

Gas phase sodium hydroxide is produced at room temperature in a conventional flow tube by two different reaction sequences. The direct method involves the addition of hydrogen peroxide to atomic sodium,



This reaction has been studied previously² and it has been shown that $k_{3a}/k_{3a}+k_{3b} = 0.6$. This ratio can be raised to unity upon the addition of excess CO, which reacts only with sodium monoxide and creates a chain reaction sequence resulting in the eventual conversion of all of the sodium to NaOH:



The second NaOH production method is a two-step conversion of atomic sodium using N₂O and H₂:



In excess N₂O and H₂, reactions 5 and 6 cycle until NaOH is the sole product. The value of $k_5 = 8 \times 10^{-13} \text{ cm}^{-3} \text{ molecule}^{-1} \text{ s}^{-1}$ was measured by us and is discussed in Section 3 of this report. Ager and Howard report the

$$k_{5a} = 2.6 \times 10^{-11} \text{ cm}^3 \text{ molecule}^{-1} \text{ s}^{-1} \text{ and } k_{5b} = 1 \times 10^{-11} \text{ cm}^3 \text{ molecule}^{-1} \text{ s}^{-1.3}$$

In all cases atomic sodium concentrations were monitored using laser induced fluorescence. Although this method does not produce a signal linear to the sodium concentration at values of $[\text{Na}] > 10^{11} \text{ cm}^{-3}$, it can be used to show when all of the Na has been chemically removed (our sensitivity to sodium in these experiments is estimated at 10^7 cm^{-3}). Absolute determination of the sodium concentration in our detection zone was accomplished by titration with known amounts of Cl_2 . In these experiments, $[\text{Na}]$ was varied from 10^{12} - $3 \times 10^{14} \text{ atoms cm}^{-3}$. Although we did not detect NaOH directly, we still believe that it was produced in concentrations equivalent to the $[\text{Na}]$ in the system. Besides observing the loss of Na upon addition of H_2O_2 or N_2O , we also could observe, for the first NaOH production method, changes in infrared H_2O_2 absorptions which approximately correspond to the magnitude of the Na concentration changes. Furthermore, past experience has shown that upon addition of H_2O_2 to Na, OH appears² (seen via laser induced fluorescence), presumably as the product of reaction 3a.

7.3 Detection of NaOH

The methods and techniques for measuring infrared absorption of gaseous species with tunable diode lasers has been well described elsewhere.⁴⁻⁵ This method was chosen for the detection of NaOH since it is expected to be fairly sensitive, given the expected large dipole moments of alkali compounds.⁶⁻⁸ No viable visible or ultraviolet optical detection techniques have been demonstrated.

The infrared absorption spectrum of NaOH is not well known. Sodium hydroxide is a linear molecule,⁹⁻¹⁰ and has three infrared active vibrational modes - a low frequency bend, an Na-OH stretch, and an O-H stretch. Observation of the latter two modes of NaOH or polymeric forms of NaOH have been reported. Spinar and Margrave¹¹ heated powdered NaOH in an absorption cell to 850 - 1000 degrees (Celsius?) and using a broadband source of light,

observed a feature centered at $437 \pm 10 \text{ cm}^{-1}$, which they attributed to $[\text{NaOH}]_x$. Acquista and Abramowitz¹⁰ made broadband absorption measurements of NaOH and NaOD on an argon matrix and reported seeing a number of bands between 200 and 600 cm^{-1} . Their source of NaOH was a Knudsen cell with a double boiler arrangement which they felt could help distinguish between monomer and polymer bands by changing the oven temperatures. Large isomer shifts led to the assignment of $337 \pm 1 \text{ cm}^{-1}$ as the ν_2 mode. Certain changes in intensity of the $431 \pm 1 \text{ cm}^{-1}$ band relative to the other bands led them to tentatively assign this feature to the ν_1 band of NaOH. However, they observed but did not assign strong absorptions at 400, 360, 285, and 273 cm^{-1} . Although the assignments for ν_1 in these two experiments agree fairly well, it must be noted that the frequencies obtained in matrix isolation studies are lower than the corresponding frequencies found in the gas phase.¹² In fact, alkali metal compounds may exhibit the largest differences. The alkali halides show gas phase frequencies which are 6-9% higher than the corresponding argon matrix value. If one models the OH ligand as a fluorine atom, then we might expect a frequency shift similar to that of NaF, i.e. 7%, or an expected value of $\sim 460 \text{ cm}^{-1}$ based on the assignment of Acquista and Abramowitz.¹⁰

Another approach for estimating the location of ν_1 is to compare the gas phase ν_1 frequencies of other alkali hydroxides and fluorides. For Rb, the difference is 7 cm^{-1} and for K, 15 cm^{-1} .¹¹⁻¹³ For NaF $\nu_1 = 529.2 \text{ cm}^{-1}$,¹³ so that one might expect a band center in the $480 - 500 \text{ cm}^{-1}$ region.

Finally, theoretical calculations for NaOH have been performed by Long, et al.,⁹ using a 6-21G basis with MP3 and CID electronic correlation. The frequencies determined were $\nu_3 = 3628 \text{ cm}^{-1}$ in agreement with predictions of Kuijpers et al.,¹⁴ $\nu_2 = 322 \text{ cm}^{-1}$ in good agreement with Acquista and Abramowitz¹⁰ (although one might have expected a gas phase prediction somewhat higher than the matrix measurement), and $\nu_1 = 710 \text{ cm}^{-1}$. This last prediction appears high. However, it is unclear from the experiments¹⁰⁻¹¹ whether or not any unassigned absorptions were seen in this spectral region.

7.4 Results

Using second-derivative techniques, infrared absorption spectra were taken at 376, 378, 407.5, 424, 448, 477 and 497 cm^{-1} . Each scan covered a range of at least twice that of the NaOH rotational constant, in order to assure the observation of a rotational line. All measurements were performed using the same diode laser, and detection of the laser beam was made using a liquid nitrogen-cooled Hg:Cd:Te detector which was selected for peak response near 25 μm . A typical spectrum is shown in Figure 7.1. In most of the data, etalons within the White cell limited the measurable fractional absorption limit to about 1%. At the lowest frequencies, both laser power and detector response drop, so that the detection limit was only a few percent absorption. Even with these poor sensitivities, with estimated concentrations of NaOH greater than 10^{13} cm^{-3} , we would expect⁶⁻⁹ fractional absorptions greater than one percent and in most of the cases studied greater than ten percent.

No absorption feature attributable to NaOH was observed at any of the frequencies studied. The diode/detection system was working, as evidenced by observation of H_2O_2 absorptions as well as known absorptions of CS_2 , which was added to the flow for wavelength calibration purposes.

In order to assure ourselves that the IR diode absorption system could detect alkali species, we looked for absorption lines of KF, made by reacting K with excess F_2 . Its vibrational spectrum (actually the first overtone spectrum) has been measured with a diode laser,¹⁵ so that the band center is accurately known. The rotational lines were observed at approximately 407.8, 430, and 431.4 cm^{-1} . Based on the measured concentration of potassium and the observed amount of absorption, we conclude that if rotational lines of NaOH are to be seen with the present system, they will appear using more intense laser modes, due to the problems of large internal etalons and system noise. A more thorough search using a number of diodes (to assure complete wavelength coverage at reasonable intensity) should be able to detect NaOH at levels useable for simple kinetic measurements.

The lack of an observed NaOH absorption feature leads us to the conclusion that the previously detected bands near $430\text{--}440\text{ cm}^{-1}$ do not belong to monomeric NaOH or that we happened to look exactly at band center, where the spacing between the P(1) and R(0) lines would exceed the spectral range of the scan at that diode frequency. It is clear that this problem needs further investigation.

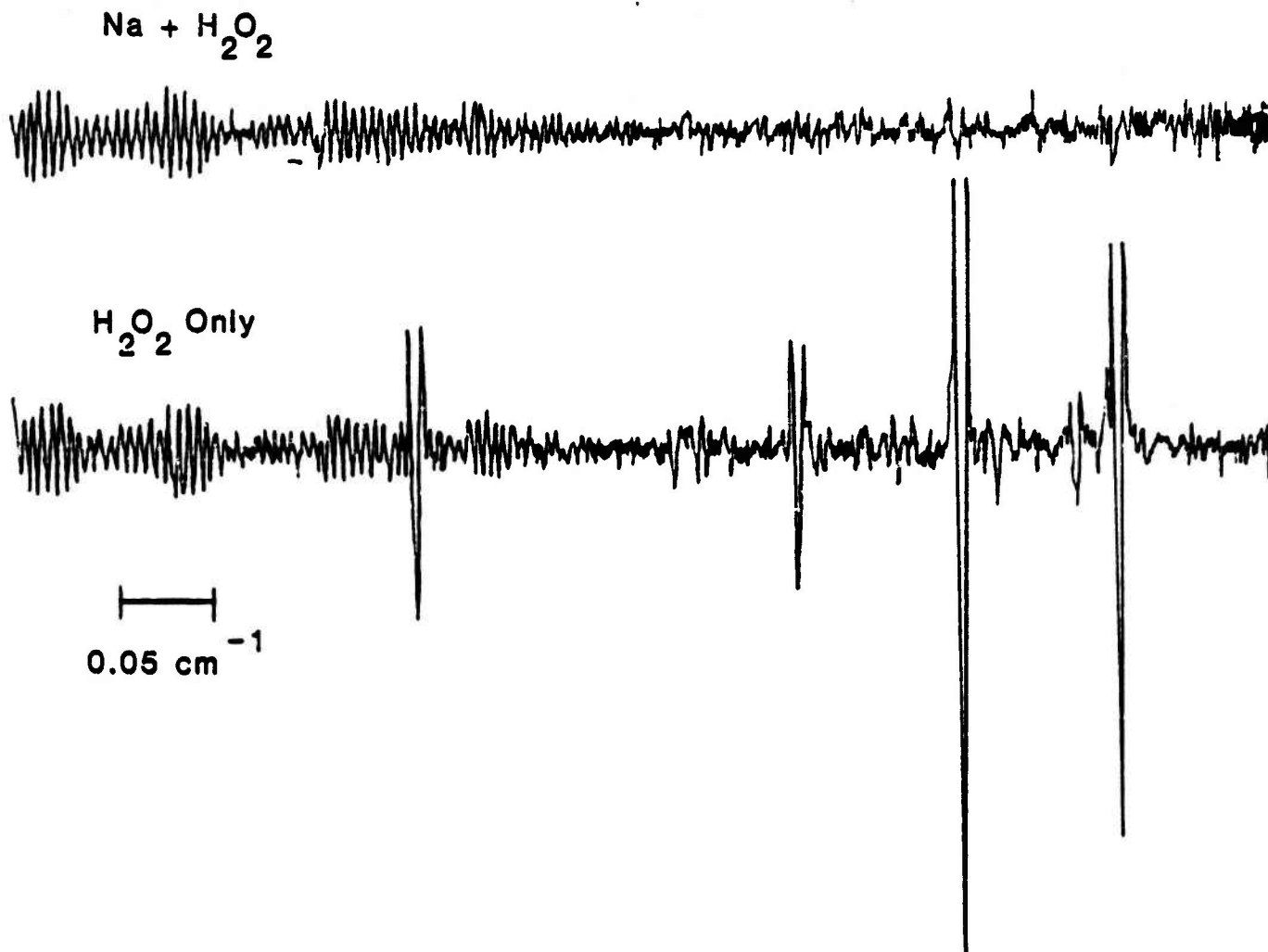


Figure 7.1 Typical Second-Derivative Absorption Spectrum for Na+H₂O₂. Upper curve is with both reactants present. Lower curve is with the sodium oven turned off.

75 References

1. E. Murad, W. Swider and S.W. Benson, *Nature* 289, 273 (1981).
2. J.A. Silver, A.C. Stanton, M.S. Zahniser, and C.E. Kolb, *J. Phys. Chem.* 88, 3123 (1984).
3. J. Ager and C. Howard, University of Colorado at Boulder, private communication, 1985.
4. A.C. Stanton and C.E. Kolb, *J. Chem. Phys.* 72, 6637 (1980).
5. J.C. Wormhoudt, A.C. Stanton, and J.A. Silver, *Proc. SPIE* 452, 88 (1984).
6. E.S. Rittner, *J. Chem. Phys.* 19, 1030 (1951).
7. D.R. Bedding and T.I. Moran, *Phys. Rev. A* 9, 2324 (1974).
8. R.D. Nelson, Jr., D.R. Lide, Jr., and A.A. Maryott, *NSRDS-NBS* 10 (1967).
9. G.A. Long, J.F. Capitani, and L. Pederson, *J. Mol. Struct.* 105, 229 (1983).
10. N. Acquista and S. Abramowitz, *J. Chem. Phys.* 51, 2911 (1969).
11. L.H. Spinar and J.L. Margrave, *Spectrochimica Acta* 12, 244 (1958).
12. M.E. Jacox, *J. Mol. Spec.* 113, 286 (1985).
13. K.P. Huber and G. Herzber, "Molecular Spectra and Molecular Structure IV Constants of Diatomic Molecules", Van Nostrand Reinhold, New York, 1979.
14. P. Kuijpers, T. Topping, and A. Dymanus, *Chem. Phys.* 15, 160 (1976).
15. A.G. Maki and F.J. Lovas, *J. Mol. Spec.* 95, 80 (1982).

8. DISCUSSION AND SUMMARY RESULTS

From the work presented in the preceding sections, it is clear that a great deal of progress has been made in the past five years in both recognizing and then understanding the role which sodium compounds of meteoric origin play in atmospheric chemistry. A list of the reactions of sodium compounds rate constants measured during this period is shown in Table 8-1. We now believe that the observed mesospheric atomic sodium profile can be explained, and its diurnal and seasonal variations understood.¹²⁻¹⁴ A schematic diagram which illustrates the evolution of sodium from the time it enters the lower thermosphere to its removal from the stratosphere is shown in Figure 8.1.

We see that as the ablated sodium metal in its neutral form descends below ~100 km, it begins to react with ozone and molecular oxygen. The latter reaction dominates below 85 km as the O_2 concentration and total atmospheric pressure increase. Sodium monoxide reacts at these altitudes with atomic oxygen to produce electronically excited sodium atoms, which emit the familiar D-line radiation at 590 and 596 nm.

As atomic sodium disappears below 80 km, it is converted through the above mechanisms to NaO and NaO₂. The NaO rapidly reacts with any traces of water vapor to produce NaOH. At these altitudes, photolysis will recycle these species to atomic sodium, resulting in a steady state mixture of mostly NaO₂ and NaOH, with little NaO and virtually no atomic sodium. The question of which of the first two compounds dominates will depend on how rapidly NaO₂ is converted to NaO (see Figure 8.1) relative to its photodissociation rate. These reaction rate constants and photolysis rates have not yet been measured.

Once the alkali end products of the mesospheric chemistry reach the upper stratosphere, reactions with chlorinated compounds, most notably HCl, become important. Photolysis of NaCl will cause atomic chlorine to be released,

Table 8-1 Recent Experimental Rate Constants of Gas-Phase Sodium Compounds

Reaction	T(K)	k(cm ³ molecule ⁻¹ s ⁻¹)	Reference
Na + O ₂ + M → NaO ₂ + M (M = N ₂)	320-698 571-1016 1650-2400	(1.9±0.4)×10 ⁻³⁰ (T/300) ^{-1.1±0.5} (a) (1.11±0.08)×10 ⁻²³ T ^(2.47±0.14) (a) 2×10 ⁻²⁸ T ⁻¹ (a)	Silver, et al. ¹ Husain, et al. ² Hynes, et al. ³
Na + O ₃ → NaO + O ₂	293 290 500	(3.01±0.4)×10 ⁻¹⁰ (7±2)×10 ⁻¹⁰ 4(±4,-2)×10 ⁻¹⁰	Silver, Kolb ⁴ Ager, Howard ⁵ Husain, et al. ⁶
Na + N ₂ O → NaO + N ₂	295 290 349-917	(7.7±0.9)×10 ⁻¹³ (8.2±1.5)×10 ⁻¹³ (1.9±0.3)×10 ⁻¹⁰ exp (-12.5±0.6 kJ/mole/RT)	Silver, Kolb ⁴ Ager, Howard ⁵ Husain, Marshall ⁷
Na + Cl ₂ → NaCl + Cl	294 284-305	(6.7±0.9)×10 ⁻¹⁰ (1.08±0.2)×10 ⁻⁹	Silver ⁸ Talcott, et al. ⁹
Na + H ₂ O ₂ → NaOH + OH → NaO + H ₂ O	308 308	4.1×10 ⁻¹¹ 2.8×10 ⁻¹¹	Silver, et al. ¹⁰ Silver, et al. ¹⁰
NaO + O ₃ → NaO ₂ + O ₂ → Na + 2O ₂	293 290 293 290	-1.5×10 ⁻¹⁰ 1.8×10 ⁻¹⁰ -5×10 ⁻¹¹ 1×10 ⁻¹⁰	Silver, Kolb ⁴ Ager, Howard ⁵ Silver, Kolb ⁴ Ager, Howard ⁵
NaO + H ₂ O → NaOH + OH	290	(2±1)×10 ⁻¹⁰	Ager, Howard ⁵
NaO + HCl → NaCl + OH	308	2.8×10 ⁻¹⁰	Silver, et al. ¹⁰
NaO + H → Na + OH	308	>4×10 ⁻¹²	Silver, et al. ¹⁰
NaO ₂ + HCl → NaCl + HO ₂	295	(2.3±0.4)×10 ⁻¹⁰	Silver, Kolb ⁴
NaOH + HCl → NaCl + H ₂ O	295	(2.8±0.9)×10 ⁻¹⁰	Silver, et al. ¹⁰
NaOH + H → Na + H ₂ O	295	>4×10 ⁻¹²	Silver, et al. ¹⁰
NaCl + H → Na + HCl	308	5×10 ⁻¹⁴ (±1)	Silver, et al. ¹⁰
NaCl + hν → Na + Cl	300	σ _{max} =1×10 ⁻¹⁷ cm ² at 235 nm	Silver, et al. ¹¹

(a) rate constant in units of cm⁶ molecule⁻² s⁻¹

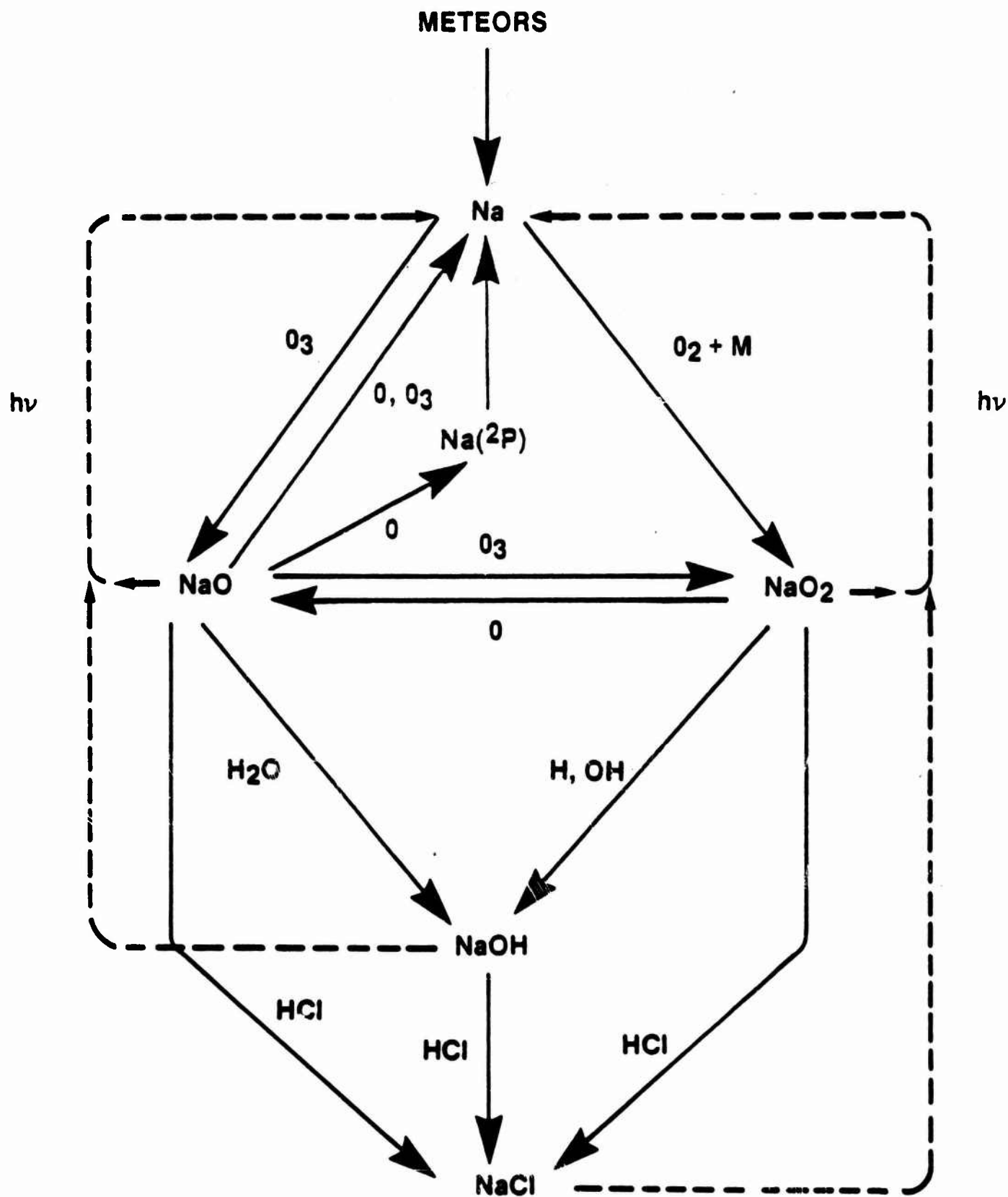


Figure 8.1 Schematic Diagram of Meteoric Sodium Chemistry

creating an additional source for chlorine catalyzed destruction of stratospheric ozone.

The importance of sodium catalyzed chlorine release relative to that caused by the reaction of OH with HCl remains to be determined. If only these gas phase processes are considered, this process might well increase the previously recognized chlorine release rate by as much as 30 percent. However, one must consider both homogeneous and heterogeneous loss processes for these atmospheric metal species. The most likely pathways for losses are condensation onto atmospheric dust, smoke, water droplets or other aerosols. No experimental data quantifying the magnitude of these effects exist, and simple estimates of the effectiveness of alkali loss range from no removal to total removal, depending on one's choice of parameters. Because of the potential importance on stratospheric ozone, we believe that in situ measurements of the stratospheric gas phase alkali content are required.

Finally, we would like to point out that sodium comprises only a few percent of meteoric metals, and that the effects of the more abundant species on atmospheric chemistry should be investigated. This is especially true for iron and silicon. The former is expected to exhibit a fair bit of reactivity with atmospheric constituents. Although silicon oxides are fairly stable, their reactions with halogen compounds are only beginning to be understood and this area should be studied more thoroughly.

8.1 References

1. J.A. Silver, A.C. Stanton, M.S. Zahniser, and C.E. Kolb, 20th Symposium (International) on Combustion, The Combustion Institute, pg. 604 (1984).
2. D. Husain, P. Marshall, and J.M.C. Plane, J. Chem. Soc. Faraday Trans. 2 81, 301 (1985).
3. A.J. Hynes, M. Steinberg, and K. Schofield, J. Chem. Phys. 80, 2585 (1984).
4. J.A. Silver and C.E. Kolb, J. Phys. Chem., submitted for publication (1985).

5. J.W. Ager III, and C.J. Howard, private communication (1985).
6. D. Husain, P. Marshall, and J.M.C. Plane, J. Chem. Soc. Chem. Commun., 1216 (1985).
7. D. Husain and P. Marshall, Comb. Flame 60, 81 (1985).
8. J.A. Silver, J. Chem. Phys., in press (1986).
9. C.L. Talcott, J.W. Ager III, and C.J. Howard, J. Chem. Phys., submitted for publication (1986).
10. J.A. Silver, M.S. Zahmiser, A.C. Stanton, and C.E. Kolb, J. Phys. Chem. 88, 3123 (1984).
11. J.A. Silver, D. Worsnop, A. Freedman, and C.E. Kolb, J. Chem. Phys., in press (1986).
12. V.W.J.H. Kirchoff and B.R. Clemensha, J. Geophys. Res. 88, 442 (1983); V.W.J.H. Kirchoff, Geophys. Res. Lett. 10, 721 (1983).
13. L. Thomas, M.C. Isherwood, and M.R. Bowman, J. Atmos. and Terres. Phys. 45, 587 (1983).
14. W. Swider, Geophys. Res. . Lett. 12, 589 (1985).

9. PAPERS AND PRESENTATIONS

This section lists the papers published and presentations made of the reactions studied in this program.

9.1 Publications

"Temperature Dependent Termolecular Reaction Rate Constant for Potassium and Sodium Superoxide Formation, by J.A. Silver, M.S. Zahniser, A.C. Stanton, and C.E. Kolb, 20th Symposium (Int.) on Combustion, The Combustion Institute 605 (1984).

"The Gas Phase Reaction Rate of Sodium Hydroxide with Hydrochloric Acid", J.A. Silver, A.C. Stanton, M.S. Zahniser, and C.E. Kolb, J. Phys. Chem., 88, 3123 (1984).

"Measurement of Atomic Sodium and Potassium Diffusion Coefficients", J.A. Silver, J. Chem. Phys., 81, 5125 (1984).

"Absolute Photodissociation Cross Sections of Gas-Phase Sodium Chloride at Room Temperature", by Joel A. Silver, Douglas R. Worsnop, Andrew Freedman, and Charles E. Kolb, Journal of Chemical Physics, in press (1986).

"Gas-Phase Reaction Rate of Sodium Superoxide with Hydrochloric Acid", by Joel A. Silver and Charles E. Kolb, submitted for publication to the Journal of Physical Chemistry, 1985.

"Determination of the Absolute Rate Constants for the Room Temperature Reactions of Atomic Sodium with Ozone and Nitrous Oxide", by J.A. Silver and C.E. Kolb, submitted for publication in the Journal of Physical Chemistry, 1985.

9.2 Presentations

"The Reaction Rates of $\text{Na} + \text{O}_2 + \text{M}$, $\text{K} + \text{O}_2$ and $\text{NaOH} + \text{HCl}$ ", by J.A. Silver, M.S. Zahniser, A.C. Stanton, and C.E. Kolb, at the 1983 Fall American Geophysical Union meeting in San Francisco, CA on December 7, 1983.

"Atmospheric Chemistry of Meteoric Metals", by J.A. Silver for a colloquium at the Air Force Geophysics Laboratory on April 19, 1984.

"Temperature Dependent Termolecular Reaction Rate Constant for Potassium and Sodium Superoxide Formation", by J.A. Silver, M.S. Zahniser, A.C. Stanton, and C.E. Kolb, at the 20th International Symposium on Combustion in Ann Arbor, MI in July, 1984.

"The Chemistry of Alkali Oxides in the Atmosphere, by J.A. Silver at the XVI Informal Conference on Photochemistry in Cambridge, MA in August, 1984.

"Gas Phase Alkali Chemistry in the Post-Molecular Beam Age", by C.E. Kolb at MIT on 6 November 1984.

"Measurements of the Photodissociation Cross Section of Sodium Chloride", J.A. Silver, presented at the 1984 International Chemical Congress of Pacific Basin Societies, Honolulu, HA, December 1984.

"Mesospheric Chemistry of Meteor Metals: Reaction Rate Measurements for $\text{Na} + \text{O}_3$, J.A. Silver and C.E. Kolb, 1985 Spring Meeting of the American Geophysical Union, Baltimore, MD, May 27, 1985.

"Stratospheric Chemistry of Meteoric Metals: Measurements of the Rate Constant for $\text{NaO}_2 + \text{HCl}$ and of Photodissociation Cross Sections for NaCl ", J.A. Silver and C.E. Kolb, 1985 Spring Meeting of the American Geophysical Union, Baltimore, MD, May 27, 1985.

"Gas Phase Oxidation Chemistry of Sodium", J.A. Silver, International Conference on Chemical Kinetics, National Bureau of Standards, Gaithersburg, MD, June 17-19, 1985.